International Scientific Journal

Quantum Computers & Computing

This issue is devoted to the Conference on Theoretical Physics, which held in Moscow Open University in Summer 2011. It was organized by professor T.F.Kamalov and brought together researchers from Russia, USA, India, Kanada, EU and other countries. The Conference had the wide scope of topics many of them fit to the Journal "Quantum Computers and Computing". We publish articles, which have been submitted to the journal and passed through the referee process. We hope that this issue will be interesting for many scientists working in close areas to the topic of our journal and will give new impulse to the development of to Quantum Informatics in Russia and abroad.

Yuri Ozhigov,
Editor

CONTENTS

Volume 11

M. Agüero[1,2], **O. Gonzalez**[1], **A. Aguilar**[1]

[1] **Universidad Autonoma del Estado de Mexico,**
Instituto Literario No. 100, Toluca, C.P. 50000, Edo.Mex., México, Mexico
[2] **Institute for General Physics, Russian Academy of Science,**
119991, Babilov Str. 38, Moscow Russia

Generalized coherent states in the study of dynamics of nonlinear processes

A nonlinear saturated Schrödinger equation is obtained as a result of application to the model of DNA, the method of generalized coherent states (GCS). The studied DNA model was introduced by Takeno and Homma in their pioneering work [3]. In this model the DNA macromolecule is subjected to the influence of thermal phonons. We have obtained for particular values in the parameter space, a compacton–anticompacton couple solutions that could be responsible for maintaining the DNA health.

Keywords: nonclassical solutions; generalized coherent states; DNA; compactons.
PACS number(s):02.40.Gh,04.60.Kz,98.80.Qc

1. Introduction

The existence of regimes where nonlinear optical propagation and DNA (or BEC) evolution models obeys the same type of equations are well known [1,2]. Among them the resulting for intense light pulses or spatial beams, the most fascinating is certainly the formation of solitons, which can also be considered in DNA dynamics.

The theoretical studies of DNA macromolecule dynamics in many aspects show the appearance of nonlinear traveling structures along the chain. That studies have led to many interesting types of solutions in the past such as the soliton solutions, the cnoidal solutions, the compacton solutions, the peakon solutions. However, finding these solutions has not been easy at all as is evidenced in the literature.

The model we use in this contribution is the quasi spin variant proposed by Takeno and Homma [3]. In this paper, evolutionary PDEs describing wave patterns inside the DNA macromolecule with compact support are studied. It is assumed that open states of the DNA is a principal requirement for arising other important features of this molecule, specifically for transcription and replication processes. Therefore, it is obvious that the opposite type of states the anti - open sates are suggested to appear inside the DNA molecule. In case of existence of these waves, this inverse process dual to the open ones, will repair the disruption or elongation of hydrogen bonds.

Different approaches for variety of models of the DNA molecule have been applied. After the first proposal made by Englander [4], the model that is being deal with rotational degrees of freedom, and the first one was proposed by Yomosa [5]. Along this type of model the principal one in the sense of dynamics of the hydrogen bonds, is due to the Peyrard - Bishop model [2]. These two version of modeling DNA received a great improvements by many important contributions that one can find for example in the papers [3, 6, 7] and citation therein. In his pioneering work Yomosa S. [5] presented an important DNA model which include the rotation of pair bases along the spiral model proposed by Watson and Crick. This approach takes into consideration a dynamic

of a plane base rotation perpendicular to the helical axis z around the backbone structure. Further improvements were done in the papers [3, 8].

On the other order of things, the study of many body problems whose Hamiltonian has been explicitly written in terms of spin or quasi-spin operators, can be reduced by appropriated approximations to a quasi-classical treatment. For doing this, certain reduction procedure from the quasi - spin operator description to a classical one is needed. This procedure consists in choosing trial functions which can be used for averaging the Hamiltonian. Then it is natural to choose for this aim, coherent states since these states are the most classical and minimized the uncertainty relation [9–11].

In this contribution we study a dynamical model related to the emergence of traveling waves in the DNA molecule by using the quasi - classical approximation due to the generalized coherent states approach. This treatment was possible to implement because of the quasi spin character of the Hamiltonian of the DNA that is written in terms of the Spin operators $\mathbf{S}$ proposed by Takeno-Homma (TH) in [3]. The approach to derive analytical solutions was implemented explicitly for the case of traveling waves. In the next section we briefly expose the main features of the Takeno-Homma model. The third section is devoted to the generalized coherent state approach applied to the nonlinear lattice equation of DNA. The equation of motion derived from the application of GCS method is reported in section 4. The nonlinear soliton like patterns are obtained by analyzing the equations in the continuum limit of the nonlinear lattice equation, that is reported in the fifth section. In the 6-th section we analyze the analytical solutions for hydrogen bond displacements. Comments and conclusion are done in the last section.

2. The quasi-spin model of DNA

We will use the model proposed by Takeno and Homma [3]. In this model the quasi spin operators $\mathbf{S_n} = (S_x, S_y, S_z)$ are related to the rotational angles θ_n and ϕ_n as

$$\mathbf{S_n} = (S_x, S_y, S_z) = (\sin\theta_n \cos\phi_n, \sin\theta_n \sin\phi_n, \cos\theta_n). \tag{2.1}$$

This representation is given for the two strands that compose the DNA. The notation for the second strand will differ to the first one by the apostrophe in the mathematical expressions for its corresponding magnitudes. The rotational angles $\theta_n(\theta_n^{'})$ and $\phi_n(\phi_n^{'})$ represent the angles of rotation of the bases in the n^{th} base pair in the xz and xy plane respectively. Details on this proper DNA model can be found in the works [3, 8, 12, 14]. We will analyze the symmetric case when $z_n = z_n^{'}$. Thus the Hamiltonian for description the nonlinear dynamics of the isotropically homogeneous coupled quasi-spin chain model in the nearest neighboring interactions can be written as

$$H_1 = -\sum_n [J(\mathbf{S_n} \cdot \mathbf{S_{n+1}} + \mathbf{S_n^{'}} \cdot \mathbf{S_{n+1}^{'}}) + \mu(\mathbf{S_n} \cdot \mathbf{S_n^{'}})]. \tag{2.2}$$

This Hamiltonian formally coincides with the generalized Heisenberg spin model used in many branches of physics. In some sense here the double strand DNA model is mapped onto a two coupled spin chain model or a spin ladder system with ferromagnetic legs. The first term of the Hamiltonian (2.2) corresponds to the stacking interaction between the base with number n and its nearest neighbors and the second term represents the inter strand interaction at the nth site or hydrogen bond interaction.

Since the functions of DNA are switched on under the biological temperature, then it is necessary to include thermal surrounding phonon contribution. Let us denote by X_n as the displacement of the bases along the hydrogen bond at the nth site and by $p_n = m_1 \dot{X}_n$ the corresponding momentum of displacements X_n. The coupling between the oscillation of the hydrogen atom due to

thermal fluctuation and the rotation of bases is denoted by α_1. The proposed phonon contribution to the previous Hamiltonian can be written as

$$H_2 = \sum_n [\frac{p_n^2}{2m_1} + k_1(X_n - X_{n+1})^2 + \alpha_1(X_{n+1} - X_{n-1})(\mathbf{S_n} \cdot \mathbf{S_n^{'}})]. \tag{2.3}$$

Thus, the total Hamiltonian that will be analyzed is written as

$$H = \sum_n \Big[-J(\mathbf{S_n} \cdot \mathbf{S_{n+1}} + \mathbf{S_n^{'}} \cdot \mathbf{S_{n+1}^{'}}) - (\mu - \alpha_1(X_{n+1} - X_{n-1}))(\mathbf{S_n} \cdot \mathbf{S_n^{'}}) + \\ + \frac{p_n^2}{2m_1} + k_1(X_n - X_{n+1})^2 \Big]. \tag{2.4}$$

3. Generalized coherent state approach

The correspondence between the collective nonlinear effects in classical and quasi-quantum models has been extensively discussed by many authors. For some details we can address the work [15]. The reduction procedure from quasi spin treatment to classical one have been done by different key approaches. Among those there is a powerful method of the generalized coherent state. This method allows to obtain a quasi-classical version of the model by averaging the quantum or quasi-quantum Hamiltonian over some states that minimizes uncertainties.

Next, we expose some main properties of the generalized coherent states. Let G be an arbitrary Lie Group and $\hat{T}$ be its irreducible unitary representation acting in the Hilbert space $\mathcal{H}$. Any vector of this space is denoted by the symbol $|\psi >$, meanwhile the scalar product of the vectors $|\psi >$, and $|\varphi >$; linear on $|\psi >$, and anti-linear on $|\varphi >$; by the symbol $< \varphi|\psi >$. Finally, the projection operator on the vector $|\psi >$, by $|\psi >< \varphi|$. Let $|\psi_0 >$ be some fixed vector in the space $\mathcal{H}$. Consider the set of vectors $\{|\psi_g >\}$, constructed with the help of the operation: $|\psi_g >= T(g)|\psi_o >$ where g goes over all the group G. These state vectors belong to the orbit of the group in the Hilbert space. It is easy to see that two vectors $|\psi_{g_1} >$ and $|\psi_{g_2} >$ in the same orbit will differ from one another only by a phase factor ($|\psi_{g_1} >= e^{i\alpha}|\psi_{g_2} >, |e^{i\alpha}| = 1$), or in other words will determine the same state only if $T(g_2^{-1}.g_1)|\psi_0 >= e^{i\alpha}|\psi_0 >$.

Let $P = \{p\}$ be the set of elements of the group G such that $T(p)|\psi_0 >= e^{i\alpha(p)}|\psi_0 >$. It is evident that P is a subgroup of the group G and we call it the stationary group of the state $|\psi_0 >$. Over an orbit the stationary subgroups are conjugated.

From the above assumptions it is easily seen that the vectors $\mid \psi(g) >$ are embedded in the left adjoin class $g_{1p} \in g_1 P$ and will differ from each other only in the phase. It means that they define the same state, or, in other words, the whole equivalence class is assigned to the state. When realized the procedure described, one concludes that different vectors (states) will correspond to different elements g_m that belong to the factor space $M = G/P$. As usual, it will be only necessary to consider specific representatives from each class. Since a geometrical point of view, the group G is treated as a fiber-bundle space with a base $M = G/P$ and fiber P. Then the choosing of certain g_m corresponds to some element of this fiber-bundle space. Formally we have the triplet: $\langle\, G, \pi, G/P \,\rangle$, where π is the continuum projector. The idea of a section map is:

$$S : G/P \to G$$

Where the diagram: $S \circ \pi = \pi \circ S$ holds. So, in this sense, the elements of the group are considered as sections of this bundle. The set of vectors:

$$\mid \psi_m >= T(g_m) \mid \psi_0 >$$

where $g_m \in G/P$ is what we will call a system of Generalized Coherent States (GCS) on the group G with a referent vector $\mid \psi_0 >$.

Usually, the choose of the referent vector $|\psi_0>$ is determined by thinking on simplicity and with the states being nearly classical. For our aims the group $SU(2)$ plays a crucial role. This group will be the group G of the above described scheme. It is known that the system of spin coherent states (GCS constructed on the $SU(2)/U(1)$ space; which is the classical Hopf fib-ration $S^1 \to S^3 \to S^2$) may be written as:

$$|\psi>= T(g)|\psi_0>= e^{\alpha S^+ - \hat{\alpha} S^-}|0>= \left(1+|\psi|^2\right)^{-j} e^{\psi S^+}|0>; \tag{3.5}$$

with $\hat{S}^{\pm} = \hat{S}^x + i\hat{S}^y$, $\psi = \dfrac{\alpha}{|\alpha|} Tan|\alpha|$, α, ψ are complex numbers, $|0>= |j, -j>$ and j defines the unitary representation of the group $SU(2)$.

Here as mentioned above, we investigate the particle-like localized nonlinear excitation in the quasi quantum Hamiltonian for DNA obtained by Takeno-Homma [3] by making use the reduction procedure, based on the generalized coherent states (GCS) on the group SU(2)/U(1). We consider the homogeneous system that means all exchange integrals in the Hamiltonian (2.4) are constants and do not differ from point point to point. The quasi-spin piece of the Hamiltonian (2.4) is formally written in terms of spin operators with spin value $j = 1/2$. Since, the spin Hamiltonian and the SU(2) coherent states are constructed on the operators of the same group, here is not necessary to carry out the bozonization procedure of the Hamiltonian. The exchange integrals in the x, y, z direction are the same so we have a quasi spin system with zero anisotropy. This type of system according to Makhankov [18] has the SU(2) symmetry. Also we can consider the easy axis of the model the axis z that is the direction of helical axis of anisotropy. All these qualities permit us to use the approach of generalized coherent states based on SU(2) group.

Let us pass from quasi-quantum system to classical description. Since spin operators $\widehat{S_j^+}$ commute in neighboring sites of both DNA strands, the generalized coherent state for all the lattice is the direct product of GCS taken at separate sites.

$$|\psi>= \prod_j |\psi>_j; \qquad j = 1, 2, 3, \ldots N \tag{3.6}$$

Thus we have for the spin averaging

$$<\psi|\widehat{S_j^+}\,\widehat{S_{j+1}^+}|\psi>=<\psi_j|\widehat{S_j^+}|\psi_j><\psi_{j+1}|\widehat{S_{j+1}^+}|\psi_{j+1}> \tag{3.7}$$

The averaged values of quasi-spin operators $\mathbf{S} = (S^x, S^y, S^z)$ by using the SU(2) GCS can be written in the following stereographic projection forms, that subsequently will be used for averaging the lattice Hamiltonian (2.4)

$$S^+ =<\psi|\widehat{S^+}|\psi>= \frac{\overline{\psi}}{1+|\psi|^2}; \quad S^- =<\psi|\widehat{S^-}|\psi>= \frac{\psi}{1+|\psi|^2}; \tag{3.8}$$

$$S^z =<\psi|\widehat{S^z}|\psi>= -\frac{1-|\psi|^2}{2(1+|\psi|^2)} \tag{3.9}$$

with $S^+ = S^x + iS^y$ and $S^- = S^x - iS^y$. The variables $\psi_n, \theta_n \;\; and \;\; \phi_n$ from the Eq. (2.1) are interrelated by the formula

$$\psi_n = \tan(\theta_n/2)\, e^{i\phi_n} \tag{3.10}$$

After averaging the Hamiltonian (2.4) with the aid of SU(2) GCS we obtained

$$
\begin{aligned}
H \;=\; \sum_{n} \Bigg\{ & -\frac{J}{2}\left(\frac{(\overline{\psi_n}\psi_{n+1}+\overline{\psi_n}\psi_{n+1})+(1-|\psi_n|^2)(1-|\psi_{n+1}|^2)}{(1+|\psi_n|^2)(1+|\psi_{n+1}|^2)} \right. \\
& \left. + \; \frac{(\overline{\xi_n}\xi_{n+1}+\overline{\xi_n}\xi_{n+1})+(1-|\xi_n|^2)(1-|\xi_{n+1}|^2)}{(1+|\xi_n|^2)(1+|\xi_{n+1}|^2)} \right) \\
& -\frac{1}{4}(\mu-\alpha_1(X_{n+1}-X_{n-1}))\frac{2\overline{\psi_n}\xi_n+2\overline{\xi_n}\psi_n+(1-|\xi_n|^2)(1-|\psi_n|^2)}{(1+|\xi_n|^2)(1+|\psi_n|^2)} \\
& +\frac{p_n^2}{2m_1}++k_1(X_n-X_{n+1})^2 \Bigg\}. \qquad (3.11)
\end{aligned}
$$

4. Equations of motion

We will study the continuum version of the Hamiltonian model (3.11). Therefore, we consider the inter-site distance between nucleotides are quite small in comparison with the DNA length. Introducing the new variable fields $X_n \to X(z,t)$ with $z = na$ and as usual making the standard procedures we have $\psi_{n\pm1} = \psi(z,t) \pm a\psi_z + \frac{a^2}{2!}\psi_{zz} + ...$, also $|\psi_{n\pm1}|^2 = |\psi|^2 \pm a(|\psi|)_z + + \frac{a^2}{2!}(|\psi|)_{zz} + ...,$ and $\sum_n - > \int \frac{dz}{a}$. The similar expansion can be straightly done for $\xi_{n\pm1}$ and $|\xi_{n\pm1}|^2$. These last variables correspond to the complementary strand (apostrophe variables) of the double ladder of DNA. Also similar approximation is done for $X_{n\pm1}$. After some algebra we obtain the quasi-classical Hamiltonian

$$
\begin{aligned}
H \;=\; \int \Bigg\{ & \frac{aJ}{2}\left(\frac{|\psi_z|^2}{1+|\psi|^2}+\frac{|\xi_z|^2}{1+|\xi|^2} \right) \\
& - \; \frac{(\mu-2\alpha_1 a X_z)}{4a}\left(\frac{2(\psi\overline{\xi}+\overline{\psi}\xi)+(1-|\xi|^2)(1-|\psi|^2)}{(1+|\xi|^2)(1+|\psi|^2)} \right) \\
& + \; \frac{p^2}{2am_1}+k_1 a(X_z)^2 \Bigg\} dz + \text{const.} \qquad (4.12)
\end{aligned}
$$

The equation of motion for the unknown variables can be obtained using the standard Hamiltonian method. Thus, for finding the unknown displacements $X(z,t)$ from the Eq.(4.12) we can use the standard Hamiltonian equations of motion $\dot{X} = \frac{\partial H}{\partial p}$ and its canonical conjugate counterpart. The equation of motion for the unknown field functions $\psi(z,t)$ and $\xi(z,t)$ can be written using the variational derivative as [19].

$$
i\psi_t = -(1+|\psi|^2)^2 \frac{\delta H}{\delta \overline{\psi}}. \qquad (4.13)
$$

The similar equation of motion is directly built also for the field variable ξ. Therefore, finally

we have obtained the following system of nonlinear differential equations:

$$i\psi_t = -\frac{Ja}{2}\psi_{zz} + aJ\frac{2\psi_z^2\overline{\psi}}{1+|\psi|^2} - \left(\frac{\mu - 2a\alpha_1 X_z}{2a}\right)\left(\frac{\xi - \psi + \psi|\xi|^2 - \overline{\xi}\psi^2}{1+|\xi|^2}\right), \quad (4.14)$$

$$i\xi_t = -\frac{Ja}{2}\xi_{zz} + aJ\frac{2\xi_z^2\overline{\xi}}{1+|\xi|^2} - \left(\frac{\mu - 2a\alpha_1 X_z}{2a}\right)\left(\frac{\psi - \xi + \xi|\psi|^2 - \overline{\psi}\xi^2}{1+|\psi|^2}\right), \quad (4.15)$$

$$m_1 X_{tt} = 2ak_1 X_{zz} + \frac{\alpha_1}{2}\left(\frac{2(\psi\overline{\xi} + \overline{\psi}\xi) + (1-|\xi|^2)(1-|\psi|^2)}{(1+|\xi|^2)(1+|\psi|^2)}\right)_z. \quad (4.16)$$

From the equations (4.14) and (4.15) one finds $\psi = -\xi$. Thus after some algebra we can find the next nonlinear differential equation

$$i\psi = -\frac{Ja}{2}\psi_{zz} + aJ\frac{\psi_z^2\overline{\psi}}{1+|\psi|^2} + \left(\frac{2\mu}{a} - 4\alpha_1 X_z\right)\frac{1-|\psi|^2}{1+|\psi|^2}\psi. \quad (4.17)$$

This equation belongs to the family of Nonlinear Schrodinger equation with saturation. Subsequently, for description the hydrogen bond displacements $X(z,t)$ we found the equation

$$m_1 X_{tt} = 2ak_1 X_{zz} + \frac{\alpha_1}{2}\left(\frac{1+|\psi|^4 - 6|\psi|^2}{(1+|\psi|^2)^2}\right)_z. \quad (4.18)$$

We will look forward for traveling wave solutions. For doing this we change the variables $\sigma = z - vt$. Applying the procedure due to Vasumathi and Daniel [8] i.e. making $X_z = W(z,t)$, after some algebra it yields

$$X_z = \frac{\alpha_1}{2(m_1 v^2 - 2ak_1)}\frac{1+|\psi|^4 - 6|\psi|^2}{(1+|\psi|^2)^2}. \quad (4.19)$$

Replacing the equation (4.19) in to the nonlinear Schrodinger equation (4.17) one obtains

$$i\psi_t = -\frac{Ja}{2}\psi_{zz} + aJ\frac{\psi_z^2\overline{\psi}}{1+|\psi|^2} + \left(\frac{2\mu}{a} - \beta\frac{1+|\psi|^4 - 6|\psi|^2}{(1+|\psi|^2)^2}\right)\frac{1-|\psi|^2}{1+|\psi|^2}\psi, \quad (4.20)$$

$$\text{with } \beta = 2\alpha_1/(m_1 v^2 - 2ak_1). \quad (4.21)$$

Further, we will make several simplifications in order to find analytical solutions. First of all we will make a parametric change of the independent variable z as $z = s\sqrt{\frac{Ja}{2}}$. Second, we will assume that in the first approximation the parameter μ that is the exchange integral between strands and the separation of nucleotides satisfies the strong inequality $\frac{\mu}{a} \gg 1$. Thus, after these restrictions the nonlinear generalized Schrodinger equation is transformed to the following saturable one.

$$i\psi_t = -\psi_{ss} + \frac{2\mu}{a}\left(\frac{1-|\psi|^2}{1+|\psi|^2}\right)\psi - \left(\beta\frac{1+|\psi|^4 - 6|\psi|^2}{(1+|\psi|^2)^2}\right)\frac{1-|\psi|^2}{1+|\psi|^2}\psi. \quad (4.22)$$

5. Nonlinear traveling waves

Since the analytical solution of equation (4.22) is quite difficult to find, we will restrict ourselves for the specific particular case of weakly saturating approximation. This approximation is well documented in various important contribution on nonlinear optics and Bose Einstein condensation theories [9,20]. The equation (4.22) possesses terms proportional to $M = F(I)(1+I)^{-1}$ with $I = |\psi|^2$. Therefore, for the resulting equation not lose saturation properties, we will use the expansion $M = F(I)(1-I)$. We make the following redefinition $\frac{\mu}{a} \to \mu$. Making such approximation after some algebra we obtain the following Cubic-Quintic Nonlinear Schrödinger Equation (CQNSE):

$$i\psi_t + \psi_{ss} + \kappa_1\psi + \kappa_3|\psi|^2\psi - \kappa_5|\psi|^4\psi = 0 \tag{5.23}$$

with the following parameter relations

$$\kappa_1 = -2\mu + \beta, \quad \kappa_3 = 4\mu - 10\beta, \quad \kappa_5 = 4\mu - 34\beta. \tag{5.24}$$

Let us analyze some particular interesting cases of the obtained equation (5.23)

I. Case $\kappa_5 = 0$. In this particular case, the equation (4.22) reduces to the well known nonlinear Schrödinger equation

$$i\phi_t + \phi_{ss} + \gamma|\phi|^2\phi = 0. \tag{5.25}$$

With the following redefined functions and parameters $\psi = \phi\, e^{i\kappa_1 t}$ and $\kappa_1 = -\frac{9}{8}\gamma$, $\kappa_3 = \gamma = 24\beta$. The previous nonlinear equation is the famous nonlinear Schrödinger equation that is completely integrable. Thus there does exist a method for instance an inverse scattering or Hirota methods for finding its N-soliton solutions. The nonlinear Schrödinger equation is a key model describing wave processes in weakly dispersive and weakly nonlinear media [9]

Next our aim is to obtain analytical solutions for the hydrogen bond displacement of the DNA macromolecule. For obtaining some information on DNA properties let us take some solution that supports the Schrodinger nonlinear equation.

First we consider the sign of the parameter γ be positive. For this case as is well known [16] when $\gamma > 1$ the solution of the NSE (5.25) with the trivial boundary condition (that means when the field tends to zero as $|x| \to \infty$) is

$$\phi(s,t) = \left(-\frac{2\nu}{\gamma}\right)^{1/2} \mathrm{Sech}\left[\sqrt{-\nu}s\right] \exp\{-i\nu t\} \tag{5.26}$$

being ν an arbitrary constant. Since we are interested in obtaining traveling wave solution, we will use the well established fact that NSE is invariant under the Galilean transformations

$$\zeta = s - Vt, \quad \tau = t, \quad \phi' = \phi\, \exp\left\{-\frac{iV}{2}\left(s - \frac{1}{2}V\tau\right)\right\}, \tag{5.27}$$

where $\zeta = \sigma/\sqrt{\frac{Ja}{2}}$, $V = v/\sqrt{\frac{Ja}{2}}$ that finally gives us the traveling soliton

$$\phi(s,t) = \left(-\frac{2\nu}{\gamma}\right)^{i/2} \mathrm{Sech}\left[\sqrt{-\nu}\,\zeta\right] \exp\left[\frac{iV}{2} - \frac{i}{2}\left\{\left(\frac{V}{2}\right)^2 + 2\nu\right\}t\right]. \tag{5.28}$$

This solution applied to DNA molecular dynamics should imply that a collective wave of bell type forming a certain open state for the angle deviation defined by $|\psi|^2 = |\phi|^2 = (tan(\theta/2)^2$ should be propagated along the chain due to the interaction of the DNA molecule with thermal

phonons surrounding molecule. This because the collective wave is constructed by the two types of bell solutions for ψ and for ξ field variables correspondingly.

II. **Case.** $\alpha_3 = 0$ In this case we have the Quintic Schrödinger equation.

$$i\phi_t + \phi_{ss} + \gamma_2|\phi|^4\phi = 0. \tag{5.29}$$

This nonlinear equation supports soliton solution in the attractive case when the coefficient γ_2 is positive. The solution that divides the scenario of the evolution equation in two sectors is possible to exist [17]

$$\phi(s,t) = \frac{3^{1/4}(-w)^{1/4}}{\sqrt{\cosh(2\sqrt{-ws})}}e^{-iwt}. \tag{5.30}$$

The first sector as is well known is the sector of collapse when the amplitude of the solution infinitely grows in a finite time. The second scenario correspond to the dispersion solution when the amplitude decays and the area of its localization grows. The collapse is not physical well solution. Then in this case it is convenient to introduce other effects perhaps dissipative ones for compensate the blow up of solutions. These can be numerous nonlinear dissipation mechanisms such as inelastic collisions of the pair of base of DNA with surrounding proteins molecules which results in loss of energy by emitting heat. This interesting issue could be studied further.

6. Hydrogen bond displacements

The mixture of both solutions ψ and $-\psi$ will maintain a certain configuration state along the chain for angle rotations θ and ϕ. For instance, we can see a configuration made by $\mathrm{Sech}^2(\zeta)$ and by $-\mathrm{Sech}^2(\zeta)$ in such a manner that along the DNA chain should be created a wooden spinning top state, for the angle θ deviation. In this case, one can observe the envelope of the edges of quasi-spin arrows. The angle that forms the arrows of quasi spins with respect to the axes ζ represents the angle deviation from equilibrium position. Far from the central part the excitation zone, the angle deviations θ in the middle site acquires the maximum value while outside of the center the angles vanish.

For calculating the traveling waves for displacements X along the hydrogen bonds we can use the analytical solution (5.26). We replace this solution into the equation (4.19) and integrate once with respect to the variable ζ. After integration we have obtained a traveling solution for the displacements $X(\zeta)$ with an arbitrary constant of integration X_0. This constant of integration can be considered by some initial condition imposed to the nonlinear equation (4.19). Further, the integration has been done numerically and we found the pair compacton structure represented in the Fig. (1), by virtue of satisfying the trivial boundary condition at infinity and initial conditions. Resuming, we found a solutions for the hydrogen bond displacements that can be represented by

$$X(\zeta) = X(s - Vt) = \delta \int F(|\phi|^2)d\zeta, \quad \text{for} \quad -\zeta_0 \le \zeta \le \zeta_0, \tag{6.31}$$

$$X(\zeta) = 0, \quad \text{elsewhere} \tag{6.32}$$

$$\text{with} \qquad F(|\phi|^2) = \frac{1 + |\phi|^4 - 6|\phi|^2}{(1 + |\phi|^2)^2} \text{ and } \quad \delta = \frac{\beta}{4}\sqrt{\frac{Ja}{2}}. \tag{6.33}$$

This solution represents a couple of compac and anti-compact fused structures. Specifically, the sector for negative values of independent variable $-\zeta_0 \le \zeta \le 0$ corresponds to the compact piece of the solution and in the region of $0 \le \zeta \le \zeta_0$ lives the anticompacton branch of the solution. Thus, this solution is made of two different contributions of the waves. As it is well common for similar

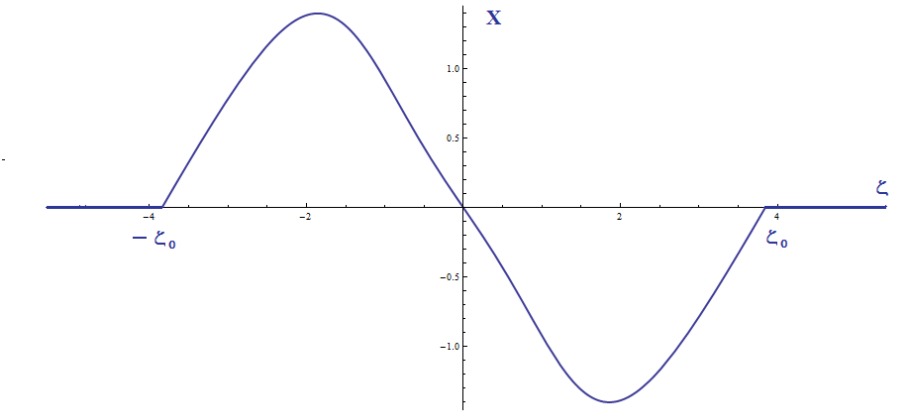

Fig. 1. A couple compacton anti-compacton solution for hydrogen bond displacements along the DNA. The positive values of displacements elongate the separation of the two strands while the negative ones stretch this separation. The values of $\beta = 1$ was used for numerical integration of the corresponding equations.

compact structures [13] we observe the discontinuity on its first derivative at points $\pm\zeta_0$. Thus, the compacton sector ensure the formation of open states due to positive values of displacement of hydrogen bonds, while the anti-compacton sector represents the reconstruction of hydrogen bonds, see Fig. (1). The compacton and the anti-compacton parts collaborate each other in such a manner that the DNA molecule preserves its identity. We observe here a natural mechanism of healing the open states that profusely can be created along the different sector of DNA molecule.

For the second case or the quintic Schrödinger equation, the hydrogen bond displacements can be obtained analytically and we have the particular solution for example when $w = -1$

$$X(\zeta) = \frac{1}{2}\delta\left(2\zeta + 4\sqrt{6}\,\mathrm{arctanh}\left[\frac{\left(-1+\sqrt{3}\right)\tanh(\zeta)}{\sqrt{2}}\right] - \frac{12\sinh(2\zeta)}{\sqrt{3}+\cosh(2\zeta)}\right) \tag{6.34}$$

For $-\zeta_0 \leq \zeta \leq \zeta_0$.

The profile of this solution has the similar fashion of the previous solution found for the case of cubic Schrödinger equation with the Fig. (1). Again this solution represents a typical couple of compacton and anti-compacton pair solution. Although the angle deviations undergo collapse effects, the corresponding hydrogen displacement shows a regular behavior.

The energy of the compacton pair can be easily calculated by virtue of equation (2.3). The integration with respect to the variable ζ in the interval $[-\zeta_0, \zeta_0]$ of first pair compacton anticompacton can be evaluated directly using the energy density

$$E = g(X_\zeta^2) + hX_\zeta F(|\phi|^2) \tag{6.35}$$

with $G = \dfrac{mv^2}{Ja} + \dfrac{2k_1 a}{Ja}$, $h = \dfrac{\alpha_1}{\sqrt{2Ja}}$ and $F(|\phi|^2)$ is defined by the relation (6.33). The compacton

solution can emerge only when the velocities do not satisfy the relation $mv^2 - 2ak_1 = 0$. Otherwise, we could encounter nonphysical solutions with infinity values of energy.

7. Conclusions

We have discussed in this contribution the appearance of non classical soliton like excitations along the DNA molecular model based on the pioneering work of [3]. These solutions could eventually be responsible for various fundamental processes inside the DNA macromolecule. As is well known the relation of the quasi-classical field variable of the GCS approach ψ and the angle θ being the deviation of the angle of the classical spin $\mathbf{S}$ see Eq. (2.1) from the OZ axis is the following $|\psi|^2 = \tan^2(\theta/2)$ [9]. Thus the using of generalized coherent state approach provides us directly with the possibility to calculate the angle deviation of the "classical" spin with respect the chosen direction z. This approach allows as to find the generalized form of the NSE. This NSE for very specific parameter values represents the well known completely integrable model. The angle deviation form the axis z will completely determined by the solutions of integrable NSE . These exact solutions that could serve as a good first approximation in a complex and deep theoretical and experimental analysis of the DNA molecule. The hydrogen bond displacements, shows unexpected behavior represented by the couple of compacton anti-compacton solution. The velocity of this couple is restricted by the relation $\beta > 0$ being β defined by equation (4.21).

The evaluation of displacements of the hydrogen bonds along the DNA can be carried out straightaway by integrating their corresponding nonlinear equations (4.19). We considered that for displacements that occur sufficiently far from the excitation zone, vanish. Therefore, in both direction of the axis ζ we will observe the physical interesting case of vanished values of hydrogen bond displacements at long distances from the active zone. By taking in mind this physical reason and integration of the equation (4.19) we obtain for specific parameter values the compacton anti-compacton couple while the angle θ deviation evolves like a bell soliton along the DNA macromolecule.

As soon as the nonlinear excitations in whichever segment of the DNA molecule is being activated by the presence of phonons, nonlinear waves of coupled compacton and anti-compacton pieces could appear, describing the evolution of hydrogen bonds. The last one could be interpreted as a healing wave piece that cures the bubble or open states on the DNA segments. As is well known the open states of DNA chain is considered the precursors of denaturation of this macromolecule. Thus, we observe that it is very possible that soon after defects of elongation for bond hydrogens along the chain appear, its dual counter part of a wave immediately turns on restoring its previous perturbation. We can observe again that the wave of displacements travels in a fashion that resemble the Cooper pair in electronics dynamics or virtual particles in field theories.

Acknowledgements

We acknowledge the efforts of SIEA-UAEMEX for supporting the fundamental research.

References

[1] V N Serkin, Akira Hasegawa, T L Belyaeva, Phys. Rev. Lett. 03/2007; 98(7):074102.

[2] M. Peyrard and A.R. Bishop, Phys. Rev. Lett. 62 (23) , 2755-2758, (1989)

[3] Takeno S. y Homma B. Prog. Theor. Phys.70 (1983)308 ; Takeno S. y Homma B. Prog. Theor. Phys. 72 (1984) 679.

[4] S.W. Englander, N.R. Kallenbach, A.J. Heeger, J.A. Krumhansl, 0927 and S. Litwin.// Proc. Natl. Acad. Sci (U.S.A.) 77, 7222 (1980)

[5] S. Yomosa, Phys Rev. A 27 (1983) 2120; Phys. Rev. A 30 (1984) 474

[6] Yakushevich L. V. Nonlinear Physics of DNA, Wiley (Chichester) (1998) Second edit. (2004).

[7] G. Gaeta, C. Reiss, M. Peyrard and Th. Dauxois, Simple models of non-linear DNA dynamics, Rivista del Nuovo Cimento 17 (1994) n.4, 148

[8] M. Daniel, Vasumathi, Physica D 231 (2007) 10-29; Physical Review E, 80, (2009) 061904

[9] V.G. Makhankov. Soliton Phenomenology, Kluwer Academic Publishers (1990).

[10] A. Perelomov Generalized Coherent States and their applications. Springer. Berlin (1986).

[11] Klauder J. R. Skagerstam B. S. Coherent states, Applications in Physics and Mathematical Physics. World Scient (2010).

[12] Takeno S., Homma S. Prog. Theor. Phys.77 (1987) n03 548-562

[13] P. Rossenau and J. M. Hyman, Phys. Rev. Lett. 70, 564 (1993).

[14] Takeno S. Phys. Lett. A 339 (2005) 352-360

[15] Kosevich A.M. Ivanov B.A. and Kovalyov A.S. Phys Rep. **194**, 1 (1990)

[16] Debnath L. Nonlinear PDEs for scientists and engineers (Birkhauser, (1997)

[17] G. L. Alfimov, V. V. Konotop, and P. Pacciani, Arxiv:nlin/0605035v2 (2006).

[18] Makhankov V.G., Makhankov A.V. Phys. Stat Sol. (b) 145, 669 (1988).

[19] L. Fadeev, L. Takhtajan, Hamiltonian methods in the theory of solitons. Springer (1987).

[20] Y.Kivshar, G. Agrawal, Optical Solitons. Academic Press (2003).

V.A. Andreev
P.N. Lebedev Physical Institute RAN, Moscow, Russia*

Supersymmetric models in quantum optics

The supersymmetrical structure of some quantum optics models is studied. The notion of the degree of supersymmetry is introduced. This concept is valid for discerning the supersymmetry of the quantum systems with different ground-state (vacuum) structure. The examples of Hamiltonians with a certain value of the supersymmetry degree are given.

Keywords: quantum optics; Supersymmetric models. PACS number(s): 42.50.Ex

1. Introduction

The notion of supersummetry is widespread in the modern physics. It started with the field theories uniting bosons and fermions, but with Witten's supersymmetrical quantum mechanics the similar structures become quite common [1, 2]. In many problems there are no bosons and fermions anymore, however, the present terminology is historically still being used. The general formulation of the concept of supersymmetric quantum mechanics and its structure is described in [3]- [6]. This paper contains a formal description of the supersymmetric quantum mechanics as algebraic theory consisting of the Hamiltonian, special operators, which are called superchargers and the algebraic form distinguishing between "boson" and "fermion" sectors of the model. These structures are define certain Clifford algebra. In the simplest case the baseline construction of this theory is the existence of a Hamiltonian H_1. This Hamiltonian is a factorable operator, i.e. it can be presented as a product of two operators

$$H_1 = AB, \tag{1.1}$$

here A,B are some operators.

Now, along with the Hamiltonian H_1 one can consider the Hamiltonian H_2, obtained from the H_1 by permuting the factors A,B.

$$H_2 = BA. \tag{1.2}$$

The Hamiltonians H_1, H_2 can be combined into a unit Hamiltonian

$$H = \begin{pmatrix} H_1 & 0 \\ 0 & H_2 \end{pmatrix} = \begin{pmatrix} 0 & A \\ B & 0 \end{pmatrix}^2 = Q^2. \tag{1.3}$$

The operator Q is called supercharge. Equally with the supercharge

$$Q_1 = \begin{pmatrix} 0 & A \\ B & 0 \end{pmatrix} \tag{1.4}$$

*E-mail: andrvlad@yandex.ru

one can consider a supercharge

$$Q_2 = \begin{pmatrix} 0 & iA \\ -iB & 0 \end{pmatrix}. \tag{1.5}$$

The supercharges Q_1, Q_2 have the properties

$$\{Q_1, Q_1\} = \{Q_2, Q_2\} = 2H, \tag{1.6}$$
$$[H, Q_1] = [H, Q_2] = 0, \ \{Q_1, Q_2\} = 0.$$

Strictly speaking the spectra of the operators H_1 and H_2 should be identical, but the ground state may be different. Several cases are possible. First the spectra of the Hamiltonians H_1 and H_2 could be completely identical. This takes place in the Jaynes-Cummings model. We call the supersymmetry of the given type zeroth-degree supersymmetry:

$$\Delta S = 0. \tag{1.7}$$

There are certain examples when one of the Hamiltonians, say H_2, has one nondegenerate ground state

$$H_2\psi_0 = 0, \tag{1.8}$$

and H_1 has no such a state. So the spectra of the Hamiltonians H_1, H_2 differ by single nondegenerate level. This supersymmetry is to be called first-degree supersymmetry:

$$\Delta S = 1. \tag{1.9}$$

This type of supersymmetry takes place in the model of two-photon transitions. In the case of multy-photon transitions the supersymmetry with a degree

$$\Delta S = k \tag{1.10}$$

is realized.

This is the general structure of Witten's supersymmetric model. There are various examples of its realization. One such example is the supersymmetric quantum mechanics. It was actively studied in 80 years. In this model the Schrodinger operator, which is a differential operator of second order, is presented as product of two differential operators of first order.

$$H_1 = \frac{d^2}{dx^2} + U_1(x) = \left(\frac{d}{dx} + a(x)\right)\left(\frac{d}{dx} + b(x)\right) = AB. \tag{1.11}$$

Now one can construct the operator H_2. It can be done by permutation of the factors A, B.

$$H_2 = BA = \left(\frac{d}{dx} + b(x)\right)\left(\frac{d}{dx} + a(x)\right) = \frac{d^2}{dx^2} + U_2(x). \tag{1.12}$$

The eigenfunctions of the operators H_1, H_2 are connected by Darboux transformation. Considering them together, one can construct a supersymmetric Hamiltonian

$$H = \begin{pmatrix} H_1 & 0 \\ 0 & H_2 \end{pmatrix} = \begin{pmatrix} 0 & \frac{d^2}{dx^2} + U_1(x) \\ \frac{d^2}{dx^2} + U_2(x) & 0 \end{pmatrix}. \tag{1.13}$$

In this case the supercharges Q_1, Q_2 have the form

$$Q_1 = \begin{pmatrix} 0 & \frac{d}{dx} + a(x) \\ \frac{d}{dx} + b(x) & 0 \end{pmatrix}, \quad Q_2 = \begin{pmatrix} 0 & i(\frac{d}{dx} + a(x)) \\ -i(\frac{d}{dx} + b(x)) & 0 \end{pmatrix}. \tag{1.14}$$

The similar structures exist in quantum optics.

Here we give a short review of our results in this field. An alternative approach to the problem one can find in Refs. [7–11].

2. The Jaynes-Cummings model

The Hamiltonian of the Jaynes-Cummings model is usually written in the form

$$H_1 = \hbar\omega(a^+a + \sigma_3) + g(a^+\sigma_- + a\sigma_+). \tag{2.15}$$

Here we propose that the detuning $\Delta = \omega - \omega_0$ between the frequency of the cavity mode ω and the two-level system frequency ω_0 is zero. The operators a^+, a are the creation and the annihilation operators of the bosonic mode and $\sigma_\pm, \sigma_3$ are Pauli matrices acting on the states of the two-level system. The total number of excitations, both bosonic and fermionic, is conserved.

The observables of the system are invariant under a constant phase shift

$$a^+ \to e^{i\varphi}a^+, \quad a \to e^{-i\varphi}a. \tag{2.16}$$

The specific chose $\varphi = \frac{\pi}{2}$ is also conventional as well as $\varphi = 0$. With the help of this transformation one can get the second Hamiltonian.

$$H_2 = \hbar\omega(a^+a + \sigma_3) + ig(a^+\sigma_- - a\sigma_+). \tag{2.17}$$

The Hamiltonians (2.15),(2.17) can be considered as the components of unit Hamiltonian H (1.13). The conventional structure of suprtsymmetric theory according to [4] consists of the supercharge $Q, H = Q^2$ and the hermitian operator γ discerning bosons and fermions with properties

$$\gamma^2 = I, \quad \{Q, \gamma\} = 0.$$

Usually

$$\gamma = \begin{pmatrix} 1 & 0 & & 0 \\ 0 & 1 & 0 & 0 \\ 0 & 0 & -1 & 0 \\ 0 & 0 & 0 & -1 \end{pmatrix},$$

and this is also true with the Jaynes-Cummings model. One may try to search for supercharges having the form [12]

$$Q = \begin{pmatrix} 0 & 0 & \alpha & \gamma a \\ 0 & 0 & \beta a^+ & \delta \\ \alpha^* & \beta^* a & 0 & 0 \\ \gamma^* a^+ & \delta^* & 0 & 0 \end{pmatrix}. \tag{2.18}$$

But one can find that the supercharge in the closed form does not exist. But for the Hamiltonian

$$H_c = H + cI \tag{2.19}$$

with a shifted zero level of energy the supercharge in the form (2.18) still exists. For the Hamiltonian (2.19) the supercharges Q_1, Q_2 reads

$$Q_1 = \begin{pmatrix} 0 & 0 & \frac{g}{2\sqrt{\hbar\omega}} & -i\sqrt{\hbar\omega}a \\ 0 & 0 & \sqrt{\hbar\omega}a^+ & -i\frac{g}{2\sqrt{\hbar\omega}} \\ \frac{g}{2\sqrt{\hbar\omega}} & \sqrt{\hbar\omega}a & 0 & 0 \\ i\sqrt{\hbar\omega}a^+ & i\frac{g}{2\sqrt{\hbar\omega}} & 0 & 0 \end{pmatrix}, \tag{2.20}$$

$$Q_2 = \begin{pmatrix} 0 & 0 & i\frac{g}{2\sqrt{\hbar\omega}} & \sqrt{\hbar\omega}a \\ 0 & 0 & i\sqrt{\hbar\omega}a^+ & \frac{g}{2\sqrt{\hbar\omega}} \\ -i\frac{g}{2\sqrt{\hbar\omega}} & -i\sqrt{\hbar\omega}a & 0 & 0 \\ \sqrt{\hbar\omega}a^+ & \frac{g}{2\sqrt{\hbar\omega}} & 0 & 0 \end{pmatrix}.$$

The value of the constant

$$c = \frac{1}{2}\hbar\omega + \frac{g^2}{4\hbar\omega} \tag{2.21}$$

can be interpreted in terms of an energy gap. In fact, the energy spectrum of the Hamiltonians (2.15),(2.17) has the form

$$E_n = \frac{1}{2}\hbar\omega\left(1 + \frac{1}{2}\right) \pm g\sqrt{n+1}. \tag{2.22}$$

The constant shift c guarantees that the energy cannot be negative for any values of the constant g.

Thus, supersymmetry in the Jaynes-Cummings model is the possibility to consider together two Hamiltonian, in which photon creation and annihilation operators differ by arbitrary phase.

The supersymmetry is spontaneously broken when there is degeneracy of the ground state and there exist specific operators commuting with the Hamiltonian and transfering these ground states into each other. In the case presented, the ground state is twofold degenerate and the bosonic and fermionic vacuums are

$$|0\rangle^B = \begin{pmatrix} 0 \\ 0 \\ i|k\rangle \\ |k+1\rangle \end{pmatrix}, \quad |0\rangle^F = \begin{pmatrix} -|k\rangle \\ |k+1\rangle \\ 0 \\ 0 \end{pmatrix}. \tag{2.23}$$

Here $k = max[(g/2\hbar\omega)^2 - 1, 0]$.

The action of supercharges on these vacuums is described by

$$Q_1|0\rangle^B = -\frac{i}{\sqrt{\hbar\omega}}\left(\frac{1}{2}g - \hbar\omega\sqrt{n+1}\right)|0\rangle^F, \quad Q_1|0\rangle^F = \frac{i}{\sqrt{\hbar\omega}}\left(\frac{1}{2}g - \hbar\omega\sqrt{n+1}\right)|0\rangle^B \tag{2.24}$$

$$Q_2|0\rangle^B = \frac{1}{\sqrt{\hbar\omega}}\left(\frac{1}{2}g - \hbar\omega\sqrt{n+1}\right)|0\rangle^F, \quad Q_2|0\rangle^F = \frac{1}{\sqrt{\hbar\omega}}\left(\frac{1}{2}g - \hbar\omega\sqrt{n+1}\right)|0\rangle^B.$$

This is the supersymmetric structure of the Jaynes-Cummings model. In this model the supersymmetry with $\Delta S = 0$ is realized.

3. The supersymmetry of two-photon Hamiltonians

In this case we consider the two-photon Hamiltonians describing two proprocesses: two-photon absorption and stimulated Raman scattering. This two processes can be united into a single supersymmetric Hamiltonian. In contrast to the case of the Jaynes-Cummings model, the case of the usual Witten-type supersymmetry is realized and the ground state is non-degenerate.

The pair of the Hamiltonians is considered:

$$H_1 = \omega_1 a_1^+ a_1 + \omega_2 a_2^+ a_2 + \omega_0 \sigma_3 + g(a_1^+ a_2 \sigma_- + a_1 a_2^+ \sigma_+), \;\; \omega_0 = \omega_1 - \omega_2, \tag{3.25}$$
$$H_2 = \omega_1 a_1^+ a_1 + \omega_2 a_2^+ a_2 + \tilde{\omega}_0 \sigma_3 + g(a_1^+ a_2^+ \sigma_- + a_1 a_2 \sigma_+), \;\; \tilde{\omega}_0 = \omega_1 + \omega_2.$$

The Hamiltonian H_1 is used to describe the proprocess of stimulated Raman scattering. The quantum with frequency ω_1 is absorbed and the quantum with frequency ω_2 is emitted. The atom of the Raman-activ medium undergose transformation from the ground to the excited state. The Hamiltonian H_2 describes the proprocess of two-photon absorption when the atom to undergo transition should absorb two quanta with frequencies ω_1 and ω_2 respectively.

The compound Hamiltonian has the form

$$H = \begin{pmatrix} H_1 & 0 \\ 0 & H_2 \end{pmatrix} + \frac{1}{2}(\omega_1 + \omega_2) I. \tag{3.26}$$

The energy level shift is necessary to assure the hermiticity of operators of supercharge. The Hamiltonian H in the form (3.26) isupersymmetric and has the supercharges Q_1, Q_2 [13]

$$Q_1 = \begin{pmatrix} 0 & 0 & \alpha a_2^+ & \beta a_1 \\ 0 & 0 & \beta a_1^+ & \alpha a_2 \\ \alpha a_2 & \delta a_1 & 0 & 0 \\ \delta a_1^+ & \alpha a_2^+ & 0 & 0 \end{pmatrix}, \;\; Q_2 = i \begin{pmatrix} 1 & 0 & 0 & 0 \\ 0 & 1 & 0 & 0 \\ 0 & 0 & -1 & 0 \\ 0 & 0 & 0 & -1 \end{pmatrix} Q_1. \tag{3.27}$$

Here

$$\alpha = \sqrt{\omega}_2, \;\; \beta = \frac{\sqrt{\omega}_1}{u}, \;\; \delta = u\sqrt{\omega}_1. \tag{3.28}$$

The quantity u is the root of the equation

$$u + \frac{1}{u} = \frac{g}{\sqrt{\omega_1 \omega_2}}. \tag{3.29}$$

The equation (3.29) has two solutions u_+, u_- providing two sets of parameters β, δ. Thus, the Hamiltonian (3.26) has two parametric families of the supercharges (3.27).

The spectrum of the given model is constructed as follows.

The Hamiltonian H_1 has eigenvectors

$$\Psi_{n,m}^{1,\pm} = \begin{pmatrix} |n, m\rangle \\ \pm|n+1, m-1\rangle \end{pmatrix}, \tag{3.30}$$

with the corresponding eigenvalues

$$\tilde{E}^{1,\pm}_{n,m} = n\omega_1 + m\omega_2 + \frac{1}{2}(\omega_1 - \omega_2) \pm g\sqrt{(n+1)m}. \tag{3.31}$$

The Hamiltonian H_2 has eigenvectors

$$\Psi^{2,\pm}_{n,m} = \begin{pmatrix} |n,m\rangle \\ \pm|n+1,m+1\rangle \end{pmatrix}, \tag{3.32}$$

with the corresponding eigenvalues

$$\tilde{E}^{2,\pm}_{n,m} = n\omega_1 + m\omega_2 + \frac{1}{2}(\omega_1 + \omega_2) \pm g\sqrt{(n+1)(m+1)}. \tag{3.33}$$

After the energy level shift $\frac{1}{2}(\omega_1+\omega_2)$, which was applied for hermiticity of the supercharges, the spectrum (3.30),(3.33) obtains the form

$$E^{1,\pm}_{n,m} = (n+1)\omega_1 + m\omega_2 \pm g\sqrt{(n+1)m}. \tag{3.34}$$

$$E^{1,\pm}_{n,m} = (n+1)\omega_1 + (m+1)\omega_2 \pm g\sqrt{(n+1)(m+1)}. \tag{3.35}$$

One can see from (3.34) and (3.35) that the spectrum of the supersymmetric Hamiltonian is twice degenerate.

$$E^{1,\pm}_{n,m+1} = E^{2,\pm}_{n,m}. \tag{3.36}$$

The each eigenvalue

$$E^{ss,\pm}_{n,m} = (n+1)\omega_1 + (m+1)\omega_2 \pm g\sqrt{(n+1)(m+1)} \tag{3.37}$$

corresponds to two eigenvectors

$$\Psi^{ss,\pm}_{n,m,+} = \begin{pmatrix} |n,m+1\rangle \\ \pm|n+1,m\rangle \\ |n,m\rangle \\ \pm|n+1,m\rangle \end{pmatrix}, \quad Psi^{ss,\pm}_{n,m,-} = \begin{pmatrix} |n,m+1\rangle \\ \pm|n+1,m\rangle \\ -|n,m\rangle \\ \pm|n+1,m\rangle \end{pmatrix}. \tag{3.38}$$

The are also states

$$\Psi^{ss,\pm}_{n,-1} = \begin{pmatrix} |n,0\rangle \\ 0 \\ 0 \\ \pm|n+1,0\rangle \end{pmatrix} \tag{3.39}$$

with energy

$$E^{ss,\pm}_{n,-1} = (n+1)\omega_1.$$

And the states

$$\Psi^{ss,\pm}_{-1,m} = \begin{pmatrix} 0 \\ |0,m\rangle \\ 0 \\ \pm|0,m+1\rangle \end{pmatrix} \tag{3.40}$$

with energy

$$E^{ss,\pm}_{-1,m} = (m+1)\omega_2.$$

The ground level

$$E_0 = E^{ss,\pm}_{-1,-1} = 0 \tag{3.41}$$

is nondegenerate and the corresponding vacuum eigenvector is expressed as

$$\Psi^{ss}_{-1,-1} = \begin{pmatrix} 0 \\ 0 \\ 0 \\ |0,0\rangle \end{pmatrix}. \tag{3.42}$$

For this reason, the model realizes the conventional scheme for supersymmetric quantum mechanics in which ground state is nondegenerate. All other states are twice degenerate. So in this model the supersymmetry with $\Delta S = 1$ is realized.

4. The multiphoton transitions

We consider a two-level system interacting with electromagnetic field. There are two modes of the field and the state of the field is changed by a definite number of quanta for each emission process. We consider a multiphoton process, when the transition from the excited to the ground state of the two-level system results in the absorption of n quanta of one mode and emission of m quanta from another mode. The other process is the decay of the ground state into n quanta of one mode and m quanta of anotherb mode.

These two processes can be united into one supersymmetric model, however, one must somehow distort the Hamiltonians, describing these processes. First, we consider the standart Hamiltonians and explain what is wrong with them.

The multiphoton Raman process is described by the Hamiltonian

$$\begin{gathered} \tilde{H}_1 = \omega_1 a_1^+ a_1 + \omega_2 a_2^+ a_2 + \omega_0 \sigma_3 + g((a_1^+)^n a_2^m \sigma_- + a_1^n (a_2^+)^m \sigma_+), \\ \omega_0 = n\omega_1 - m\omega_2, \end{gathered} \tag{4.43}$$

and the two-mode absorption is described by the Hamiltonian

$$\begin{gathered} \tilde{H}_2 = \omega_1 a_1^+ a_1 + \omega_2 a_2^+ a_2 + \tilde{\omega}_0 \sigma_3 + g((a_1^+)^n (a_2^+)^m \sigma_- + a_1^n a_2^m \sigma_+), \\ \tilde{\omega}_0 = n\omega_1 + m\omega_2. \end{gathered} \tag{4.44}$$

The Hamiltonians (4.43) and (4.44) have insufficient richness of structure for supersymmetry, at least in the class of 4×4 matrices. One can overcome this difficulty if one takes into account that the self-energy of the systems H_1^0, H_2^0 commutes with the interaction parts of the Hamiltonians. This implies the conservation of the total number of exitations in yhe system by the interaction.

$$\begin{aligned} [H_1^0, H_1^{int}] &= [\omega_1 a_1^+ a_1 + \omega_2 a_2^+ a_2 + \tilde{\omega}_0 \sigma_3, (a_1^+)^n a_2^m \sigma_- + a_1^n (a_2^+)^m \sigma_+], \\ [H_1^0, H_1^{int}] &= [\omega_1 a_1^+ a_1 + \omega_2 a_2^+ a_2 + \tilde{\omega}_0 \sigma_3, (a_1^+)^n (a_2^+)^m \sigma_- + a_1^n a_2^m \sigma_+]. \end{aligned} \tag{4.45}$$

Then one can go into the interaction picture and construct a supersymmetric Hamiltonian

$$H^{int} = \begin{pmatrix} H_1^{int} & 0 \\ 0 & H_2^{int} \end{pmatrix} = \\ = \begin{pmatrix} (a_1^+)^n a_2^m \sigma_- + a_1^n (a_2^+)^m \sigma_+ & 0 \\ 0 & (a_1^+)^n (a_2^+)^m \sigma_- + a_1^n a_2^m \sigma_+ \end{pmatrix} \tag{4.46}$$

This Hamiltonian has the supercharges Q_1, Q_2 [14], [15]

$$Q_1 = \begin{pmatrix} 0 & 0 & (a_1^+)^n & 0 \\ 0 & 0 & & a_1^n \\ 0 & a_2^n & 0 & 0 \\ (a_2^+)^n & 0 & 0 & 0 \end{pmatrix}, \quad Q_2 = i \begin{pmatrix} 1 & 0 & 0 & 0 \\ 0 & 1 & 0 & 0 \\ 0 & 0 & -1 & 0 \\ 0 & 0 & 0 & -1 \end{pmatrix} Q_1. \tag{4.47}$$

The supersymmetric Hamiltonian (4.46) has the supersymmetry of degry $\Delta S = nm$.

5. Conclusion

In the work we consider some quantum optics models and show that they have a supersymmetry structure. These models are a quantum field generalization of Witten's supersymmetrical quantum mechanics. The notion of the degree ΔS of supersymmetry is introduced. Examples of supersymmetric quantum optics models with the degree of supersymmetry equal to a non-negative integer are given. The supersymmetrical model with $\Delta S = 0$ is realized in the Jaynes-Cummings model. The supersymmetrical model with $\Delta S = 1$ corresponds to the model of two photon transitions. And the supersymmetrical model with $\Delta S = n \geq 2$ is realized in the model of multiphoton transitions.

Acknowledgement

V.A. Andreev is grateful to the Russian Foundation for Basic Research for partial support under Project. 11-02-01269-a

References

[1] E. Witten, *Nucl. Phys.*, **185**, (1981) 513.
[2] E. Witten, *Nucl. Phys.*, **202**, 91982) 253.
[3] L.E. Gendenshtein and I.V. Krive, *Sov. Phys. Usp.*, **28**, (1985) 645.
[4] A. Juffe, A. Leshiewski and M. Lewenstein *Ann. Phys.*, **178**, (1987) 313.
[5] A.A. Andrianov, N.V. Borisov, M.V. Ioffe, M. I. Eides, *Teoret. Mat. Fiz.*, **61**, (1984) 17.
[6] A.A. Andrianov, N.V. Borisov, M.V. Ioffe, *Teoret. Mat. Fiz.*, **61**, (1984) 183.
[7] R.W. Haymaker and A.R.P. Rau, *Am. J. Phys.*, **54**, (1986) 928.
[8] Ling Yin-Sheng and Zhang Wei, *Phys. Lett. A*, **193**, (1994) 47.
[9] Chang Jae Lee, *Phys. Rev. A*, **50**, (1994) R4.
[10] Jian-Qi Shen , Hong-Yi Zhu and Hong Mao, *J. Phys. Soc. Jpn.*, **71**, (2002) R4.
[11] F. Coopera, A. Khareb and U. Sukhatmec, *Phys. Rep.*, **251**, (1995) 267.
[12] V.A. Andreev and P.B. Lerner, *Phys. Lett. A*, **134**, (1989) 507.
[13] V.A. Andreev and P.B. Lerner, *Opt. Commun.*, **84**, (1991) 323.
[14] V.A. Andreev and P.B. Lerner, *Nuovo Cimento*, **105 A**, (1992) 773.
[15] V.A. Andreev and P.B. Lerner, *Nuovo Cimento*, **107 A**, (1993) 1767.

I.E. Bulyzhenkov
P.N. Lebedev Physical Institute
Leninskiy pros. 53, Moscow, 119991, Russia

Ricci curvatures describe both field and particle densities

The continuous elementary source in Einstein's gravitational theory is the r^{-4} radial energy density rather than the delta-operator density in empty-space gravitation. The space energy integral of such an infinite (astro)particle is finite and determines its nonlocal gravitational charge for the energy-to-energy attractions with other nonlocal (astro)particles. The non-empty flat space of the undivided material Universe is charged continuously by the world energy density of the global ensemble of overlapping radial particles.

Keywords: gravitation; particles. PACS number(s): 73.22.-f

The integration of particles into spatial structures of their fields was assumed by Einstein: 'We could regard matter as being made up of regions of space in which the field is extremely intense... There would be no room in this new physics for both field and matter, for the field would be the only reality,' translation [1].

We rely on the metric formalism [2] of Einstein's General Relativity (GR) in order to discuss extended particles and nonlocality of classical masses. Let us consider a non-rotating probe particle with passive mass m_p in a static central field of a gravitational source with the motionless active mass M_a and active GR energy E_a. The passive GR energy $\mathcal{E}_p$ of the probe particle,

$$\mathcal{E}_p \equiv \frac{m_p c^2 \sqrt{g_{oo}}}{\sqrt{1 - v^2 c^{-2}}} \equiv \mathcal{K} + \mathcal{U}_\Delta, \tag{1}$$

incorporates its Special Relativity (SR) mechanical energy $\mathcal{K}$ and the so far undefined contribution of gravitational energy $\mathcal{U}_\Delta$. We are not going to employ Newtonian references from the classical mass-to-mass gravitation for this potential energy, $\mathcal{U}_\Delta = \mathcal{U}_\Delta(r)$, which is an unknown radial function of distance r between centers of active, E_a, and passive, $\mathcal{E}_p$, nonlocal energies. We plan to use only SR energy references $\mathcal{K} \equiv m_p c^2/\sqrt{1 - v^2 c^{-2}}$ for gravitating mass-energies. Then, Einstein's SR and GR may be discussed together as the self-contained SR-GR theory for energy-to-energy interactions of non-local inertial energies or GR charges.

Based on 'new' SR references for the mechanical energy K in (1), one can redesign the GR metric component g_{oo} of the pseudo-Riemannian metric tensor $g_{\mu\nu}$ in the following way,

$$\sqrt{g_{oo}} \equiv \frac{\mathcal{K}\sqrt{1 - v^2 c^{-2}}}{m_p c^2} + \frac{\mathcal{U}_\Delta \sqrt{g_{oo}}}{\mathcal{E}_p} \equiv \frac{\mathcal{K}\sqrt{1 - v^2 c^{-2}}}{m_p c^2 (1 - \mathcal{U}_\Delta \mathcal{E}_p^{-1})} \equiv \frac{1}{1 - \mathcal{U}_\Delta \mathcal{E}_p^{-1}}. \tag{2}$$

This metric component equally contributes to local physical time $d\tau = \sqrt{g_{oo}} dt$ for an imaginary point observer and to local proper time for probe mass centers in a static field without rotation (when $g_{oi} = 0$ and $ds^2 = g_{oo} dt^2 - dl^2$). The active mass M_a possesses a distributed active energy E_a of the nonlocal GR source, while the passive mass M_p can be associated with the distributed

passive-inertial energy E_p of the same radial carrier of matter, which have equal active and passive mass-energies. A spatial density of active energy of the distributed source-particle is locally balanced by passive sink-particle energy density in the vanishing [3] Einstein curvature, $G^o_o \equiv g^{o\nu}R_{\nu o} - -2^{-1}g^{\rho\nu}R_{\rho\nu} = 0$, for static energy-momentum carrier with locally bound source-particle (active field) and sink-particle (passive field) fractions of matter-energy.

Einstein maintained that all terms of his 1915 equation should be considered at field points and we reiterated the continuous, field distribution of gravitational bodies within their spatial field structures by assigning active mass-energy to distributed source-fields and passive mass-energy to distributed sink-fields or distributed inertial particles. The 1907 Principle of Equivalence corresponds to the strict balance of active and passive energy-momentum components of every gesamt (=whole) energy carrier.

The GR non-empty space equation for the global summary of all local energy densities, $\sum_1^\infty G^o_o = 0$, is valid for the world overlap of static continuous sources and sinks [4]. The Ricci-Tolman mass-energy density R^o_o of every gesamt carrier of paired active-passive (source-sink) energies is jointly contributed by equal densities of the distributed active source-energy E_a and the distributed passive sink-energy E_p. Two non-vanishing affine connections, $\Gamma^o_{io} = \partial_i g_{oo}/2g_{oo}, \Gamma^i_{oo} = \partial_i g_{oo}/2$, with one logarithmic potential $W \equiv -c^2 ln(1/\sqrt{g_{oo}})$ are responsible for the Ricci scalar density,

$$\frac{R}{2} = R^o_o = g^{oo}R_{oo} = g^{oo}\partial_i\Gamma^i_{oo} - g^{oo}\Gamma^i_{oo}\Gamma^o_{io} = \nabla^2 W c^{-2} + (\nabla W c^{-2})^2, \tag{3}$$

of elementary material spaces with strong static fields in their rest frames, where $g_{oi} = g^{oi} = 0$, $g^{oo} = 1/g_{oo}$, and $g_{ij} = -\delta_{ij}$. Many relativists tend to drop $(\nabla W/c^2)^2$ next to the 'linear' term $\nabla^2 W/c^2$ for Newtonian weak field limit ($-W/c^2 \approx -\mathcal{U}_\Delta/\mathcal{E}_p = +const/r \ll 1$) of the Ricci curvature R^o_o in the Einstein Equation. Such an erroneous approach to the Ricci tensor formalism contradicts the Principle of Equivalence which requires local identities, $\nabla^2 W/c^2 \equiv (\nabla W/c^2)^2$, of active and passive mass-energies for both strong and weak gravitational interactions. Even without references on Einstein's physics, it is not reasonable mathematics when one claims for the week field limit ($W \approx -const/r$) that $\nabla^2 W \equiv r^{-1}\partial_r^2(rW) \approx -r^{-1}\partial_r^2 const \equiv 0$ is the largest term in R^o_o. In fact, the 1915 Einstein equation $G^\mu_\nu = \kappa T^\mu_\nu$ cannot result mathematically in static Newtonian gravitation, unless one 'simplifies' this overloaded tensor equation by geometrization of particles in T^o_o through the Ricci tensor densities within the 'simplified' equation $G^o_o = 0$.

Contrary to the qualitative interpretation of the Principle of Equivalence for empty space gravitation of point particles, non-empty space physics with Newtonian aether of nonlocal gravitational bodies can describe the local equivalence of active and passive (inertial) mass-energy densities quantitatively,

$$\begin{aligned}\rho_a c^2 \equiv \frac{c^2\nabla^2 W}{4\pi G} &\equiv -\frac{c^4}{4\pi G r^2}\partial_r\left[r^2\partial_r ln\left(\frac{1}{\sqrt{g_{oo}}}\right)\right] \\ &= \frac{c^4}{4\pi G}\left[\partial_r ln\left(\frac{1}{\sqrt{g_{oo}}}\right)\right]^2 \equiv \frac{(\nabla W)^2}{4\pi G} \equiv \rho_p c^2,\end{aligned} \tag{4}$$

with peculiarity-free solutions for the metric tensor component (2) even in strong fields. General radial solutions of the nonlinear Poisson equation (4), $1 - \mathcal{U}_\Delta\mathcal{E}_p^{-1} \equiv 1/\sqrt{g_{oo}} = C_1 r^{-1} + C_2$, depends on two constants C_1 and C_2. One constant can be defined ($C_2 = 1$) due to the SR asymptotic behavior of the GR metric, $g_{oo}(\infty) \to 1$. The other constant ($C_1 = GE_a/c^4$) can be found after the volume integration of the active energy density from (4),

$$E_a = \int_o^\infty \rho_a(r)c^2 4\pi r^2 dr = -\frac{c^4 r^2}{G}\partial_r ln(1/\sqrt{g_{oo}})|^{r\to\infty}_{r\to o} = \frac{c^4 r^2\partial_r(\mathcal{U}_\Delta\mathcal{E}_p^{-1})}{G(1-\mathcal{U}_\Delta\mathcal{E}_p^{-1})}|^{r\to\infty}_{r\to o}. \tag{5}$$

The radial potential $\mathcal{U}_\Delta \mathcal{E}_p^{-1} = -C_1 r^{-1}$ of the active nonlocal energy-charge $E_a = c^4 C_1/G$ for the passive (probe) nonlocal energy-charge $\mathcal{E}_p$ corresponds to the energy-to-energy attraction law [3]

$$\mathcal{U}_\Delta = -\frac{GE_a}{c^4 r}\mathcal{E}_p, \tag{6}$$

in self-contained GR with SR references.

Again, we specified two constants $C_1 = GE_a/c^4 \equiv r_o$ and $C_2 = 1$ through the Principle of Equivalence for active and passive components of the Ricci-Tolman mass-energy in (3)-(4) and through the SR asymptotic metric. Therefore, we specified the GR metric tensor component $g_{oo} = = (1 + r_o r^{-1})^{-2}$ and the static flatspace metric $ds^2 = g_{oo}dt^2 - \delta_{ij}dx^i d^j$ (for rest-frame fields without rotation or net spin) without references on Newtonian gravitation. The GR vector force in static central fields [5],

$$\mathbf{f} \equiv \frac{m_p}{\sqrt{1-v^2}}\nabla ln\left(\frac{1}{\sqrt{g_{oo}}}\right) = \frac{m_p\sqrt{g_{oo}}}{\sqrt{1-v^2}}\nabla\left(\frac{1}{\sqrt{g_{oo}}}\right) = -\frac{\hat{\mathbf{r}}GE_a}{c^4 r^2}\mathcal{E}_p, \tag{7}$$

is exerted upon the passive energy-charge $\mathcal{E}_p$, which is the measure of inertia for the probe mass m_p. The strong field intensity $\mathbf{f}/\mathcal{E}_p$ keeps Gaussian surface flux ($E_a = const$) for paired energy-to-energy interactions in flat space. However, active/passive energy-charges are constant in (7) only in the absence of third bodies which can vary such gravitational/inertial charges in full agreement with Mach's ideas [6] embedded into the self-contained SR-GR dynamics (1)-(7) of nonlocal continuous energies or nonlocal gravitational bodies.

Based on the SR form of the mechanical part of the GR passive (probe) energy $\mathcal{E}_p$, Einstein's metric theory quantitatively incorporates Machian ideas and rigorously relates the local component $g_{oo} = [1+(r_o/r)]^{-2}$ to the nonlocal active energy E_a. It is worth noting that every elementary mass continuously occupies the entire Universe despite the ultrashort gravitational scale $r_o = Gm/c^2$ for the half-mass volume. Indeed, the active and passive mass-energy densities of the radial astrocarrier with equal active/passive energy charges $E_{a/p} = r_o c^4/G = E = mc^2$,

$$\rho_a(r)c^2 \equiv \rho_p(r)c^2 = E\frac{r_o}{4\pi r^2(r_o + r)^2}, \tag{8}$$

exist everywhere, at all radial distances in the nonlocal elementary microcosm of each rest-mass formation. Electrically bound elementary astrocarriers of active and passive radial GR energies constitute nonlocal molecules, nonlocal mechanical bodies (cosmism of all people), nonlocal planets, etc... Ultrashort microscopic scales, $r_o = GM_{atom}/c^2$, of electrically neutral atoms on bodies' visible surfaces are beyond the Planck quantum length, the $10^{-18}m$ instrumental resolution record, and the human perception level. Nonetheless, all surface and bulk atoms of observed gravitating bodies are nonlocal astrodistributions of radial active plus passive energies, while centers of spherical symmetries of these atoms belong to the most dense (visible) frames of an infinite body (with its low-dense invisible aether). Continuous fields and continuous particles in nonlocal energy-to-energy gravitation are (yin-yang) paired distributions of equal amounts of matter-energy.

Flat material space with Newtonian aether, specified by the astrodistribution (8) with the radial particle density $n(r) = r_o/4\pi r^2(r + r_o)^2$, differs in principle from Schwarzschild's 'point matter in empty space' model of physical reality (roughly described by operator mathematics of the non-analytical density $\delta(r)$ for the point particle approximation). Moreover, our static metric solution $ds^2 = dt^2\left(1 + r_o r^{-1}\right)^{-2} - \delta_{ij}dx^i dx^j$ for the universal attraction (6)-(7) of nonlocal passive energy-charges by the nonlocal active (source) energy-charge has been derived to criticize *ad hoc* dogmas of the empty space world with point mass-energy peculiarities. Both elementary electric charges (with the Gauss flux conservation due to spatial flatness) and masses co-exist for observations in one 3D space, which therefore must have only one universal, common 3D sub-geometry for all kinds of particles or fields.

References

[1] M.-A. Tonnelat, *The Principles of Electromagnetic Theory and Relativity* (Riedel Publishing Co., Dordrecht, 1966).

[2] A. Einstein and M. Grossmann, Zeits. Math. und Physik **62**, 225 (1913)

[3] I.E. Bulyzhenkov, *Int. J. Theor. Phys* **47**, 1261 (2008).

[4] I.E. Bulyzhenkov, *Jour. Supercond. and Novel Magn.* **22**, 723 (2009).

[5] L.D. Landau and E.M. Lifshitz, *The Classical Theory of Fields* (Pergamon, Oxford, 1975) para 106, problem 4

[6] E. Mach, *Die Mechanik in ihrer Entwickelung historisch-kritisch dargestellt* (F.A. Brockhaus, Leipzig, 1904), S. 236.

[7] W. de Sitter, Mon. Not. Roy. Astron. Soc. **77**, 155 (1916)

[8] I.I. Shapiro, R.D. Resenberg, J.F. Chandler, and R.W. Babcock, Phys. Rev. Lett. **61**, 2643 (1988); J.G. Williams, X.X. Newhall, and J.O. Dickey, Phys. Rev. D **53**, 6730 (1996)

[9] K. Schwarzschild, Sitzungsber. Deut. Akad. Wiss., Berlin 189 (1916); J. Droste, Proc. Kon. Ned. Akad. Wet. Amsterdam, **19**, 197 (1916)

[10] A. Einstein, Annals of Mathematics **40**, 922 (1939)

[11] J. V. Narlikar, *A Random Walk in General Relativity and Cosmology*, ed. by N.K. Dadhich, J. Krishna Rao and C.V. Vishveshwara (Wiley Eastern, New Delhy, 1985) p. 171; J. V. Narlikar and T. Padmanabhan, Foundation of Physics **18**, 659 (1988)

[12] C.W.F. Everitt, in *Near Zero: New Frontiers of Physics*, ed. by J.D. Fairbank *et al.* (Freeman and Co, New York, 1988), p.587

[13] L. I. Schiff, Proc. Nat. Acad. Sci. **46**, 871 (1960); Phys. Rev. Lett. **4**, 215 (1960)

[14] A. Einstein, I. Infeld, and B. Hoffmann, Ann. Math. **39**, 65 (1938)

[15] A.S. Eddington and G.L. Clark, Proc. Roy. Soc. **A166**, 465 (1938); V.A. Fock, Jour. Exp. Theor. Phys. **9**, 375 (1939) and Fiz. Zhur. AN USSR **1**, 81 (1939); B. Bertotti and J. Plebanski, Ann. Phys. **11**, 169 (1960); P. Havas and J.N. Goldberg, Phys. Rev. **128**, 398 (1962)

A. Deveikis
Department of Applied Informatics, Vytautas Magnus University, Kaunas, Lithuania*

Density matrices of the nuclear shell model

The presented two-particle translationally invariant density matrices are defined as two-particle density matrices integrated over centre-of-mass position vector of two last particles and complemented with isospin variables. In order to simplify shell-model calculations, we propose to use the set of quantum numbers containing only the number of oscillator quanta E, the total angular momentum J, the total isospin T, and only one additional integer quantum number responsible for unambiguous enumeration of the antisymmetric states. On this basis we developed simple and effective procedures for calculation of translationally invariant density matrices. The procedures concerns the calculation of the one-particle and two-particle coefficients of fractional parentage for a single j-orbit with isospin, calculation of the two-particle generalized coefficients of fractional parentage and elimination of spurious states by diagonalizing centre-of-mass Hamiltonian matrix in the basis of the antisymmetric A-particle oscillator functions with singled-out dependence on intrinsic coordinates of two last particles. An arbitrary number of oscillator quanta can be involved. The presented two-particle translationally invariant density matrices may be used for calculation of expectation values of two-particle nuclear shell-model operators within the isospin formalism. The calculated density matrices applied for analysis of the level structures of $A = 6$ and $A = 8$ isobars.

Keywords: nuclear shell model; density matrices.
PACS number(s): 73.21.La

1. Introduction

In the last decade significant progress in the nuclear calculations of light atomic nuclei present the *ab initio* no-core shell model [1]. The *ab initio* no-core nuclear shell-model approach obey the principles of antisymmetry, translational invariance and deal with the latest NN-interactions. This approach is based on calculation of wave functions for description of many particle systems. However it is well known that long series expansion of realistic nuclear wave function in shell model ones is plagued with a number of serious convergence problems. In the light of ever-increasing model space size, the more promising approach for calculation of identical particle systems may be based on translationally invariant density matrices instead of wave functions [2]. Since all operators of observables including intrinsic Hamiltonian and root-mean-square radius operators are symmetric ones, calculation of their expectation values does not require the complete wave function. Finally, the description of an A-particle system may be simplified using even a simpler quantity, namely, the density matrix integrated over the centre-of-mass position vector of two last particles, or the so-called intracule [3]. In the case of light nuclei, the intracule has to describe the A-particle system with unexcited centre-of-mass and must be complemented with isospin wariables. We call such intracule the two-particle translationally invariant density matrix. The advantage is that using two-particle translationally invariant density matrices we have to deal only with $7 + 7$ orbital, spin, and isospin variables, instead of wave functions containing $5A - 3$ variables.

*E-mail: a.deveikis@if.vdu.lt

In order to simplify shell model states classification and formation algorithms, we propose to use a well-defined of quantum numbers containing only the number of oscillator quanta E, the total angular momentum J, the total isospin T, and only one additional integer quantum number responsible for unambiguous enumeration of the antisymmetric states [4]. Rejection of the higher-order group-theoretical classification of many-particle antisymmetrical states allows one to significantly simplify the antisymmetrization procedure for A-particle states. As a consequence, higher excitations may be added to the model space and more adequate calculations performed. On this basis we developed simple and effective procedures for calculation of translationally invariant density matrices. The procedures concerns the calculation of the one-particle and two-particle coefficients of fractional parentage for a single j-orbit with isospin, calculation of the two-particle generalized coefficients of fractional parentage and elimination of spurious states by diagonalizing centre-of-mass Hamiltonian matrix in the basis of the antisymmetric A-particle oscillator functions with singled-out dependence on intrinsic coordinates of two last particles.

2. Definition of two-particle translationally invariant density matrices

The only quantities really needed for calculation of identical particle systems are two-particle translationally invariant density matrices. It is well known, that the most straightforward way to construct a density matrix is by the use of coefficients of fractional parentage. However, the calculation of translationally invariant coefficients of fractional parentage is very sophisticated and until now don't succeed even for light atomic nuclei. The translationally invariant density matrices may be calculated by no use of the translationally invariant coefficients of fractional parentage. For this, it is convenient to introduce the expansion of the product of centre-of-mass ground state function and intrinsic harmonic oscillator wave-function in terms of antisymmetric but not translationally invariant shell model wave functions [5]

$$\begin{aligned}\Psi_{00}(\vec{\xi}_0)\Psi_{E\Gamma JTM_JM_T}(\xi_1\dots\xi_{A-1})\\ =\sum_{K\Delta}\Psi_{EK\Delta JTM_JM_T}(x_1\dots x_A)\;a^{EJT}_{K\Delta;00,\Gamma}.\end{aligned}\tag{2.1}$$

Here $\Psi_{00}(\vec{\xi}_0)$ is the nucleus centre-of-mass ground-state wave function with principal and orbital angular momentum quantum numbers equal to zero and $\Psi_{E\Gamma JTM_JM_T}(\xi_1\dots\xi_{A-1})$ is translationally invariant wave function depending on Jacobi coordinates. The summation in this formula runs over all configurations K and additional quantum number Δ (Γ is the additional quantum number for differentiation of translationally invariant states). The functions from the subspace of the non-spurious motion are the eigenfunctions of the centre-of-mass Hamiltonian. Thus, the coefficients of this expansion $a^{EJT}_{K\Delta;00,\Gamma}$ can be obtained by diagonalizing the centre-of-mass Hamiltonian in the basis of not translationally invariant oscillator shell model wave functions $\Psi_{EK\Delta JTM_JM_T}(x_1\dots x_A)$.

The calculation of $\Psi_{EK\Delta JTM_JM_T}(x_1\dots x_A)$ functions should start from calculation of single-shell coefficients of fractional parentage (CFPs). Single-shell one-particle CFPs may be calculated by spectral decomposition of an antisymmetrization operator matrix $\mathbf{Y}_{A,1}$

$$\begin{aligned}&\langle(j^{A-1}\overline{(\Delta JT)};j)j^A\Delta JT|\mathbf{Y}_{A,1}|(j^{A-1}\overline{(\Delta JT)}';j)j^A\Delta JT\rangle\\ &\quad=\frac{1}{A}\delta_{\overline{(\Delta JT)},\overline{(\Delta JT)}'}+\frac{A-1}{A}(-1)^{2j+J+T+\overline{J}'+\overline{T}'}\sqrt{\left[\overline{J}',\overline{T}',\overline{J},\overline{T}\right]}\\ &\quad\times\sum_{\overline{\overline{(\Delta JT)}}}\langle j^{A-2}\overline{\overline{(\Delta JT)}};j|j^{A-1}\overline{(\Delta JT)}\rangle\langle j^{A-2}\overline{\overline{(\Delta JT)}};j|j^{A-1}\overline{(\Delta JT)}'\rangle\\ &\quad\times\begin{Bmatrix}j&\overline{J}&\overline{\overline{J}}\\ j&\overline{J}'&J\end{Bmatrix}\begin{Bmatrix}\frac{1}{2}&\overline{T}&\overline{\overline{T}}\\ \frac{1}{2}&\overline{T}'&T\end{Bmatrix}.\end{aligned}\tag{2.2}$$

Here a single bar over quantum numbers indicates the parent state. The specification of single shell is followed by its total momentums and Δ. CFPs are those eigenvectors of the $\mathbf{Y}_{A,1}$ that correspond to unit eigenvalues. With the use of the CFPs the antisymmetric angular-momentum-coupled A-particle wave function for the nuclear j-shell in an isospin formalism may be expanded in terms of a complete set of the angular-momentum-coupled parent-state wave functions with a lower degree of antisymmetry

$$\begin{aligned}&\Phi_{j^A\Delta JTM_JM_T}(x_1\dots x_A)\\&=\sum_{\overline{(\Delta JT)}}\langle j^{A-1}\overline{(\Delta JT)};j|j^A\Delta JT\rangle\left\{\Phi_{j^{A-1}\overline{(\Delta JT)}}(x_1\dots x_{A-1})\otimes\phi_{elsJ''T''}(x_A)\right\}_{JTM_JM_T}\end{aligned}\tag{2.3}$$

The two-particle CFPs may be expressed in terms of obtained one-particle CFPs [6]

$$\begin{aligned}&\langle j^{A-2}\overline{\overline{(\Delta JT)}};j^2J''T''|j^A\Delta JT\rangle\\&\quad=(-1)^{[j]+\overline{J}+\overline{T}+J+T}\frac{1}{2}[1-(-1)^{J''+T''}]\sqrt{[J'',T'']}\\&\quad\times\sum_{\overline{(\Delta JT)}}\sqrt{[\overline{J},\overline{T}]}\langle j^{A-2}\overline{\overline{(\Delta JT)}};j|j^{A-1}\overline{(\Delta JT)}\rangle\langle j^{A-1}\overline{(\Delta JT)};j|j^A\Delta JT\rangle\\&\quad\times\begin{Bmatrix}j&j&J''\\J&\overline{J}&\overline{J}\end{Bmatrix}\begin{Bmatrix}\frac{1}{2}&\frac{1}{2}&T''\\T&\overline{\overline{T}}&\overline{T}\end{Bmatrix}.\end{aligned}\tag{2.4}$$

A double bar over the list of quantum numbers indicates the $A-2$ particle state. Double primes refer to the separated two-particle subsystem.

Two-particle multishell coefficients of fractional parentage (GCFPs) may be calculated by means of the one-particle and two-particle CFPs [7]. In the first case the two particles are taken from different j-shells. This GCFP can be expressed in terms of single-shell one-particle CFP and the corresponding recoupling coefficient

$$\begin{aligned}&\langle\overline{\overline{(EK\Delta JT)}};((elj)_{A-1},(elj)_A)J''T''|EK\Delta JT\rangle\\&\quad=(-1)^{\nu_r+\nu_p-1}[2n_rn_p/(A(A-1))]^{\frac{1}{2}}\\&\quad\times\langle j^{n_r-1}\overline{(\Delta JT)}_r;j_r|j^{n_r}(\Delta JT)_r\rangle\langle j^{n_p-1}\overline{(\Delta JT)}_p;j_p|j^{n_p}(\Delta JT)_p\rangle\\&\quad\times\langle((J_1T_1\dots\overline{J_rT_r}\dots\overline{J_pT_p}\dots J_kT_k)\overline{\overline{JT}},(j_rt_r,j_pt_p)J''T'')JT|\\&\qquad|(J_1T_1\dots(\overline{J_rT_r},j_rt_r)J_rT_r\dots(\overline{J_pT_p},j_pt_p)J_pT_p\dots J_kT_k)JT\rangle.\end{aligned}\tag{2.5}$$

Here subscript r refers to the r-th shell in the configuration, and superscript n_r is the number of particles contained in the r-th shell. The recoupling coefficient is independent on one-particle quantum numbers and Δ, so their notations are not indicated in its specification. The total momentums of single shells indicated in the recoupling coefficient expression are vector coupled in an ascending order if another sequence explicitly displayed by parentheses is not introduced. The integer is $\nu_r=\sum_{i=r+1}^{k}n_i$, where sum runs over all shells standing to the right from the r-th shell.

In the second case two particles are removed from the same shell. The definition of this GCFP contains simply the two-particle single-shell CFP

$$\begin{aligned}&\langle\overline{\overline{(EK\Delta JT)}};((elj)_{A-1},(elj)_A)J''T''|EK\Delta JT\rangle\\&\quad=[n_r(n_r-1)/(A(A-1))]^{\frac{1}{2}}\langle j^{n_r-2}\overline{\overline{(\Delta JT)}}_r;j_r^2J''T''|j_r^{n_r}(\Delta JT)_r\rangle\\&\quad\times\langle((J_1T_1\dots\overline{\overline{J_rT_r}}\dots J_kT_k)\overline{\overline{JT}},J''T'')JT|\\&\qquad|(J_1T_1\dots(\overline{\overline{J_rT_r}},J''T'')J_rT_r\dots J_kT_k)JT\rangle.\end{aligned}\tag{2.6}$$

The expectation value of the two-particle operator (centre-of-mass Hamiltonian) can be obtained by expressing them into the single-particle form. This may be accomplished by means of Jacobi coordinates

$$\begin{cases} \vec{\xi}_{-1} = \dfrac{1}{\sqrt{2}}(\vec{r}_{A-1} + \vec{r}_A) \ , \\ \vec{\xi}_2 = \dfrac{1}{\sqrt{2}}(\vec{r}_{A-1} - \vec{r}_A) \ . \end{cases} \tag{2.7}$$

The antisymmetric two-particle oscillator shell model functions may be expanded in terms of vector coupled products of the functions depending on the intrinsic Jacobi variable ξ_2 with the functions depending on the Jacobi coordinate with the nonpositive index $\vec{\xi}_{-1}$

$$\begin{aligned} &|((elj)_{A-1},(elj)_A)J''T''\rangle \\ &\quad = \sum_{(el)_{-1},elsj} |((el)_{-1},elsj)J''T''\rangle\langle((el)_{-1},elsj)J''T''|((elj)_{A-1},(elj)_A)J''T''\rangle. \end{aligned} \tag{2.8}$$

The coefficients for the transition from the antisymmetrical two-particle shell model functions to the function of ξ_2 we call the *Jacobi* coefficients. The *Jacobi* coefficients may be expressed via *Trlifaj*, $6j$ and $9j$ coefficients

$$\begin{aligned} &\langle((elj)_{A-1},(elj)_A)J''T''|((el)_{-1},elsj)J''T''\rangle \\ &\quad = \frac{1-(-1)^{l+s+T''}}{\sqrt{2\left(1+\delta_{(elj)_{A-1},(elj)_A}\right)}}(-1)^{l_{A-1}+l_A+s+J''}\sqrt{[j_{A-1},j_A,s,j]} \\ &\quad \times \sum_L [L]\langle(el)_{A-1},(el)_A : L|(el)_{-1},el : L\rangle_1 \begin{Bmatrix} l_{-1} & l & L \\ s & J'' & j \end{Bmatrix} \begin{Bmatrix} l_{A-1} & \frac{1}{2} & j_{A-1} \\ l_A & \frac{1}{2} & j_A \\ L & s & J'' \end{Bmatrix}. \end{aligned} \tag{2.9}$$

It is convenient to introduce the coefficients of expansion of the oscillator shell model functions in terms of the ones with singled out dependence on the intrinsic coordinates of two last particles (SCFPs). The SCFPs are composed of GCFPs and *Jacobi* coefficients

$$\begin{aligned} &\langle\overline{\overline{(EK\Delta JT)}},((el)_{-1},elsj)J''T''|EK\Delta JT\rangle \\ &\quad = \sum_{(elj)_{A-1},(elj)_A} \langle\overline{\overline{(EK\Delta JT)}};((elj)_{A-1},(elj)_A)J''T''||EK\Delta JT\rangle \\ &\quad \times\langle((elj)_{A-1},(elj)_A)J''T''|((el)_{-1},elsj)J''T''\rangle. \end{aligned} \tag{2.10}$$

The procedure for spurious state elimination is based on projecting out the unexcited centre-of-mass subspace by diagonalizing real symmetric centre-of-mass Hamiltonian matrix ($\mathbf{H}_{\text{c.m.}}$) in the basis of the antisymmetric A-particle oscillator functions with singled-out dependence on intrinsic coordinates of two last particles – SCFPs

$$\begin{aligned} &\frac{1}{\hbar\omega}\langle EK\Delta JT|\mathbf{H}_{\text{c.m.}}|EK'\Delta'JT\rangle \\ &\quad = \left(E+\frac{3}{2}\right)\delta_{K\Delta,K'\Delta'} - (A-1)\sum_e e \sum_{((el)_{-1},lsj)J''T''} \\ &\quad \times \sum_{\overline{\overline{(EK\Delta JT)}}} \langle\overline{\overline{(EK\Delta JT)}};((el)_{-1},elsj)J''T''|EK\Delta JT\rangle \\ &\quad \times\langle\overline{\overline{(EK\Delta JT)}};((el)_{-1},elsj)J''T''|EK'\Delta'JT\rangle. \end{aligned} \tag{2.11}$$

The centre-of-mass Hamiltonian matrix is expressible as the spectral decomposition of idempotent matrices $\mathbf{P}_\alpha$ that may be expressed in terms of the original matrix and its eigenvalues

$$\mathbf{P}_\alpha = \prod_{\substack{\beta=1 \\ \beta\neq\alpha}}^{n} \left(\lambda_\beta - \frac{\mathbf{H}_{\text{c.m.}}}{\hbar\omega} \right) / \prod_{\substack{\beta=1 \\ \beta\neq\alpha}}^{n} (\lambda_\beta - \lambda_\alpha) \ . \tag{2.12}$$

Here λ_α denote the distinct eigenvalues of the matrix $\mathbf{H}_{\text{c.m.}}$. The diagonalization of matrices $\mathbf{P}_\alpha$ was performed with `rs()` procedure from EISPAC and obtained eigenvectors are coefficients $a^{EJT}_{K\Delta;00,\Gamma}$.

Finally, we may define the only coefficients needed for calculation of two-particle translationally invariant density matrices (CESOs). CESOs are the coefficients of expansion of the oscillator shell model functions in terms of A-particle oscillator functions with singled-out dependence on intrinsic coordinates of two last particles and with eliminated spurious states

$$\begin{aligned} &\langle \overline{\overline{(EK\Delta JT)}}, ((el)_{-1}, elsj) J''T'' || E\Gamma JT \rangle \\ &\quad = \sum_{K\Delta} \langle \overline{\overline{(EK\Delta JT)}}, ((el)_{-1}, elsj) J''T'' || EK\Delta JT \rangle a^{EJT}_{K\Delta;00,\Gamma}. \end{aligned} \tag{2.13}$$

The two-particle translationally invariant density matrices may be expressed in terms of CESOs

$$\begin{aligned} W^{EJT;\Gamma\Gamma'}_{sjT'';el,e'l'} = \sum_{\overline{\overline{(EK\Delta JT)}},(el)_{-1},J''} & \langle \overline{\overline{(EK\Delta JT)}}, ((el)_{-1}, elsj) J''T'' || E\Gamma JT \rangle \\ \times \langle \overline{\overline{(EK\Delta JT)}}, & ((el)_{-1}, e'l'sj) J''T'' || E\Gamma' JT \rangle. \end{aligned} \tag{2.14}$$

The two-particle translationally invariant density matrices satisfies the usual normalization relation which may be used for the evaluation of the accuracy of the calculations

$$\sum_{elsjT''} W^{EJT;\Gamma\Gamma'}_{sjT'';el,el} = \delta_{\Gamma,\Gamma'}. \tag{2.15}$$

3. Calculations and Results

The procedures for calculation of two-particle translationally invariant density matrices were implemented in computer code. The theoretical formulation have been illustrated by calculation of translationally invariant density matrices for $E_x = 0, 1, 2, 3, 4$ excitations in the case of $A = 6$ and $JT = 21$ nucleus. The efficiency of the proposed procedures was tested on Pentium 3 GHz PC with 1 GB RAM. The FORTRAN90 program for two-particle translationally invariant density matrices calculation were run on *Fortran PowerStation 4.0*. The computational results are presented in Table 1. The columns of the table are: E_x is the number of excitation quanta; #SCFP is the number of SCFPs; d_H is the dimension of centre-of-mass Hamiltonian matrix; r_P is the rank of $\mathbf{P}_\alpha$ matrix ($\lambda_\alpha = 3/2$); #a is the number of $a^{EJT}_{K\Delta;00,\Gamma}$ coefficients; #CESO is the number of CESOs; #DM is the number of two-particle translationally invariant density matrices; d_W is the dimension two-particle translationally invariant density matrices; *accuracy* is the accuracy of two-particle translationally invariant density matrices computation.

The obtained density matrices may be used for approximate analysis of the light nuclei spectrum in the framework of reduced Hamiltonian method [2]. In this method the binding energies of the ground and excited states of the atomic nucleus may be expressed in terms of the NN-potential characteristics, given by the corresponding reduced Hamiltonian operator

$$E_\Lambda = \sum_i \varepsilon_i \omega_{i,\Lambda}, \tag{3.16}$$

Table 1. The $A = 6$, $JT = 21$ calculation data of two-particle translationally invariant density matrices for up to 4 $\hbar\omega$ excitation quanta.

E_x	#SCFP	d_H	r_p	$\#a$	#CESO	#DM	d_W	*accuracy*
0	68	–	–	–	104	7	2	3.55E-15
1	2286	18	15	270	6840	14	15	5.77E-15
2	38860	116	72	8352	178560	21	72	9.10E-15
3	361355	507	260	131820	2621060	31	260	1.88E-14
4	2831348	1869	789	1474641	27324648	40	789	4.24E-14

here the set of quantum numbers Λ defnes the nuclear state under investigation, ε_i is the eigenvalue of the reduced Hamiltonian operator in the two nucleon channel i, and $\omega_{i,\Lambda}$ is the diagonal element of the exact realistic density matrix.

The major role in the stability of light atomic nuclei play the two nucleon channel ${}^3S_1 - {}^3D_1$. According to the reduced Hamiltonian method, the ${}^3D_1$ state admixture to the ${}^3S_1$ state should be maximized in the expansion of the exact realistic density matrices $\omega_{i,\Lambda}$ in terms of the model density matrices. We will use the obtained two-particle translationally invariant density matrices as the model density matrices.

Let us start from the $A = 6$ case. In zero approximation ($E_x = 0$) the diagonal entries of the calculated density matrices for the six nucleon system have some admixture of ${}^3D_1$ state only in the three $J^\Pi T = 1^+0$ states. At first glance it looks like the obtained results suggests that the first three states in the ^{6}Li nucleus should be the $J^\Pi T = 1^+0$ states. After the diagonalization of the ${}^3D_1$ density matrix only one of its diagonal entries becomes nonzero value. So, only one state of the six nucleon system acquire the nonzero ${}^3D_1$ state admixture in the two-nucleon reduced Hamiltonian channel and, as consequence, this state should be the most bound one. In the $A = 6$ case there exists only one stable state – the ground state of the ^{6}Li nucleus. We obtain the good agreement between theoretical and experimental results in this case. The excited states of the $A = 6$ acquire the nonzero ${}^3D_1$ state admixture only for higher $E_x > 0$ excitations. However, in this case the sequence of $A = 6$ $J^\Pi T$ energy levels do not follow to the sequence of maximal values of diagonal elements of the calculated density matrices after the diagonalization. This may be explained by peculiarities of the realistic NN-potential and values of the reduced Hamiltonian operator ε_i.

In the $A = 8$ case the computational results of ${}^3D_1$ translationally invariant density matrices for zero excitation ($E_x = 0$) are presented in Table 2. The columns of the table are: $J^\Pi T$ are the total angular momentum, parity and isospin of the eight nucleon system; #DM is the total number of two-particle translationally invariant density matrices; d_W is the dimension of the ${}^3D_1$ density matrices; #N is the number of nonzero diagonal entries of the ${}^3D_1$ density matrix after its diagonalization; $W_{j,j}$ is the largest diagonal entry of of the ${}^3D_1$ density matrix after its diagonalization. $W_{j,j}$ entry have the largest value for the 0^+0 isobars state. This is in the full agreement with experimental results – the ground (stable) state of the ^{8}Be nucleus. The sequence of excited states of the ^{8}Be: 2^+0 and 4^+0 correspond to the sequence of maximal values of diagonal elements of the calculated ${}^3D_1$ density matrices after the diagonalization. It should be pointed, that computation results for 2^+1 state do not fit the experimental data and can't be explained in the zero approximation. The sequence of excited states of the ^{8}Li: 1^+1 and 3^+1 correspond to the sequence of calculated diagonal entries ${}^3D_1$ density matrices after their diagonalization. In the case of 0^+2 there is no ${}^3D_1$ density matrix. So, this state is unbound comparing with the isobars states which

have the $^3D_1$ two-particle state. That $J^\Pi T$ values correspond to the high lying ground states 0^+2 of ^{8}He and ^{8}C in full agreement with experimental situation.

Table 2. The $A = 6$ calculation data of two-particle translationally invariant density matrices in zero approximation ($E_x = 0$).

$J^\Pi T$	#DM	d_W	#N	$W_{j,j}$
0^+0	12	5	3	4.21E-2
2^+0	12	8	5	2.85E-2
4^+0	11	3	1	1.46E-2
2^+1	12	7	3	2.29E-2
1^+1	12	8	5	2.61E-2
3^+1	12	5	2	1.59E-2
0^+2	–	–	–	–

4. Conclusions

The presented formalism consistently lines the principles of antisymmetrization and translational invariance and is implicitly based on the reduced Hamiltonian method [2]. The proposed density matrices are very suitable for exact realistic density matrix expansion, since they allow one to avoid using realistic spectator functions for description of the subsystem of the rest $A - 2$ particles. Moreover, the translationally invariant density matrices may be calculated in an antisymmetric but not translationally invariant CESOs basis, so the sophisticated calculation of translationally invariant coefficients of fractional parentage may be completely avoided.

A distinct feature of this formalism is in the complete rejection of group-theoretical classification of antisymmetric many-particle states. This is a remarkable circumstance, because a benefit could be gained due to simplicity and comprehensibility of such kind of calculations. It should be noted that as is common in the *ab initio* shell-model calculations the density matrices calculation time grows exponentially with the number of nucleons and the excitation energy. However due to the simplified method for enumeration of A-particle states the effective classification procedures of A-particle states may be applied and computation of density matrices may be efficiently managed.

The new computer code proves to be quick, efficient, numerically stable, and produces results possessing only small numerical uncertainties. The efficiency of the proposed procedure was illustrated by calculation of two-particle translationally invariant density matrices in a complete basis $(0 - 4)\hbar\omega$ for $A = 6$ and $JT = 21$. The accuracy of calculated two-particle translationally invariant density matrices is extremely high ($< 10^{-12}$ in tested cases). At the same time the dimensions of matrices involved (centre-of-mass Hamiltonian) are very low. The presented in the Table 1 results clearly show that approach based on density matrices may considerably reduce the memory demand on the storage of the shell-model calculations results. The dimensions of two-particle translationally invariant density matrices are very low. Moreover, since the symmetric nature of the density matrices only their upper triangle should be stored. This number of quantities is considerably less than the corresponding number of CESOs. The obtained result indicates that the two-particle translationally invariant density matrices may be may be stored, transferred and used for calculation of expectation values of two-particle nuclear shell-model operators within the isospin formalism much more easily than the coefficients of fractional parentage.

The analysis of the level structures of $A = 6$ and $A = 8$ isobars imply that the calculated density matrices may be successfuly used for exact realistic density matrix expansion.

REFERENCES

[1] Navratil P. et al The reduced hamiltonian method in the theory of the identical particles systems bound states // 2009 J. Phys. G: Nucl. Part. Phys. 36 083101

[2] Kamuntavicius G.P. The reduced Hamiltonian method in the identical particle systems bound state theory // 1989 Sov. J. Part. Nuclei V.20, No. 2, 261-292.

[3] Coleman A.J. Structure of Fermion density matrices // Rev. Mod. Phys. 1963. V.35, No. 3, p. 668-689.

[4] Deveikis A., Kamuntavicius G.P. Intrinsic density matrices of the nuclear shell model // Lithuanian Phys. J. 1996. V.36, No. 2, P. 83-95.

[5] Deveikis A., Kamuntavicius G.P. Elimination of spurious states of oscillator shell model // Lithuanian Phys. J. 1997. V.37, No. 5, P. 371-383.

[6] Deveikis A. A program for generating one-particle and two-particle coefficients of fractional parentage for the single j-orbit with isospin // Comp. Phys. Comm. 2005, V.173, Iss.3, p. 186-192.

[7] Deveikis A., Juodagalvis A. A computer program for two-particle generalized coefficients of fractional parentage // Comp. Phys. Comm. 2008. V.179, Iss.8, p. 607-613.

I. Filikhin, S.G. Matinyan, and B. Vlahovic

Department of Physics,
North Carolina Central University,
1801 Fayetteville Street, Durham, NC 27707, USA
Phone: 1(919) 530 6645, Fax: 1(919) 530 7472*

Electron trapping in weakly coupled concentric quantum rings

We investigate the electron localization in double concentric quantum rings (DCQRs) when a perpendicular magnetic field is applied. In weakly coupled DCQRs, the situation can occur when the single electron energy levels associated with different rings may be crossed. To avoid degeneracy, the anti-crossing of these levels has a place. We show that in this DCQR the electron spatial transition between the rings occurs due to the electron level anti-crossing. The anti-crossing of the levels with different radial quantum numbers (and equal orbital quantum numbers) provides the conditions for electron tunneling between rings. To study electronic structure of the semiconductor DCQR, the single sub-band effective mass approach with energy dependence was used. Results of numerical simulation for the electron transition are presented for DCQRs of geometry related to one fabricated in experiment.

Keywords: quantum dots, single electron levels, single-electron tunneling
PACS 73.21.La, 73.22.Dj, 85.35.G

1. Introduction

Quantum Rings (QR) are remarkable meso- and nanostructures due to their non-simply connected topology and attracted much attention last decade. This interest supported essentially by the progress in the fabrication of the structures with wide range of geometries including single and double rings [1-5]. This interest rouse tremendously in the connection to the problem of the persistent current in mesoscopic rings [6].Transition from meso - to nano -scale makes more favorable the coherence conditions and permit to reduce the problem to the few or even to single electron.

Application of the transverse magnetic field B leads to the novel effects: Whereas the quantum dots (QDs) of the corresponding shape (circular for two dimensional (2D), cylindrical or spherical for 3D) has degeneracy in the radial n and orbital l quantum numbers, QR due to the double connectedness in the absence of the magnetic field B has degeneracy only in l, and the nonzero B lifts the degeneracy in l, thus making possible the energy level crossing at some value of B [7], potentially providing the single electron transition from one state to the another.

Use the configurations with double concentric QR (DCQR) reveals a new pattern: one can observe the transition between different rings in analogy with atomic phenomena. For the DCQR, the 3D treatment is especially important when one includes the inter ring coupling due to the tunneling. The dependence on the geometries of the rings (size, shape and etc.) [7, 8] becomes essential.

In the light of above mentioned, it is not surprising that numerous papers were devoted in the recent years to the different aspects of DCQR [9-12].

*E-mail: ifilikhin@nccu.edu

In the present paper, we visualize interesting features occurring in DCQR composed of GaAs in an $Al_{0.70}Ga_{0.30}As$ substrate [4] and the electron transition between rings under influence of the transverse magnetic field B. Therefore, we concentrate here, in contrast with some previous related papers, to the electron spatial transition between inner and outer rings of DCQR which is accompanied by energy levels transition with different radial quantum numbers n. The present work is close, in essence, to Ref. [12] where the effect of a magnetic field on the energy levels of electron and holes for cylindrical shaped DCQR was determined for fixed size and for radial quantum number n=1,2, with orbital quantum number $|l|$changing from 1 to 4.

We will see that the spatial transition of electrons in DCQR between rings occur due to the level anti-crossing providing the conditions for tunneling between rings. In this study we use realistic confining potentials including ones motivated by the experimental fabrication of QRs [4]. Due to the small sizes of the considering DCQRs, we use approximation in which the non-parabolicity of the conduction band is taken into account. That results a shift energy levels and increases the electron effective mass from the bulk value. Proposed model reproduces the observed PL data [4] including levels with different radial quantum numbers. We show principal possibility for the electron trapping in inner ring (or dot) of DCQR which may have application in quantum computing.

2. Model

The GaAs DCQRs rings, embedded into the $Al_{0.70}Ga_{0.30}As$ substrate, are considered. We use the single sub-band approach, what is justified due to the relatively large band gap of GaAs. The problem can be expressed by the following Schrödinger equation

$$\left(\hat{H}_{kp} + V_c\left(r\right)\right)\Psi\left(r\right) = E\Psi\left(r\right). \tag{2.1}$$

Here $\hat{H}_{kp}$ is the single band ***kp***-Hamiltonian operator $\hat{H}_{kp} = -\nabla\frac{\hbar^2}{2m(r,E)^*}\nabla$, $m^*\left(r,E\right)$ is the electron effective mass, and $V_c\left(r\right)$ is the band gap potential, $V_c\left(r\right) = 0$ inside the QR and is equal to E_c outside the QR, where E_c is defined by the conduction band offset for the bulk. The Ben-Daniel-Duke boundary conditions are used on interface of the material of QR and substrate. This consideration was restricted by the electron and heavy hole carriers, and the Coulomb interaction was excluded. In order to account for the non-parabolic effect, the energy dependence of the carrier effective mass is introduced: $m^*/m_0 = f\left(E,r\right)$, where m_0 is the free electron mass, and$f\left(E,r\right)$ is a function of confinement energy [8,13-15]. This function is described by Kane formula [16]. We used the linear dependence of the electron effective mass on energy. The effective mass in QR varies between the bulk values for effective mass of the QR and substrate materials and the energy is rearranged by the quantum well depth.

The Schrödinger equation (2.1) with the energy dependence of effective mass is solved by the iteration procedure. For each step of the iterations the equation (2.1) is reduced to Schrödinger equation with the effective mass of the current step which does not depend on energy. Obtained eigenvalue problem is solved numerically by the finite element method. After that, a new value for effective mass is taken by using $f\left(E,r\right)$ and procedure is repeated. The convergence of the effective mass during the procedure has a place after 3-5 steps.

For each step of the procedure the Schrödinger equation (2.1) is written in cylindrical coordinates, with constant magnetic field in the z direction ($B = B\hat{z}$), as follows:

$$\begin{aligned} &-\frac{\hbar^2}{2}\left(\frac{\partial}{\partial\rho}\left(\frac{1}{m^*}\frac{\partial\Phi_{n,l}}{\partial\rho}\right) + \frac{1}{m^*\rho}\frac{\partial\Phi_{n,l}}{\partial\rho} - \frac{l^2}{m^*\rho^2}\Phi_{n,l}\right) + \\ &+\frac{\hbar l\omega_c}{2}\Phi_{n,l} + \frac{m^*\omega_c^2\rho^2}{8}\Phi_{n,l} + \left[V_c\left(\rho,z\right) - E\right]\Phi_{n,l} - \frac{\hbar^2}{2m^*}\frac{\partial^2\Phi_{n,l}}{\partial z^2} = 0, \end{aligned} \tag{2.2}$$

$\Psi_{n,l}(\rho,z,\varphi)=\Phi_{n,l}(\rho,z)\,e^{il\varphi}$, where $n=1,2,\ldots$ are radial and $l=\pm0,\pm1,...$ are orbital quantum numbers. $\omega_c=|e|B/m^*$ is the cyclotron frequency. First magnetic field term in (2.2) is orbital Zeeman term, the second - diamagnetic term. The electron spin Zeeman effect has been ignored here since it is small.

The values m*=0.067m_0 and 0.093m_0 is used for the bulk values of the electron effective masses in the materials of DCQR and substrate respectively. The effective mass of DCQR differs from the bulk value, and this difference is defined by energy of the electron in the considered state. The confinement potential $V_c(r)$ is zero in the rings and 0.262 eV in the substrate [4]. The contribution of strain was ignored in this paper because the lattice mismatch between the rings and the substrate is small. For the effective mass of heavy hole we used the value of 0.51m_0 in GaAs and 0.57m_0 in $Al_{0.70}Ga_{0.30}As$. The confinement potential $V_c(r)$has the value of 0.195 eV [4].

There is a problem of notation for states for DCQR. If we consider single QR (SQR) then for each value of the orbital quantum number $|l|=0,1,2,...$ in Eq. (2.2) we can definite radial quantum number $n=1,2,3,....$corresponding to the numbers of the eigenvalues of the problem (2.2) in order of increasing. One can organize the spectrum by sub-bands defined by different n. When we consider the weakly coupled DCQR, in contrast of SQR, the number of these sub-bands is doubled due to known splitting the spectrum of double quantum object [17]. Electron in the weakly coupled DCQR can be localized in the inner or outer ring. In principle, in this two rings problem one should introduce a pair of separate sets of quantum numbers (n_i,l) where index $i=1,2$ denoted the rings where electron is localized. However, it is more convenient, due to the symmetry of the problem , to have one pair (n,l) numbers ascribed to the different rings (inner or outer), in other words, we use a set of quantum numbers (n,l),p where p is dichotomic parameter attributed to the electron localization (“inner“ or “outer“).

Since we are interested here in the electron transition between rings and, as we will see below, this transition can occur due to the electron levels anti-crossing followed a tunneling, we concentrate on the changing of the quantum numbers n. The anti-crossing is accompanied by changing the quantum numbers n and p of the $(n,l),p$ set.

3. Experimentally fabricated DCQR

The GaAs QRs and DQRs rings, embedded into the $Al_{0.70}Ga_{0.30}As$ substrate, are considered. We use the geometry of the DCQR which are close to one proposed in [4]. The DCQR cross section is presented in Fig. 1a. Since a profile of the quantum dots in [4] was not explicitly given, this geometry slightly differs from original one used in [4]. However our calculations for the electron energy with this geometry lead to similar results as it was obtained in [4]. To compare with results of [4], we neglected the non-parabolic effect, discussed above, and use the effective masses of the carriers, and the confinement potentials, as in [4]: m^*_{GaAs}/m^*_{AlGaAs}=0.067/0.093, E_c=262 meV for the electron, and m^*_{GaAs}/m^*_{AlGaAs}=0.51/0.57, E_c=195 meV the for heavy hole.

An interesting problem related to the GaAs self-assembled structures deals with the increase of the electron effective mass of QD, QR and DQR, respectively. The non-parabolic effect leads to a change in the effective mass of the carriers in quantum nanosize objects [1,13]. The initial GaAs QDs are quite large in size [4]; therefore for the QD this effect is minimal. The effective electron mass of the QD is practically equal to a bulk mass of the GaAs. It should be noted that the fabrication of DCQRs is accompanied by decreasing of the object size in one or two directions. Taking the energy dependence of the electron effective mass into account, we calculated the effective masses of the DCQR. The results of the calculations are shown in Fig. 1b, where a simple energy dependence of the effective mass (function $f(E,r)$ in Eq.(2.1)) is represented as a linear function connecting the points corresponding to the bulk values of the effective mass in GaAs and AlGaAs

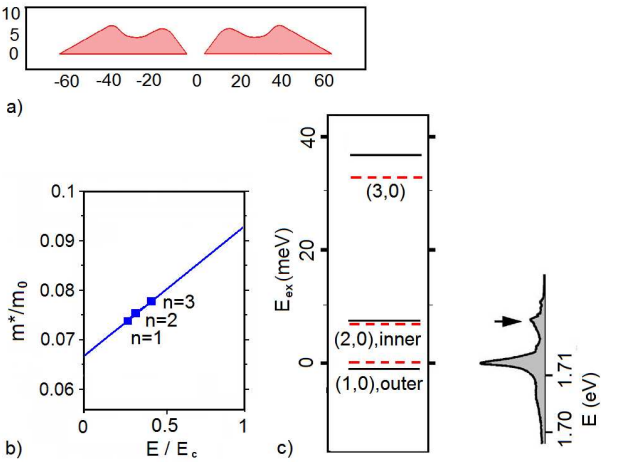

Fig. 1. a) Cross section of DCQR. The sizes are given in nm. b) The effective mass and energy of electron in the states $n = 1, 2, 3$ $(l = 0)$ c) The optical transmission spectrum and experimental data from [4]. The solid lines are results of calculation [4]; dashed lines are results of the present work. The arrow shows the (2,0) pick of the PL transition relative the (1,0) exciton energy.

materials, respectively. We obtained for the electron effective mass of the ground state the value of $0.074m_0$, which is slightly larger than the bulk value of $0.067m_0$. For the excited states, the effective mass will increase with respect to the bulk value of the AlGaAs substrate. In Fig. 1c the few energy peaks of the optical transmission spectrum are shown along the experimental data [4] and calculated results. One can see that our calculated levels are shifted relative the results of [4] due the non-parabolic effect. The effect can be neglected for first two levels, but for higher levels it becomes to be important. The experimental peaks are well reproduced by our calculations.

4. Electron transfer between rings of DCQR in magnetic field

Electron transfer in the DCQR considered is induced by external factor like a magnetic or electric fields. Probability for this transfer strongly depends on the geometry of DCQR. The geometry has to allow the existing the weakly coupled electron states. To explain it, we note that DCQR can be described as a system of double quantum well. It means that there is splitting of energy spectrum on two sub-bands [17,18] relative the one for single quantum object. In the case non interacting wells (no electron tunneling between wells) the each sub-band is related with left or right quantum well. The wave function of the electron is localized in the left or right quantum well. When the tunneling is possible (strong coupling state of the system), the wave function is spread out over whole volume of the system. In a magnetic field, it is allowed an intermediate situation (weak coupled states) when the tunneling is possible due to anti-crossing of the levels.

Strongly localized states exist in the DCQR with the geometry motivated by the fabricated DCQR in Ref. [4]. The wave functions of the two s-states of the single electron with $n = 1, 2$ are shown in Fig. 2, where the electron state $n = 1$ is localized in outer ring, and the electron state$n = 2$ is localized in inner ring. Moreover all states of the sub-bands with $n = 1, 2$, and $|l| = 1, 2, 3, \ldots$, are well localized in the DCQR. The electron localization is in outer ring for $n = 1$, $|l| = 0, 1, 2...$, and in inner ring for $n = 2$, $|l| = 0, 1, 2....$ It is shown in Fig. 3 for several

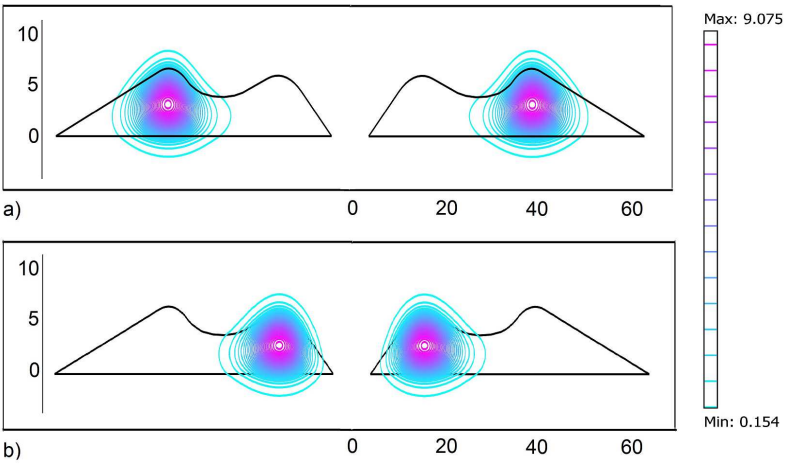

Fig. 2. The squares of wave functions for the a)$(1,0)$,outer ($E = 0.072$ eV) and b)$(2,0)$,inner ($E = 0.080$ eV) states are shown by contour plots. The contour of the DCQR cross-section is given. The sizes are in nm.

low-lying electron levels. The difference between spectra of the two sub-bands presented Fig. 3 can be explained by competition of two terms of the Hamiltonian of Eq. (2.2) and geometry factor. The first term includes first derivative of wave function over ρ in kinetic energy; the second is the centrifugal term. For $|l| \neq 0$ the centrifugal force pushes the electron into outer ring. One can see that the density of the levels is higher in the outer ring. Obviously, the geometry plays a role also. In particular, one can regulate density of levels of the rings by changing a ratio of the lateral sizes of the rings.

Summarizing, one can say that for B=0 the well separated states are only the states $(1,l),p$ and $(2,l),p$. Thus, used notation is proper only for these states. The wave functions of the rest states $(n > 2,l)$ are distributed between inner and outer rings. These states are strongly coupled states. In Ref. [12] the $(2,l),p$ and $(1,l),p$ states are denoted as the L and H states, respectively. We have to note that difference of the both descriptions is in that the notation [12] does not describe the position change of the electron in the states $(2,l),p$ or $(1,l),p$ under increasing magnetic field.

Crossing of electron levels in the magnetic field B are presented in Fig. 4. There are crossings of the levels without electron transfer between the rings. This situation is like when we have crossing levels of two independent rings. There are two crossings when the orbital quantum number is changed due to the Aharonov-Bohm (AB) effect. It occurs at about 0.42 T and 2.5 T. There are two anti-crossings: the first is at 4.8 T, another is at 5.2 T. These anti-crossings are for the states with different n; the first are states (1,0) and (2,0) and the second are states (1,-1) and (2,-1). In these anti-crossings the possibility for electron tunneling between rings are realized. In Fig. 5 we show how the root mean square (rms) of the electron radius is changed due to the tunneling at anti-crossing. One can conclude from Fig. 4–5 that the electron transition between rings is only possible when the anti-crossed levels have different radial quantum numbers and equal orbital quantum numbers. Transformation of the profile of the electron wave function during the process of anti-crossing with increasing B is given in Fig. 6. The electron state $(1,-1)$,outer is considered as "initial" state of an electron ($B = 0$). The electron is localized in outer ring. Rms radius is calculated to be R=39.6 nm. For $B = 5.2$ T, the second state is the tunneling state corresponding

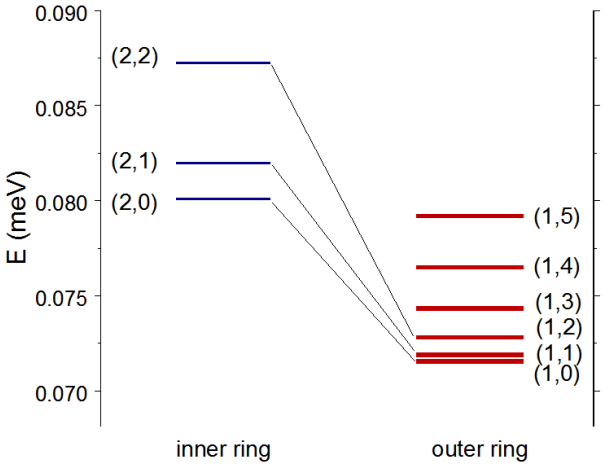

Fig. 3. Electron energy$E$ and position of single electron in DCQR for the states with $n = 1, 2$,$l = = 0, 1, 2, ...5$. The quantum number each state is shown. Fine lines connect the upper and lower members of the "doublets" $((n = 1, 2), l)$, for $l = 0, 1, 2$. Energy is measured from bottom edge of conduction bands alignment.

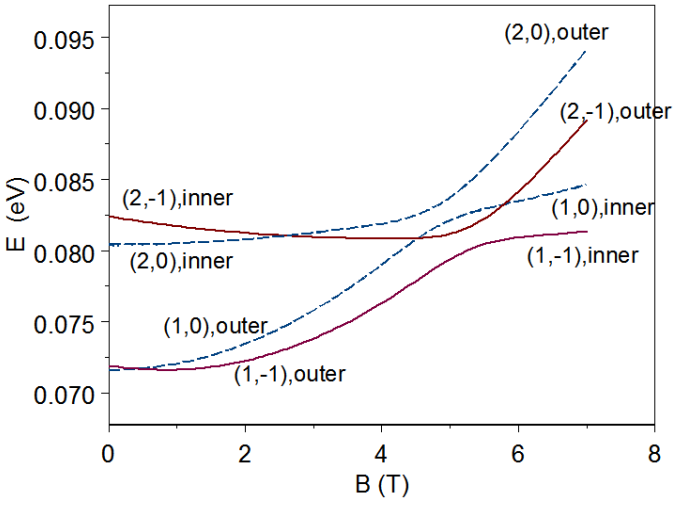

Fig. 4. Single electron energies of DCQR as a function of magnetic field magnitude B. Notation for the curves: the double dashed (solid) lines mean states with $l = 0$ ($l = -1$) with $n = 1, 2$. The quantum numbers of the states and positions of the electron in DCQR are shown.

to the anti-crossing with the state (0,-1). The wave function is spreading out in both rings with $R = 32.7$ nm. The parameter p has no definite value for this state. The "final" state is considered at $B = 7$ T. In this state the electron localized in inner ring with $R = 17.6$ nm. Consequently connecting these three states of the electron, we come to an electron trapping, when the electron

of outer ring ("initial" state) is transferred to the inner ring ("final" state). The transfer process is governed by the magnetic field.

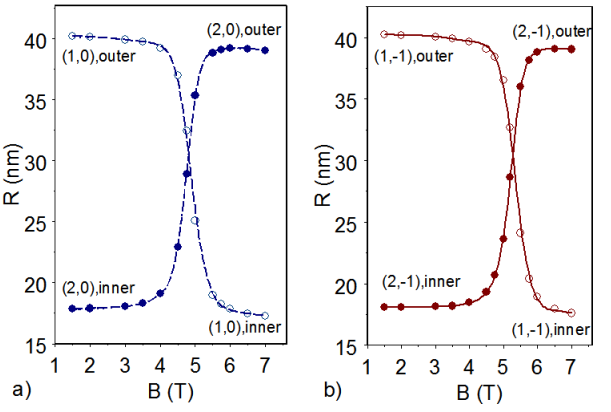

Fig. 5. Rms radius of an electron in DCQR as a function of magnetic field for the states a) $((n = 1, 2), l = 0)$ and b) $((n = 1, 2), l = -1)$ near point of the anti-crossing. The calculated values are shown by solid and open circles. The dashed (solid) line, associated with states of $l = 0$ ($l = -1$), fits the calculated points.

In the case of planar QRs ($H \ll R$) the relationship between the energy and the magnetic flux Φ can approximately be described by the following relation for the ideal quantum ring of radius R in a perpendicular magnetic field B: $E_p(l) = \hbar^2/(2m * R_p^2)(l + \Phi/\Phi_0)^2$, where $\Phi = \pi R^2 B$, $\Phi_0 = h/e$, and p means inner or outer ring, $\Phi_0 = 4135.7$ T nm2. It is clear that this relation leads to the periodic oscillations of the energy with the AB period $\Delta B = \Phi_0/\pi R^2$. Using rms radius as R, one can obtain for the inner ring $\Delta B/2 = 2.1$ T, for the outer ring $\Delta B/2$=0.42 T. The R are 17.7 nm and 39.6 nm, respectively. The obtained values for $\Delta B/2$ corresponding to the level crossing $(n, 0)$ and $(n, -1)$, where $n = 2, 1$, shown in Fig. 4, about at 2.5 T and 0.42 T, respectively. Thus, this rough estimation qualitatively reproduces the results for the AB period presented in the Fig. 4.

Note that the energy gap between anti-crossed levels, which one can see in Fig. 4, can be explained by the general theory for double interacting quantum well (see [18], for instance). The value of the gap depends on separation distance between the rings, governed by the overlapping wave functions corresponding to the each ring, and their spatial spread which mainly depends on radial quantum number of the states.

Other interesting quantum system is the system representing as QR with QD located in the center of the QR. The cross section of the system is given in Fig. 7a. In Fig. 7b we present the results of calculations for electron energies of the (1,0) and (3,0) states in the magnetic field B (see [19], also). Once more, we can see the situation of the level anti-crossing for about of 12.5 T. This anti-crossing is accompanied by exchange of electron localization between the QD and the QR. It means that if initial state (for $B < 12.5$ T) of electron was the state (1,0),outer, then the "final" state (for $B > 12.5$ T) will be (1,0),inner. The energy of the dot-localized state grows more slowly than the envelope ring-localized state. It is interesting that at the enough large B the dot-localized state becomes the ground state [20] (by choosing appropriate geometry). When the Landau orbit of electron becomes smaller then dot size, electron can enter the dot without an extra increase of kinetic energy. It will be useful variant of trapping of electron in QD for quantum computing.

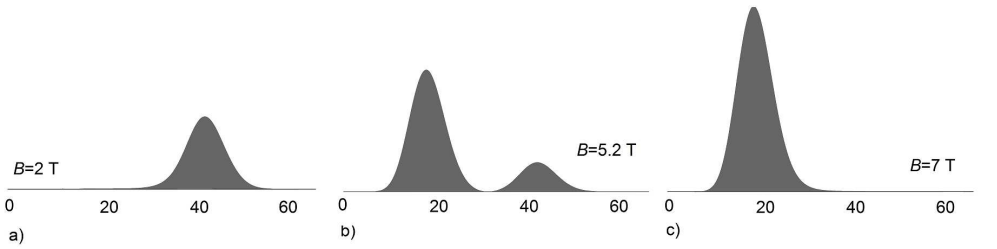

Fig. 6. Profiles of the normalized square wave function of electron in the states a) $(1,-1)$, outer; b) $(1,-1)$,n/a and c) $(1,-1)$, inner for different magnetic field B. a) is the "initial" state ($B=0$) with R=39.6 nm, b) is the state of electron transfer (B=5.2 T) with R=32.7 nm, c) is the "final" state (B=7 T) with R=17.6 nm. The radial coordinate ρ is given in nm (see Fig. 1 for the DCQR cross section).

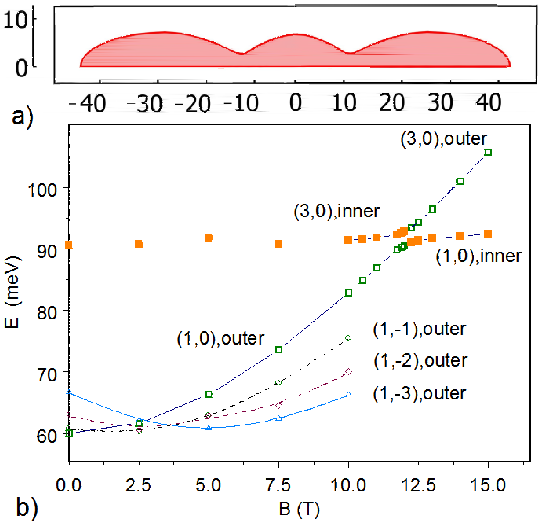

Fig. 7. a) Cross section of the QR with QD system. Sizes are given in nm. b) Energies of the (1,0) and (3,0) states in the magnetic field B for the QR with QD system. The open symbols mean that the electron is localized in the ring. The solid circles mean that the electron localized in QD.

5. Conclusion

Nanosize quantum rings were studied in the single sub-band approach, taking into account the non-parabolicity of the conduction band due to energy dependence of the electron effective mass. Realistic 3D geometry relevant to the experimental DCQR fabrication was considered.

We make visible main properties of this weakly coupled DCQD established by several level anti-crossings that occurred for the states with different radial quantum number ($n=1,2$) and equal orbital quantum number l.

We may conclude that the fate of the single electron in DCQRs is governed by the structure of the energy levels with their crossing and anti-crossing and changing with magnetic field. The above

described behavior is the result of the nontrivial excitation characteristic of the DCQRs. Effect of the trapping of electron in inner QR (QD) of DCQR may be interesting from the point of view of quantum computing.

Acknowledgements

This work is supported by the NSF (HRD-0833184) and NASA (NNX09AV07A).

References

[1] A. Lorke and R.J. Luyken, Physica (Amsterdam) 256B, 424 (1998); A. Lorke, R.J. Luyken, A.O. Govorov, J.P. Kotthaus, J.M. Garcia and P.M. Petroff, Phys. Rev. Lett. 84, 2223 (2000).

[2] A. Fuhrer, S. Locher, T. Ihn, T. Heinzel, K. Ensslin, W. Wegscheider, M. Bichle, Nature 413, 822 (2001).

[3] U. F. Keyser, S Borck, R J Haug, M Bichler, G Abstreiter and W Wegscheider, Semicond. Sci. Technol. 17, L22 (2002).

[4] T. Mano, T. Kuroda, S. Sanguinetti, T. Ochiai, T. Tateno, J. Kim, T. Noda, M. Kawabe, K. Sakoda, G. Kido, and N. Koguchi, Nano Letters 5, 425 (2005); T. Kuroda, T. Mano, T. Ochiai, S. Sanguinetti, K. Sakoda, G. Kido and N. Koguchi, Phys. Rev. B 72, 205301 (2005).

[5] M. Abbarchi, T. Kuroda, T. Mano, K. Sakoda, G. Gurioli, Phys. Rev. B 81 035334 (2010).

[6] M. Buttiker, Y. Imry and R. Landauer, Phys. Lett. A 96, 365 (1983).

[7] A.G. Aronov and Yu.V. Sharvin, Rev. Mod. Phys. 59, 755 (1987); T. Chakraborty and P. Pietilainen, Phys. Rev. B 50, 8460 (1994); B.C. Lee, O. Voskoboynikov and C.P. Lee, Physica E 24, 87 (2004); J. Simonin, C.R. Proetto, Z. Barticevic, and G. Fuster, Phys. Rev. B 70, 205305 (2004); J. I. Climente, J. Planelles, M. Barranco, F. Malet, and M. Pi, Phys. Rev. B 73, 235327 (2006.)

[8] O. Voskoboynikov, Y. Li, H. M. Lu, C.F. Shih, and C.P. Lee, Phys. Rev. B 66, 155306 (2002); Y. Li, H.M. Lu, O. Voskoboynikov, C.P. Lee and S.M. Sze. Surf. Sci. 532, 811 (2003); J. Cui, et al. Appl. Phys. Lett. 83, 2907 (2003).

[9] B. Szafran and F.M. Peeters, Phys. Rev. B *72*, 155316 (2005).

[10] M. Bayer, M. Korkusinski, P. Hawrylak, T. Gutbrod, M. Michel, A. Forchel, Phys. Rev. Lett. 90, 186801 (2003.)

[11] J.-L. Zhu, S. Hu, Zh. Dai, and X. Hu, Phys. Rev. B 72 (2005) 075411; Guang-Yin Chena, Yueh-Nan Chen, and Der-San Chuu, Solid State Communications 143, 515 (2007); B. Szafran, Phys. Rev. B 77, 205313 (2008); S. Sanguinetti, M. Abbarchi, A. Vinattieri, M. Zamfirescu, and M. Gurioli, T. Mano, T. Kuroda, and N. Koguchi, Phys. Rev. B 77, 125404 (2008).

[12] V. Arsoski, M. Tadic and F.M. Peeters, Acta Physica Polonica 117, 733 (2010).

[13] C. Wetzel, R. Winkler, M. Drechsler, B.K. Meyer, U. Russler, J. Scriba, J.P. Kotthaus, V. Hurle, F. Scholz, Phys. Rev. B 53, 1038 (1996).

[14] J. L. Climente and J. Planells, Phys. Rev. B 68 (2003) 075307; J. L. Climente, J. Planells, F. Rajadell, J. Phys.: Condens. Matter 17, 1573 (2005).

[15] I. Filikhin, V.M. Suslov and B. Vlahovic, Phys. Rev. B 73, 205332 (2006).

[16] E. Kane, J. Phys. Chem. Solids 1, 249 (1957).

[17] G. Bastard, Wave Mechanics Applied to Semiconductor Heterostructures, Halsted Press (1988).

[18] O. Manasreh, Semiconductor Heterojunctions and Nanostructures, McGraw-Hill (2005) pp. 78-80.

[19] I. Filikhin, S. Matinyan, J. Nimmo, B. Vlahovic, Physica E: Low-dimensional Systems and Nanostructures, 43, 1669 (2011).

[20] B. Szafran, F. M. Peeters, and S. Bednarek, Phys. Rev. B 70 205318 (2004).

V.A. Harutyunyan, M. Mkrtchyan
Physics Department, State Engineering University of Armenia, Gyumri Branch, 3103 Gymri, Armenia*

Semiconductor quantum ring in strong lateral electrostatic field

The specificity of single-particle and electron-hole pair's states in semiconductor quantum ring in the presence of strong external homogeneous electrostatic field is examined theoretically. The finiteness of the ring thickness in both radial and perpendicular to the radial plane direction is taken into account. The analytic form of wave functions and results of numerical calculations for the energy spectrum of interacting electron-hole pair in the ring in the presence of external field are presented. The relevant characteristics for interband electro-optical transitions in the ring are calculated analytically also. It is shown that absorption intensities and threshold frequencies of interband electro-optical transitions depend explicitly on geometrical sizes of sample, on intensities of external field, and on effective masses of charge carriers.

Keywords: nanoring, homogeneous field, electroabsorption.
PACS numbers: 78.67.-n, 78.67.Ch, 78.20.Jq

1. Introduction

During the last decades electronic and optical properties of low-dimensional semiconductor structures have been studied both experimentally and theoretically. Along with long-known systems like quantum wells (quantum films), quantum wires, quantum dots and superlattices, the novel confined structures called quantum rings (QRs) attract much attention [1–4]. It is common knowledge that the electronic, optical and kinetic properties of low-dimensional structures such as semiconductor quantum rings (SQR's) are strongly affected by the external static electric fields. Investigations of optical properties of these nanostructures and external electric fields' effects are one of the important foundations for further exploration of potential applications of such nanostructures in nanoelectrononic and optoelectronic devices. In Ref. [5] the electronic states of a semiconductor quantum ring under an applied lateral electric field are theoretically investigated and the direct optical absorption are reported as a function of the electric field. The effects of an external electric field on the electronic and optical spectra of SQR threaded by a magnetic flux have studied in Ref. [6]. The excitonic absorption spectra of nanoring double quantum wells subjected to radial and lateral electric fields are theoretically investigated in Ref. [7]. It was shown also, that the electro-optic excitonic absorption spectra show very different behaviors for different electric-field configurations. The optical Aharonow-Bohm effect for an exciton in SQR in the presence of a perpendicular electric field is studied in Ref. [8]. The electrical tuning of intersubband transitions in SQR was studied in Ref. [9]. It should be noted that the discussion of strong fields' effect on SQRs is interesting in the sense that these fields significantly alter the energy profile of confining potential of nanoheterostructure along the corresponding direction. In this paper the specificity of single-particle states of charge carriers in semiconductor quantum ring in the presence of strong lateral homogeneous electrostatic field, and electrooptical transitions in such structure are examined theoretically. The paper is organized

*E-mail: volhar@mail.ru

as follows. In Sec.II we describe the modeling approaches of the problem. Analytical expressions for wave functions and energy spectrum of single-electron states in QR at the absence of external fields are obtained in that Section also. In Sec.III analytical expressions for the wave functions and energy spectrum of the single-electron states in QR in the presence of external fields are obtained. The analytical expressions for the wave functions and energy spectrum of electron-hole pair in QR in the presence of external fields are obtained in Sec.IV. The results are discussed in Sec.V, and the conclusions are presented in Sec.VI.

2. General assumption and physical model

We present the system under consideration in the form of nanoring-"nanowasher" (Fig.1) with the thickness $L = R_2 - R_1$ and height d.Confining potential of the QR in the absence of external fields is approximated by the infinitely deep rectangular potential wells:

$$U^{(0)}(r,z) = \begin{cases} 0, \ when \ R_1 \leqslant r \leqslant R_2; \ 0 \leqslant z \leqslant d; \\ \infty, \ when \ r < R_1, \ r > R_2; \ z < 0, \ z > d; \end{cases} \tag{2.1}$$

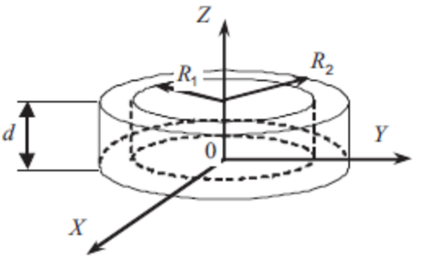

Fig. 1. The geometry of the system

Connecting to the geometrical sizes of the sample we assume that the following conditions take place

$$L, d \ll a_{ex}; \ L, d \ll R_1, \tag{2.2}$$

where a_{ex} is the Bohr radius of a bulk exciton in the SQR's material.

Let us assume now that the external electric field with intensity $\left|\vec{E}\right|$ is directed along the x-axis: $\vec{E} = (E_x, 0, 0)$. By resolving the corresponding placeLaplace equation [10] we obtain the following expression for electrostatic energy $V(r,\varphi)$ of the longitudinal motion of charge carrier within the QR:

$$V(r,\phi) = \left(Br + \frac{C}{r}\right)\cos\phi \equiv V(r)\, F_x \cos\phi \tag{2.3}$$

Here $F_x = eE_x$, and the constants B and C are as follows:

$$B = F_x \frac{2(\varepsilon_{2,1}+1)R_2^2}{(\varepsilon_{2,1}+1)^2 R_2^2 - (\varepsilon_{2,1}-1)^2 R_1^2} \equiv F_x B_0 \tag{2.4}$$

$$C = F_x \frac{2\left(\varepsilon_{2,1}-1\right) R_1^2 R_2^2}{\left(\varepsilon_{2,1}+1\right)^2 R_2^2 - \left(\varepsilon_{2,1}-1\right)^2 R_1^2} \equiv F_x C_0, \tag{2.5}$$

where $\varepsilon_{2,1} = \varepsilon_2/\varepsilon_1$, and $\varepsilon_1, \varepsilon_2$are the static dielectric constants of medium and QR's material, respectively.

3. Single-electron states in the presence of lateral external field

The corresponding Schrodinger equation for the particle's motion in (r,ϕ) plane in isotropic effective mass (μ)approximation has the form

$$-\frac{\hbar^2}{2\mu}\left[\frac{1}{r}\frac{\partial}{\partial r}\left(r\frac{\partial}{\partial r}\right)+\frac{1}{r^2}\frac{\partial^2}{\partial\phi^2}\right]\psi(r,\phi)+V(r,\phi)\psi(r,\phi)=E_{tr}\psi(r,\phi); \tag{3.6}$$

Here E_{tr} is the total energy of transversal motion of particle in (r,ϕ)plane.

Now taking into account the condition (2.3) it is obvious that the functions $1/r^2$ and $Br + C/r$alter comparatively "slowly" in the $[R_1, R_2]$ interval:

$$\left|\frac{R_2^{-2}-R_1^{-2}}{R_1^{-2}}\right| < \frac{L}{R_1}; \quad \left|\frac{V(R_2)-V(R_1)}{V(R_1)}\right| < \frac{L}{R_1}\frac{1}{\varepsilon_{2,1}}; \ (\varepsilon_{2,1}>1)$$

In view of that, it is possible to replace these functions in Eq.(3.6) by their adiabatic average meanings, built on the "non-perturbed" radial functions $\Phi_n^{(0)}(r)$. It allows us to present full wave function $\psi(r,\phi)$ of particle's transversal motion in the following form [11]:

$$\psi(r,\phi)=\Phi_n^{(0)}(r)\,u(\langle r\rangle,\phi); \quad \Phi_n^{(0)}(r)=\sqrt{\frac{2}{L}}\frac{\sin\dfrac{\pi n(r-R_1)}{L}}{\sqrt{r}}; \ n=1,2,\ldots \tag{3.7}$$

After this substitution the radial and angular variables in Eq. (3.6) can be separated and we will come to the following equations by the ϕ- variable:

$$-\frac{\hbar^2}{2\mu}\left\langle\frac{1}{r^2}\right\rangle\frac{\partial^2 u(\phi)}{\partial\phi^2}+\langle V(r)\rangle F_x\cos\phi u(\phi)=E_{ang}u(\phi). \tag{3.8}$$

Here E_{ang} is the particle's energy along the angular motion in the presence of field:$E_{tr} = E_{ang} + E_{rad}$; $E_{rad} = \pi^2\hbar^2 n^2/2\mu L^2$, and E_{rad} is the radial motion's energy. Correspondingly, instead of Eq.(3.9) we can write after averaging:

$$\frac{d^2u(\vartheta)}{d\eta^2}+\frac{8\mu R_n^2}{\hbar^2}E_{ang}u(\vartheta)+\frac{8\mu R_n^2 V_0 F_x}{\hbar^2}u(\vartheta)\cos 2\vartheta=0; \quad \left(\vartheta=\frac{\phi-\pi}{2}\right). \tag{3.9}$$

Here

$$V_0=\langle V(r)\rangle\cong B_0R_1\left(1+\frac{L}{2R_1}\right)+\frac{C_0}{L}\ln\frac{R_2}{R_1};$$

$$R_n^{-2}=\langle r^{-2}\rangle\cong R_1^{-2}\left[1-\frac{L}{R_1}+\frac{L^2}{R_1^2}\left(1-\frac{3}{2\pi^2n^2}\right)\right].$$

If the external field is "strong" enough, i.e. the condition

$$\frac{V_0 F_x}{E_l} \gg 1 \tag{3.10}$$

is fulfilled, we can present $\cos 2\vartheta$ in the following form: $\cos 2\vartheta \cong 1 - 2\vartheta^2$. After that we will come to the following oscillator-type Schrodinger equation:

$$\frac{d^2 u(\vartheta)}{d\eta^2} + \frac{8\mu R_n^2}{\hbar^2}\left(E_{ang} + V_0 F_x\right) u(\vartheta) - \sigma_n^2 \vartheta^2 u(\vartheta) = 0; \quad \sigma_n^2 = \frac{16\mu R_n^2 V_0 F_x}{\hbar^2}. \tag{3.11}$$

For corresponding energy $E_{ang}$and wave function $u(\eta)$ we obtain now:

$$E_{ang} \equiv E_k(F) = \sqrt{\frac{\hbar^2 V_0 F_x}{\mu R_n^2}}\left(k + \frac{1}{2}\right) - V_0 F_x \equiv \hbar\Omega_n\left(k + \frac{1}{2}\right) - V_0 F_x; \ (k = 0, 1, 2...) \tag{3.12}$$

$$u_k(\vartheta) = \left(\frac{1}{2^k}\frac{1}{k!}\sqrt{\frac{\sigma_n}{\pi}}\right)^{\frac{1}{2}} \cdot H_k\left(\sqrt{\sigma_n}\vartheta\right)\exp\left(-\frac{\sigma_n \vartheta^2}{2}\right). \tag{3.13}$$

Here $H_k(x)$ are Hermit polynomials, and $k = 0, 1, 2, ...$ It is clear that in framework of model under considered we will have the same equations and same results for the hole.

At the same time, in this case, when the Coulomb interaction between the electron and hole is neglected, we can use the known results to describe the motion along the *z*-axis [12]:

$$w_i(z_i) = \sqrt{\frac{2}{d}}\sin\frac{\pi s_i}{d} z_i; \ E_{s_i} = \frac{\pi^2 \hbar^2 s^2}{2\mu_i d^2}; \ (s = 1, 2, ...; i = e, h). \tag{3.14}$$

4. Electron–hole pair in QR in the presence of strong external field

Let us now consider the electron-hole pair's states in the ring when the Coulomb interaction is taking into account. Correspondingly for the energy and wave functions of pair's transversal motion we can write:

$$E_{tr} = (E_{tr})_e + (E_{tr})_h; \ \ \psi_{e,h}(r_e, r_h; \phi_e, \phi_h) = \Phi_{n_e}^{(0)}(r_e)\,\Phi_{n_h}^{(0)}(r_h)\,u_{k_e}(\phi_e)\,u_{k_h}(\phi_h) \tag{4.15}$$

Taking into account the conditions (2.2) - (2.3), we obtain for pair's interacting potential the following expression:

$$\begin{aligned} U_{eh} = -\frac{\alpha}{|\vec{r}_e - \vec{r}_h|} = -\frac{\alpha}{\sqrt{(z_e - z_h)^2 + r_e^2 + r_h^2 - 2r_e r_h\cos(\phi_e - \phi_h)}} \cong \\ \cong -\frac{\alpha}{\sqrt{(z_e - z_h)^2 + b^2}}. \end{aligned} \tag{4.16}$$

Here α is the effective interacting constant, and $b = 2R_1(1 + L/2R_1)$; $(d, z_e, z_h \ll b)$.

For pair's motion by z - coordinate we can write now the following equation:

$$\left[-\frac{\hbar^2}{2\mu_e}\frac{\partial^2}{\partial z_e^2} - \frac{\hbar^2}{2\mu_h}\frac{\partial^2}{\partial z_h^2} - \frac{\alpha}{\sqrt{(z_e - z_h)^2 + b^2}}\right] g(z_e, z_h) = E_{eh} g(z_e, z_h) \tag{4.17}$$

By the taking into account the conditions (2.2) and (2.3) it is possible to present in interacting potential U_{eh} in the form

$$U_{eh} \approx -\frac{\alpha}{b}\left[1 - \frac{z_e^2}{2b^2} - \frac{z_h^2}{2b^2} + \frac{z_e z_h}{b^2}\right]. \tag{4.18}$$

Correspondingly, it is possible to account the member $\left(-\frac{\alpha}{b}\frac{z_e z_h}{b^2}\right)$ as a perturbation. Ohere-fore, instead of the Eq.(4.17) we can write now two "non- perturbed" equations:

$$\begin{gathered}\left[-\frac{\hbar^2}{2\mu_i}\frac{\partial^2}{\partial z_i^2} - \frac{\alpha}{2b}\left(1 - \frac{z_i^2}{2b^2}\right)\right] g_i^{(0)}(z_i) = E_i^{(0)} g_i^{(0)}(z_i);\\ \left(g_i^{(0)}(0) = g_i^{(0)}(d) = 0; i = e, h\right).\end{gathered} \tag{4.19}$$

The solution of this equation can be presented in the following form [13]:

$$\begin{gathered}g_i^{(0)}(z_i) = C_i \exp\left(-\frac{\lambda_i^2 z_i^2}{2d^2}\right)\left(\frac{\lambda_i z_i^2}{d^2}\right)^{\frac{1}{2}} {}_1F_1\left(\frac{3}{4} - \frac{\beta_i}{4\lambda_i}, \frac{3}{2}, \frac{\lambda_i z_i^2}{d^2}\right);\\ \beta_i = \frac{2\mu_i d^2}{\hbar^2}\left(E_i^{(0)} + \frac{\alpha}{2b}\right).\end{gathered} \tag{4.20}$$

Here $C_i = \left[\int_0^d \left|g_i^{(0)}(z_i)\right|^2 dz_i\right]^{-\frac{1}{2}}$ is the normalization constant, $\lambda_i^2 = \mu_i d^4 \alpha/\hbar^2 b^3$, and ${}_1F_1(a, c, x)$ is Kummer confluent hypergeometric function. The energy spectrum $E_i^{(0)}$ is defined from the boundary condition

$${}_1F_1\left(\frac{3}{4} - \frac{\beta_i}{4\lambda_i}, \frac{3}{2}, \lambda_i\right) = 0. \tag{4.21}$$

In Table 1 the first five values of parameter β_i are presented for the five values of λ_i.

Table 1. First five β - roots of equation ${}_1F_1\left(\frac{3}{4} - \frac{\beta_i}{4\lambda_i}, \frac{3}{2}, \lambda_i\right) = 0$

$\lambda\lambda$ /$\beta\beta$	β_{i1}	β_{i2}	β_{i3}	β_{i4}	β_{i5}
0.01	9.86963	39.47845	88.82647	157.9137	246.7401
0.05	9.87031	39.47922	88.82726	157.9145	246.7409
0.08	9.87141	39.48047	88.82854	157.9158	246.7422
0.1	9.87243	39.48162	88.82972	157.9171	246.7434
0.2	9.88091	39.49124	88.83955	157.9269	246.7534

For the "non-perturbed" energy $E_{eh}^{(0)}$of *e-h* pair we obtain, correspondingly:

$$E_{eh}^{(0)} = E_e^{(0)} + E_h^{(0)};\ \ (E_i^{(0)})_{s_i} = \frac{\hbar^2 \beta_{i,s_i}}{2\mu_i d^2} - \frac{\alpha}{2b};\ \ (i = e, h;\ s_i = 1, 2, 3, ...). \tag{4.22}$$

Full "non-perturbed" wave function $\Psi_{eh}^{(0)}(\vec{r}_e, \vec{r}_h)$of pair takes the following form:

$$\Psi_{eh}^{(0)}(\vec{r}_e, \vec{r}_h) = \Phi_{n_e}^{(0)}(r_e)\,\Phi_{n_h}^{(0)}(r_h)\,u_{k_e}(\phi_e)\,u_{k_h}(\phi_h)\,g_e^{(0)}(z_e)\,g_h^{(0)}(z_h). \tag{4.23}$$

First-order energy correction $E_{eh}^{(1)}$, calculated using the asymptotic behavior of functions $g_i^{(0)}(z_i)$ at $d \ll b$[12], is presented in the following form:

$$E_{eh}^{(1)} = \langle e,h|(-\frac{\alpha}{b}\frac{z_e z_h}{b^2})|e,h\rangle \cong -\frac{\alpha}{b}\left(1+\frac{11}{12}\frac{d^2}{b^2}\right). \tag{4.24}$$

5. Discussion of results

From the results obtained in the first place one should highlight the fact that under the influence of strong external electrostatic field, the spatial separation of electron and hole takes place in QR.

The strong external field creates a new deep potential well by the angular variable. Because of this, along with the quantum confinement in the radial direction, the charge carriers in the QR are additionally localized also along their angular motion in (ϕ, r)plane.

The external field separates electron and hole along the field's direction and traps them to the opposite ends of the ring's diameter. Instead of the rotation in the QR circle the particle under action of a strong external field vibrates now in a narrow angular cone of the azimuth variable. The localization cones of opposite charges are disposed at opposite edges of the QR's diameter directed along the external homogeneous field.

Simultaneously, the presence of external field leads to the explicit dependence of the wave functions on the effective masses of charge carriers.

These factors undoubtedly have an influence on the optical transitions in QR.

Let us consider the interband optical dipole transitions between the states of valence$(|v\rangle)$ and conductive$(|c\rangle)$ bands and examine the influence of external field on these transitions. For the perturbation *A,* related to the light wave, we will have in dipole approximation [12]:

$$A = \frac{|q|\,A_0}{m_0 c}\,(\vec{e}\cdot\vec{p})\,. \tag{5.25}$$

Here $A_0$is the amplitude of vector-potential, $\vec{p}$is a *3D* operator of momentum, $m_o$is the mass of free electron, and c is wave's velocity in free space. The incident light wave with frequency $\omega$is directed along the *Y* – axis and is polarized linearly along the *X*- axis: $\vec{e} = \vec{e}(1,0,0)$. Note that using the asymptotic behavior of functions $g_i^{(0)}(z_i)$at $z_i, d \ll b$, with sufficient accuracy we can obtain that

$$g_i^{(0)}(z_i) \cong \sqrt{\frac{2}{d}}\sin\frac{\pi s_i}{d}z_i;\ E_{s_i}^{(0)} \cong \frac{\pi^2\hbar^2 s_i^2}{2\mu_i d^2};\ s_i = 1,2,3,... \tag{5.26}$$

When such orientation of the sample and the incident wave takes place we obtain the following selection rules:

1. by radial quantum number: $n_c = n_v \equiv n$;
2. by oscillator quantum number: number: $|k_c - k_v| = 0,2,4,...$;
3. by quantum number along z – axis: $s_c = s_v \equiv s$.

For the "partial" threshold frequencies $(\omega_{c,v})$ of these transitions we will have:

$$\hbar\omega_{c,v} = E_g + \frac{\pi^2\hbar^2 n^2}{2\mu_{cv}L^2} + \hbar\Omega_c\left(k_c+\frac{1}{2}\right) + \hbar\Omega_v\left(k_v+\frac{1}{2}\right) + \frac{\pi^2\hbar^2 s^2}{2\mu_{cv}d^2} + E_{eh}^{(1)};$$
$$\left(\mu_{cv}^{-1} = \mu_c^{-1} + \mu_v^{-1}\right). \tag{5.27}$$

Using the explicit form of the functions and taking into account the above selection rules let us represent the results of calculations of "oscillator" matrix elements $J_{c,v} = \langle u_{k_c}(\eta) \mid u_{k_v}(\eta) \rangle$ for the transitions between the first few lowest states:

$$\begin{aligned}
&a)\, k_c = k_v = 0; |J_{0,0}|^2 = 8\frac{\tau^{1/2}}{1+\tau};\\
&b)\, k_c = k_v = 1;\ |J_{1,1}|^2 = 4\,|J_{0,0}|^2\,\frac{\tau}{(1+\tau)^2};\ (\tau = \mu_v/\mu_c);\\
&c)\, k_v = 0; k_c = 2;\ |J_{2,0}|^2 = |J_{0,0}|^2\,\frac{1}{2}\left|\frac{1-\tau}{1+\tau}\right|^2;\\
&d)\, k_v = 1;\ k_c = 3;\ |J_{3,1}|^2 = |J_{0,0}|^2\,\frac{6\tau}{(1+\tau)^2}\left|\frac{1-\tau}{1+\tau}\right|^2.
\end{aligned} \tag{5.28}$$

Because of the complete discrete spectrum of charge carriers, the absorption will have a strongly resonant character. Experimental observation of the specificity of the electroabsorption in the considered system is "secured" by the supervision of the resonance absorption peaks. The positions of these peaks are determined by the values of the threshold frequencies.

Specified values of these frequencies, as seen from the above results, are determined by the intensity of the external field and its own geometric dimensions of the sample.

6. Conclusions

In the results obtained in this study we can conclude the following:

The energy spectrum of charge carriers in SQR in the presence of strong lateral homogeneous electric field is a strongly discrete. This spectrum is a substructure, which is characterized by a set of three quantum numbers.

Under the influence of strong external field the rotational motion of carriers around the circumference of the ring disappears. Instead, the electron and hole begins to oscillate in a narrow angular cone at the opposite ends of a diameter in the direction of the field.

Because of this spatial separation of electron and hole, the Coulomb interaction between them in the ring with sufficient accuracy can be regarded as a perturbation.

It is possible to modify the optical-energy parameters of the system by variation of geometrical sizes of the sample and the intensity of external field in a controlled manner. At the same time the dependence of absorption coefficient upon ratio μ_v/μ_c opens a possibility to define the value μ_v experimentally, when the value μ_c is known.

As a consequence, we can conclude that in the application plan there is a real opportunity to use the theoretical results obtained for the electrical tuning of optical transitions in quantum ring.

References

[1] T.Chacraborty and P.Pietilainen, Phys. Rev. 50, 8460 (1994).

[2] T. Chacraborty, Adv. In address Sol. St. Phys. 43, 71 (2003).

[3] B.Szafran, Phys. Rev. B 77, 205313 (2008).

[4] S.Viefers, P.Koskinen, P.Singha Deo, M.Manninen, Physica E 21, 1 (2004); N.R.Das and S.Sen, Physica B 403, 3734 (2008).

[5] J.M. Llorens, C. Trallero-Giner, A. Garciia-Cristobal and A. Cantarero, Microel. Journ. 33, 355 (2002).

[6] Z. Barticevic, G. Fuster, and M. Pacheco Phys. Rev. B 65, 193307 (2002).

[7] X.G.Guo and J.C.Cao, J. Appl. Phys. **100**, 083112 (2006).

[8] Bin Li, W.Magnus, and F.M.Peeters, J. Phys.: Conference Series 210, 012030 (2010).

[9] S. Bhattacharyya, N. R. Das, Susmita Sen, Journ. of Appl. Phys. 105, 053108 (2009).

[10] W.R.Smythe, *Static and Dynamic Electricity,* (McGraw-Hill, New York, 1968).

[11] V.A.Harutyunyan, J. Appl. Phys. 109, 014325 (2011); V.A.Harutyunyan, Physics of Solid States, 52, 1744 (2010) [Original Russian Text: V.A.Harutyunyan, Fizika Twerdogo Tela 52, 1621 (2010)].

[12] G.Bastard, *Wave Mechanics Applied to Semiconductor Heterostructures*, (Les Editions de Physique, Les Ulis, 1998); P. Harrison, *Quantum Wells, Wires, and Dots* (Wiley, StateplaceNew York, 2000).

[13] M.Abramovitz, I.A.Stegun, (Eds.), *Handbook of Mathematical Functions,* (Dover, New York, 1972).

T.F. Kamalov
Physics Department, Moscow State Open University*
Home Page: http://www.timkamalov.narod.ru/

Axiomatization of classical and quantum physics of non-inertial reference frames

The problem of axiomatization of physics formulated by Hilbert as early as 1900 and known as the Sixth Problem of Hilbert. This naturally evokes the following questions: Is it possible, without drastically changing the mathematics apparatus, to set up the axiomatics of physics so as to transform physics, being presently a multitude of unmatched theories with inconsistent axiomatics, into an integrated Classical and Quantum Physics? Is it possible, maybe through expanding their scopes, to generalize of transform the existing axiomatics into an integral system of axioms in such a manner that existing axiomatics of inconsistent Classical and Quantum theories would follow there from as a particular case?

Keywords: axiomatic mechanics, jeceleration, seleration, Kinematic Principle, Dynamic Principle, Static Principle.
PACS: 05.45.Mt, 03.65.Ud.

An axiom is a statement adopted without proof. Therefore, there is no other way of obtaining an axiom than to merely guess it. It is rather hard to resist the temptation of declaring an axiom every phenomenon inexplicable in the framework of a particular theory. In such a case, on the one hand, the consistency of a theory would not be compromised, and on the other hand, the problem of explanation of this phenomenon is avoided. However, this approach is erroneous and fallacious, as the number of axioms cannot grow in an uncontrollable manner; the number of axioms shall be minimized. Only this way one can expect minimization of likely errors should some axioms be guessed inadequately. At the same time, it is impossible to avoid axioms at all, because, according to Godel theorem, each theory comprises statements impossible to be proved within the framework of this theory. It is these statements that constitute the foundation of the theory, governing its results and implications.

On the one hand, it seems evident that having altered a single word in an axiom, we could obtain dramatic changes in the theory. Hence, arbitrary altering of axioms is inadmissible, as otherwise we would get a chaotic set of axioms rather than an axiomatic system. On the other hand, science is not a church doctrine, but rather, a system of theories based on guessed axioms. Therefore, one should be extremely careful in altering axioms to adapt them to the obtained new results. Otherwise, the description of the physical reality would result as a multitude of inconsistent, often mutually contradicting, axioms. And, as it has been mentioned, the number of axioms should be reduced to the minimum.

Historically, the axiomatics of physics has by all means experienced alterations. For example, if we compare the classical Newtonian physics with its predecessor, Aristotelian physics, we can easily see that while axiomatics of Aristotelian physics presumed motion to occur only provided a force being applied to the body, the axiomatics of Newtonian classical physics states that motion may occur also if no force is applied to the body. Therefore, Aristotelian physics postulates

*E-mail: timkamalov@gmail.com

that the dynamics of bodies is described by first order differential equations, whereas Newtonian physics (with the Laws of Newton being from the mathematical viewpoint the axiomatics of classical physics[1]) postulates proportionality of the force applied to the body to its acceleration. In other words, the Laws of Newton postulate the description of body dynamics by the second order differential equations. Newton employed the concept of the absolute space being the space related to fixed stars. Such space can be called Euclidian.

Is it correct to consider the Laws of Newton to be the axiomatics of classical physics? The answer is definitely positive. Shall we, and may we, expand their scope of application to microobjects? Quantum mechanics is a physical description of particles employing the definition of inertial reference frame, hence employing the First Newton's Law. The First Law states that any body free form interactions with other bodies would have constant velocity. So, how is velocity defined in quantum mechanics? It is done through the average with wave function ψ

$$< \dot{x} >= \int \psi^* \dot{x} \psi dx. \tag{1}$$

In a quantum (real) reference frame $< \dot{x} >= \text{const}$ there always exist infinitesimal fields, waves, and forces perturbing an ideal inertial reference frame. This follows from one of the general definitions of Mach principle [2]: "Local physical laws are determined by large-scale structure of the Universe". Commenting the Mach principle, let us note that in this case the definition of inertial properties of a body is determined by multi-particle interactions with all bodies in the Universe. The description of the case of particle motion with higher derivatives of coordinates in time has been for the first time published in 1850 by M. Ostrogradsky; it is known as an Ostrogradsky Canonical Formalism [3]. Being a mathematician, Ostrogradsky considered coordinate systems rather than reference systems. This case corresponds to a quantum (real) reference frame comprising not only inertial reference frames, but also non-inertial ones, determined, according to Mach principle, by multi-particle interactions with all bodies moving in the Universe. Inertial reference frames defines by all bodies moving in the Universe [2]

$$\frac{d^2}{dt^2}\left(\frac{\int \rho(r) r dV}{\int \rho(r) dV}\right) = 0.$$

Here $\rho(r)$ is the function of the distribution of all masses in the Universe with the volume V.

Definition

A kinematic state of a mechanical system with constant higher derivative $\dot{x}^{(n)} = const$ is called defined if the kinematics of the body is described with a differential equation

$$F(x, \dot{x}, \ddot{x}, \dddot{x}, ..., \dot{x}^{(n)}) = 0. \tag{2}$$

Let us assume that if in an arbitrary (any) reference frame the average value of a higher derivative is constant,

$$< \dot{x}^{(n)} >=< \frac{d^n x}{dt^n} >= \text{const}. \tag{3}$$

then the function F is finite.

Kinematic Principle (Inertial Principle)

A kinematic state of a mechanical system free from interactions with other bodies is observer-dependent and persists until its interaction with other bodies alters its kinematic state.

The acceleration for a body with free from interactions with other bodies is a constant for the observer in the constant-accelerated reference frame. In this case the acceleration is define the kinematic state of the body because in that case the acceleration is the invariant for the reference frame of the observer.

Let us call an invariant of a reference frame the constant higher derivative that does not change in case of transformation of coordinates

$$x' = f(x, \dot{x}, \ddot{x}, \dddot{x}, ..., \dot{x}^{(n)}) \tag{4}$$

$$t' = t. \tag{5}$$

Then the kinematic state of a mechanical system free form interactions with other bodies depends on the invariant of the observer's reference frame.

Let us call a harmonic reference system the reference system with a clock and an observer oscillating harmonically, in which any body free from interactions with other bodies would maintain the average value of its higher derivative. For a reference system oscillating harmonically let us consider the invariant the $< \dot{x}^{(n)} >= const$. In a harmonic reference frame a coordinate of the body may be described by the function of classic, quantum, and geometrized relativistic physics of the general relativistic theory does not in the least fade away, but on the contrary, becomes more pronounced each year. This naturally evokes the following questions: 1. Is it possible, without drastically changing the mathematics apparatus, to set up the axiomatics of physics so as to transform physics, being presently a multitude of unmatched theories with inconsistent

$$\varphi(t, x) = \varphi_0 \exp i(kx + \omega t) \tag{6}$$

being φ_0 the amplitude of oscillation, k and ω the wave vector and angular frequency of oscillations, respectively.

In the particular case,

$$\varphi(t, x) \approx kx + \omega t = K_i X^i \tag{7}$$

and being K_i 4-dimensional wave vector and X^i 4-coordinate of the body, $i = 0, 1, 2, 3$ in a harmonic reference frame. In this case, function φ describes the 4-coordinate of the body multiplied by a constant coefficient. In a vibrating reference frame the coordinate of a body may be expressed with arrays of harmonic oscillations.

Dynamic Principle

There exist reference frames in which the dynamics of a body is described by the equation:

$$k_1\dot{x} + k_2\ddot{x} + k_3\dddot{x} + ...k_{2n}\dot{x}^{(2n)} = F(x, \dot{x}, \ddot{x}, \dddot{x}, ..., \dot{x}^{(n)}). \tag{8}$$

We will call such reference frames real. Or

$$k_1 v + k_2 a + k_3 j + k_4 s + ...k_{2n}\dot{x}^{(2n)} = F(x, \dot{x}, \ddot{x}, \dddot{x}, ..., \dot{x}^{(n)}), \tag{9}$$

where the jerk (jeceleration) $j = \dfrac{da}{dt} = \dddot{x}$ can be finding like the derivation of the vector of bodies acceleration a with respect of time and the vector of snap (seleration) is the forth derivation with respect of time $s = \dfrac{dj}{dt} = \dot{x}^{(4)}$.

Let us call a force F the quantitative measure of the interaction between the bodies.

The generalized principle of relativity of Galileo means in this case that the order of the differential equation (8) describing the dynamics of a mechanical system with the invariant of the reference frame $\dot{x}^{(n)} = const$ does not alter at transformation (4,5).

The differential equation (8) corresponds to the description of the body dynamics in a non-isolated (open) mechanical system with the external forces of the system with odd derivatives, corresponding, for example, to losses due to friction and radiation. Odd derivatives correspond to losses (friction or radiation) and describe irreversible cases for open systems not satisfying

variational principles of mechanics. The case of an isolated (close) mechanical system corresponds the differential equation with even derivatives.

$$k_2\ddot{x} + k_4\ddot{\ddot{x}} + ...k_{2n}\dot{x}^{(2n)} = F(x, \dot{x}, \ddot{x}, \ddot{\ddot{x}}, ..., \dot{x}^{(n)}) \tag{10}$$

The reference frames, in which the dynamics of a system is described by the equation

$$< k_2\ddot{x} >=< F(x, \dot{x}, \ddot{x}, \ddot{\ddot{x}}, ..., \dot{x}^{(n)}) >, \tag{11}$$

we will call inertial reference frames. Here, the proportionality coefficient in the equation k_2 of dynamics (9) is the mass of a body.

Static Principle.

If a particle rests along an arbitrary direction, then the resultant force acting thereon along this direction is zero.

For inertial frames, the Lagrangian L depends only on coordinates and their first derivatives $L = L(x, \dot{x})$ [4]. For the case of quantum (real) reference frames the Lagrangian depends on coordinates and their higher derivatives and has the form $L = L(x, \dot{x}, \ddot{x}, \ddot{\ddot{x}}, ..., \dot{x}^{(n)})$.

Let us consider in more detail such precise description of dynamics of bodies motion accounting for quantum (real) reference frames determined, according to our model, by complex multi-particle interactions with all bodies in the Universe.

For an accurate description of dynamics of bodies motion accounting for higher derivatives, let us consider the body in an arbitrary reference frame, denoting the position r of the body in the space as and time as t. Then, expanding the function $r = r(t)$ into Taylor's series in the zero point, we get

$$r = r_0 + \dot{r}t + \frac{1}{2!}\ddot{r}t^2 + \frac{1}{3!}\ddot{\ddot{r}}t^3 + ... + \frac{1}{n!}\dot{r}^{(n)}t^n + ... \tag{12}$$

Let us denote

$$r_N = r_0 + \dot{r}t + \frac{1}{2!}\ddot{r}t^2$$

and the additional correction variables q_r for our model with arbitrary reference frames as , where - is a value equal to zero in the classical Newtonian mechanics

$$q_r = \frac{1}{3!}\ddot{\ddot{r}}t^3 + ... + \frac{1}{n!}\dot{r}^{(n)}t^n + ... \tag{13}$$

Then

$$r = r_N + q_r.$$

In our case the description discrepancy and *uncertainty between the two models* h is equal to the difference in descriptions of a test particle in the extended Newtonian dynamics with the Lagrangian $L = L(x, \dot{x}, \ddot{x}, \ddot{\ddot{x}}, ..., \dot{x}^{(n)})$ and Newtonian dynamics in the inertial reference frames with the Lagrangian $L = L(x, \dot{x})$:

$$\int (L(x, \dot{x}, \ddot{x}, \ddot{\ddot{x}}, ..., \dot{x}^{(n)}) - L(x, \dot{x}))dt = S(x, \dot{x}, \ddot{x}, \ddot{\ddot{x}}, ..., \dot{x}^{(n)}) - S(x, \dot{x}) = h \tag{14}$$

Let us apply the least action principle [5]:

$$\delta S = \delta \int L(\dot{r'}, r')dt = \int \sum_{n=0}^{N} (-1)^n \frac{d^n}{dt^n}\frac{\partial L}{\partial \dot{r}^{(n)}}\delta\dot{r}^{(n)}dt = 0. \tag{15}$$

Then the generalized Euler-Lagrange equation for real reference frames will take on the form

$$\sum_{n=0}^{N}(-1)^N \frac{d^N}{dt^N}\frac{\partial L}{\partial \dot{r}^{(N)}} = 0. \tag{16}$$

Or,

$$\frac{\partial L}{\partial r} - \frac{d}{dt}\frac{\partial L}{\partial \dot{r}} + \frac{d^2}{dt^2}\frac{\partial L}{\partial \ddot{r}} - ... + (-1)^N \frac{d^N}{dt^N}\frac{\partial L}{\partial \dot{r}^{(N)}} = 0. \tag{17}$$

Then the generalized Euler-Lagrange equations will take on the form

$$\frac{\partial L}{\partial r} - \frac{d}{dt}\frac{\partial L}{\partial \dot{D}^{(1)}r} + \frac{d^2}{dt^2}\frac{\partial L}{\partial \dot{D}^{(2)}r} - ... + (-1)^N \frac{d^N}{dt^N}\frac{\partial L}{\partial \dot{D}^{(N)}r} = 0$$

For $L = L(q, \dot{q}, \ddot{q})$

$$E = \beta_0 q^2 + \beta_1 \dot{q}^2 + \beta_2 \ddot{q}^2. \tag{18}$$

Denoting the Appel's energy of acceleration [5] Q, $\beta_1, \beta_2, \beta_3$ being constant factors, we obtain for kinetic energy W and potential energy V, respectively,

$$E = V + W + Q \tag{19}$$

$$V = \beta_0 q^2, \tag{20}$$

$$W = \beta_1 \dot{q}^2, \tag{21}$$

$$Q = \beta_2 \ddot{q}^2. \tag{22}$$

The generalized Hamilton-Jacobi equation with higher derivatives for the action function will take on the form

$$-\frac{\partial S}{\partial t} = \frac{(\nabla S)^2}{2m} + V + Q, \tag{23}$$

From purely classical trajectories considered we to find the Bohm's quantum potential [6] whereas the key is the wave function. Let's compare Q with the Bohm's quantum potential and complement Eq. (23) with the continuity equation. If $Q \approx \beta_3(\nabla^2 S/m^2)$, where the value of the constant is chosen $\beta_3 = i\hbar m/2$, in the first approximation, we obtain for the function $\psi = e^{iS/\hbar}$ the Schroedinger equation

$$i\hbar\frac{\partial \psi}{\partial t} = -\frac{\hbar^2}{2m}\nabla^2\psi + V\psi. \tag{24}$$

Then, considering quantum microobjects in the curved space, we must take into account the fact that the scalar product of two 4-vectors A^i and B^k is $g_{ik}A^iB^k$, where for weak gravitational fields one may use the value h_{ik}, which is the solution of Einstein's equations for the case of weak gravitational field in harmonic coordinates.

The correlation factor M of the projection of stochastic vector variables λ^i onto directions A^k and B^n set by the polarizers (all these vectors being unity ones) is [7,8]

$$|M| = |< AB >| = \left|< \lambda^i A^k g_{lk} \lambda^m B^n g_{mn} >\right| = \left|\frac{1}{2\pi}\int \cos\phi \cos(\phi + \theta) d\phi\right| =$$

$$= |\cos\theta|$$

due to the equations following from differential geometry,

$$\cos\phi = \frac{g_{ik}\lambda^i A^k}{\sqrt{\lambda^i \lambda_i}\sqrt{A^k A_k}},$$

$$\cos(\phi+\theta)=\frac{g_{mn}\lambda^m A^n}{\sqrt{\lambda^m\lambda_m}\sqrt{B^n B_n}}.$$

Here ϕ is the angle between λ^i and A^k, $(\phi+\theta)$ is between $\lambda^m$and B^n.

This means coincidence of the Bell's observable [9] with the experimental results in real (quantum) reference frames. All vectors here being unity ones with metrics averaging in the weak field approximation yielding unity; is the angle between polarizers, vector A^n is equal to vector B^n rotated by the angle θ, and indices taking the values $i=0,1,2,3$. Finally, we get

$$|M_{AB}|=|\cos\theta|\,. \tag{25}$$

The maximum value of the Bell's observable S is

$$|<S>|=\frac{1}{2}\,|<M_{AB}>+<M_{A'B}>+<M_{AB'}>-<M_{A'B'}>|=$$

$$=\frac{1}{2}\left|\cos(-\frac{\pi}{4})+\cos(\frac{\pi}{4})+\cos(\frac{\pi}{4})-\cos(\frac{3\pi}{4})\right|=\sqrt{2},$$

where $\theta=\frac{\pi}{4}$, being the doubled angle between direction of the polarizers A and B.

To sum it up, all equations of classical mechanics in the proposed model possess additional terms in the form of higher derivatives. At that, these additional terms are zero not always, but only in special cases, i.e. in the inertial reference frames.

Additional terms in the form of higher derivatives may play the role of hidden variables complementing both quantum and classic mechanics for the consolidation them to the Axiomatic Mechanics. Additional terms have non-local character, which enables their employment for description of non-local effects of quantum mechanics.

References

[1] I. Newton, Philosophiae naturalis principia mathematica. London, 1687. 220 p.

[2] Mach Ernst, Die Mechanik in ihrer Entwickelung: Historisch-Kritisch Dargestellt, 3rd revised & enlarged edition, F. A. Brockhaus, Leipzig (1897) [First published 1883].

[3] M. V. Ostrogradskii Memoire sur les equations differentielles relatives aux problemes des isoperim'etres // Memoires de l'Academie Imperiale des Sciences de Saint-Peterbourg, v. 6, 1850. P. 385.

[4] J.I. Lagrange, Mecanique analitique. Paris, De Saint, 1788. 131 p.

[5] Appel P., Traite' de Me'caique Rationelle, Paris, Ganthier-Villars e'diteur, 1953.

[6] Bohm D. A suggested interpretation of the quantum theory in terms of "hidden" variables I , Physical Review. 1952. v. 85, P. 166.

[7] T.F. Kamalov, A model of Extended Mechanics and non-local hidden variables for Quantum Theory, Journal of Russian Laser Research, Volume 30, Number 5, p. 466-471, 2009.

[8] T.F. Kamalov, Hidden Variables and the Nature of Quantum Statistics, Journal of Russian Laser Research, 2001, v. 22, n. 5, p. 475-479.

[9] J. S. Bell, On the Einstein, Podolsky, Rosen Paradox, Physics, 1964, v.1, n.3, 195.

N. M. Kondratiev
Faculty of Physics, Moscow State University, Leninskie Gory, Moscow, 119991, Russia*

Thermal noise and coating optimization in multilayer dielectric mirrors

Optical multilayer coatings of high-reflective mirrors significantly determine properties of Fabry-Perot resonators. Thermal (Brownian) noise in these coatings produce excess phase noise which can seriously degrade the sensitivity of high-precision measurements using these cavities. In particular, it is one of the main limiting factors at the current stage in laser gravitational-wave detectors (for example, project LIGO). We present a method to calculate this effect accurately and analyze different strategies to diminish it by optimizing the coating.

Traditionally the effect of the Brownian noise is calculated as if the beam is reflected from the very surface of the mirror's coating. However, the beam penetrates the coating and Brownian expansion of the layers leads to dephasing of interference in the coating and consequently to an additional change in the reflected amplitude and phase. Fluctuations in the thickness of a layer change the strain in the medium and hence, due to a photoelastic effect, change the refractive index of this layer. This additional effect should also be considered. It is possible to reduce the noise by changing the total number and thicknesses of high and low refractive layers preserving the reflectivity. We show how an optimized coating may be constructed analytically rather than numerically as before. We also check the possibility of using internal resonant layers, an optimized cap layer and double mirrors to decrease the thermal noise.

Keywords: dielectric mirrors; optical effects.
PACS number(s): 04.80.Nn, 42.79.Wc, 07.60.Ly, 05.40.Ca

1. Introduction

Any precise measurement faces the challenge of different noises superposing a useful signal. Brownian noise coming from chaotic thermal motion of particles is one of the enemies. A Michelson interferometer is able to detect minor changes in the lengths of its arms: two beams traveling different optical paths, interfere on the detector producing intensity which depends on the difference between phases of the beams. Thermal (sometimes also called Brownian) noise in coatings and substrates of the interferometer's mirrors results in fluctuations of their surfaces which add a random phase to the waves. This effect is one of the key factors limiting the sensitivity of laser gravitational-wave detectors [2]. Though the thickness of the multilayer coating is just several micrometers, the internal mechanical losses in layers is several orders of magnitude larger then in the substrate. That is why coating thermal noise, in accordance with the fluctuation-dissipation theorem, exceeds other noises produced in the mirrors [10].

In this paper we analyze different effects and strategies aimed at decreasing the thermal coating noise for a generalized multilayer reflective coating. Traditionally, the effect of the Brownian noise is calculated as if the beam is reflected from the surface of the mirror's coating, fluctuating as an incoherent sum of the fluctuations of each layer and of the substrate. However, the beam actually penetrates the coating and Brownian expansion of the layers leads to dephasing of interference and

*E-mail:noxobar@mail.ru

consequently to an additional change in the reflected phase [11] and amplitude. Fluctuations in the thickness of a layer change the strain in the medium and hence due to photoelastic effect change the refractive index of this layer. This additional effect should also be considered. It was proposed in [12,16] to change the number of layers and thicknesses of high and low refractive components in order to diminish the noise while preserving the reflectivity. We also check the possibility of using internal resonant layers [15], an optimized cap layer [10] and double mirrors [14] to decrease the thermal noise.

Brownian noise is not the only source of noise produced by the coating. Fluctuations of temperature, which are translated into a displacement of mirror's surface through thermal expansion (thermoelastic noise) [5,7] and a change of the optical path due to fluctuations of the refraction index (thermorefractive noise) [6] combine to produce generalized thermo-optical noise [8, 10]. Brownian fluctuations causing displacement of mirrors' surface and the previously neglected correlated photoelastic effect produced by these fluctuations form Brownian branch of noises. The Brownian branch of noises, which is the topic of this paper, and thermo-optical noise are uncorrelated as they represent uncorrelated fluctuations of volume and temperature.

2. Multilayer coating phase noise

2.1. Reflectivity

To calculate the amplitude and phase of a reflected beam the impedance method [13] will be used below. We found this method more convenient for analytical consideration than the equivalent and more widely used matrix method [9].

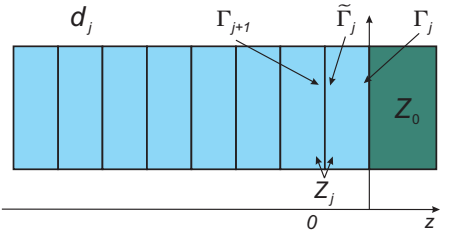

Fig. 1. A schematic of a multilayer coating

To consider the reflection of light at normal incidence on each boundary separating the layers starting from the substrate/coating boundary (see Fig. 1) we introduce an effective impedance $Z(z)$ and an amplitude reflection coefficient $\Gamma(z)$ as follows:

$$Z(z) = \frac{E(z)}{H(z)} = \frac{E_+(z) + E_-(z)}{H_+(z) + H_-(z)} = \eta(z)\frac{1+\Gamma(z)}{1-\Gamma(z)}, \tag{2.1}$$

$$\Gamma(z) = \frac{E_-(z)}{E_+(z)} = \frac{Z(z)-\eta(z)}{Z(z)+\eta(z)}, \tag{2.2}$$

$$\eta(z) = \sqrt{\frac{\mu(z)\mu_0}{\epsilon(z)\epsilon_0}} = \frac{\mu(z)}{n(z)}Z_v. \tag{2.3}$$

where E and H are tangential electric and magnetic fields in the standing wave, while E_+, H_+ and E_-, H_- are forward and backward (reflected) waves, n is the refraction index, μ and ϵ the relative

permeability and permittivity, and Z_v is the vacuum impedance ($Z_v = 1$ in the Gaussian CGS system). We assume that in a small neighborhood of the boundary μ and ϵ are piecewise-constant.

As tangential fields E and H are continuous in a medium without free currents, the effective impedance is also continuous on all boundaries, while the reflection coefficient experiences jumps. Meanwhile, the reflection coefficient changes continuously between boundaries according to the following expression:

$$\Gamma(z - d_j) = \frac{E_- e^{ik_0 n_j (z-d_j)}}{E_+ e^{-ik_0 n_j (z-d_j)}} = \Gamma(z) e^{-i2k_0 n_j d_j}, \tag{2.4}$$

where $k_0 = \dfrac{2\pi}{\lambda}$ is the wave vector of the optical field in vacuum and λ is the wavelength. This allows us to calculate reflectivity of any multilayer coating recursively, layer by layer starting from the substrate, where the impedance is equal to the impedance of the free substrate η_s, and moving to the surface, turning from the reflection coefficient $\widetilde{\Gamma}_j = \Gamma(-\sum_j d_j + 0)$ to the effective impedance $Z_j = Z(-\sum d_j - 0) = Z(-\sum d_j + 0)$ when facing the boundary and back (to Γ_{j+1}) after crossing it (see Fig. 1). It is possible also to exclude effective impedance from calculations:

$$\Gamma_{j+1} = \frac{g_{j+1,j} + \widetilde{\Gamma}_j}{1 + g_{j+1,j}\widetilde{\Gamma}_j}, \tag{2.5}$$

where $\widetilde{\Gamma}_j = \Gamma_j e^{-i\varphi_j}$ comes from (2.4), $\varphi_j = 2k_0 n_j d_j$ and $g_{ij} = \dfrac{n_i - n_j}{n_i + n_j}$. Note that the tilde sign $\widetilde{\ }$ can be read as "on the left side of the layer" (Fig. 1).

In the case of classical $\lambda/4$ layers, all impedances and reflection coefficients are real.

2.2. Interference

We now assume that each of the layers experiences a variation of thickness δd_j and a variation of its refraction index δn_j, producing changes in optical thicknesses of layers and in boundary conditions between layers. These variations may be included by changing $-\varphi_j$ for $-\varphi_j - 2k_0\delta n_j d_j - -2k_0 n_j \delta d_j = -\varphi_j + \Delta_j$ and assuming

$$\widetilde{\Gamma}'_j = \Gamma'_j e^{-i\varphi_j}(1 + i\Delta_j), \tag{2.6}$$

where the prime means modified reflectivity. We also have to substitute η_i for $\eta_i(1 + \delta\eta_i)$ in (2.1)-(2.2), which is a consequence of refraction index change $\delta\eta_j = -\dfrac{\delta n_j}{n_j}$. As before, moving layer by layer to the surface, we expand each result into a series to the first order of variations δn_j and δd_j. In this way we can build a perturbed amplitude reflection coefficient Γ'_m:

$$\begin{aligned} \Gamma'_m &= \Gamma_m(1 + \varepsilon), \\ \varepsilon &= z_m \frac{\delta n_m}{n_m} + \sum_{j=1}^{m-1} \prod_{k=j+1}^{m} \frac{z_k}{\widetilde{z}_{k-1}} \left(i\Delta_j - \zeta_j \frac{\delta n_j}{n_j} \right), \end{aligned} \tag{2.7}$$

$$z_k = \frac{(1 - \Gamma_k^2)}{2\Gamma_k},\ \widetilde{z}_k = \frac{1 - \Gamma_k^2 e^{-i2\varphi_k}}{2\Gamma_k e^{-i\varphi_k}},\ \zeta_k = \widetilde{z}_k - z_k. \tag{2.8}$$

Here m is the index of the layer of interest ($m = N + e$ for the reflectivity of the whole mirror, where N is the total number of layers, "e" represents the consideration of the top layer – vacuum boundary). Taking into account that $\Delta_j, \frac{\delta n_j}{n_j} \ll 1$, we can find an equivalent phase shift $\delta\varphi$ as well as a variation of reflectivity $\delta\Gamma$ (leading to amplitude noise which cannot be found in traditional approach) collecting all imaginary and real parts noting the decomposition $\Gamma e^{\varepsilon} \simeq \Gamma(1 + \varepsilon)$. Total fluctuations may arise both from layer thickness fluctuations δd_j (Brownian and thermoelastic noises), or from deviations of refraction index δn_j (photoelastic and thermo-refractive noises).

Using equations described above we can easily derive the inhomogenius noise ($\delta n = \delta n(z)$) of one layer applying limitation procedure: $n_j = n$, $d_j = dz \to 0$, $\sum \varphi_k = \int dz$. Then, assuming noise only inside the layer, obtain

$$\Gamma'_{N+1} = \Gamma_1 e^{-2ik_0 nL} \left(1 - 4ik_0 \int_L \delta n(z) \cos^2(k_0 nz + i\mathrm{Ln}\,\sqrt{\Gamma_1})dz)\right), \tag{2.9}$$

where Ln stands for complex logarithm, L is the layer length. This result absolutely coincides with [4] result of $\sin^2$-averaging as they had $\Gamma_1 = -1$. In multilayer coating with inhomogeneous noise equations (2.5) and (2.7) will not change their forms, while (2.8) will require a minor modification, without bringing out any new effects. A minor modification of (2.9) (as it contain transition into and out of layer) then serves as analogue of (2.4). However such non-homogeneous extension of (2.7)-(2.8) is not essential for the Brownian branch as all spectral density estimations for it are based on "thin coating approximation" giving out constant strain (and hence δn_j) in coating.

2.3. Photoelastic effect

A photoelastic effect in layers of the coating may produce additional noise correlated with Brownian noise. Photoelasticity is a phenomenon of refraction index change under deformation:

$$\Delta B_i = p_{ij} u_j, \tag{2.10}$$

where B_i is the optical indicatrix, u_j is strain tensor, p_{ij} is photoelastic tensor and indices $i, j \in 1; 6$ [19]. In the case of cylindrical symmetry we have a longitudinal effect $\Delta B_i = p_{i3} u_3 = p_{i3}\delta d/d$ and transversal effect $\Delta B_i = p_{i\rho} u_{\rho\rho}$. However, only the longitudinal effect may produce the noise correlated to the Brownian longitudinal surface noise, providing a theoretical possibility of their interference compensation. Variations of refraction indices due to longitudinal photoelasticity are the following:

$$\begin{aligned} \delta n_x &= -\frac{n_0^3}{2} p_{13} \frac{\delta d}{d}, \\ \delta n_y &= -\frac{n_0^3}{2} p_{23} \frac{\delta d}{d}. \end{aligned} \tag{2.11}$$

We neglect a nonzero δn_z component, as we consider normal incidence. It is known that tantalum oxide used in multilayer coatings Ta_2O_5 is a rutile-type crystal with tetragonal symmetry. Rutile (titanium dioxide) has $p_{13} = 0.171$, $p_{23} = 0.16$. From [18] we can also make a rough estimate for tantalum oxide $p_{Ta_2O_5} < 0.18$. For simplicity we put $p_{13} = p_{23} = p_{Ta_2O_5} = 0.17$. The other component of the coating – fused silica has $p_{13} = p_{23} = p_{SiO_2} = 0.27$.

Photoelasticity also produces a transversal effect coupled to $u_{\rho\rho}$ which should be considered separately as $u_{\rho\rho}$ noise is not correlated with $u_{zz} \propto \delta d$ noise and should be added incoherently. This component, producing a small correction, will not be considered here.

2.4. Brownian branch of noises

The photoelastic effect converts a fluctuation layer thickness into a correlated fluctuation of its refraction index, producing additional phase and boundary variations:

$$\Delta_j = -2k_0 n_j \left(1 - \frac{n_j^2}{2} p_j\right) \delta d_j = -2k_0 n_j \psi_j \delta d_j, \tag{2.12}$$

$$-\frac{\delta n_j}{n_j} = \frac{n_j^2 p_j}{2} \frac{\delta d_j}{d_j} = -\frac{n_j^2 p_j}{\varphi_j (2 - n_j^2 p_j)} \Delta_j = \gamma_j \Delta_j, \tag{2.13}$$

where p_j is the effective photoelastic index for a j-layer. Thereby coating induced deviations of reflected phase and reflection coefficient are easily obtained from (2.7)-(2.8):

$$\delta\varphi_c = \sum_{j=1}^{N} \alpha_j \delta d_j, \tag{2.14}$$

$$\delta\Gamma_c = \sum_{j=1}^{N} \beta_j \delta d_j, \tag{2.15}$$

where

$$\alpha_j = -2k_0 n_j \psi_j \operatorname{Im}\left[\prod_k \frac{z_k}{\widetilde{z}_{k-1}} (i + \zeta_j \gamma_j)\right], \tag{2.16}$$

$$\beta_j = -2k_0 n_j \psi_j \operatorname{Re}\left[\prod_k \frac{z_k}{\widetilde{z}_{k-1}} (i + \zeta_j \gamma_j)\right]. \tag{2.17}$$

Let us consider one end mirror in the arm of an interferometer. Thermal displacement of the mirror's surface produces phase fluctuations in the interferometer output. It is more intuitive to consider a case of contraction (Fig. 2) of all layers in the mirror. Then the length of additional gap for the light to travel before entering the mirror is $-\delta d$ (as $\delta d < 0$ for contracting), yielding the phase shift

$$\delta\varphi_g = -2k_0 \sum_{j=1}^{N} (-\delta d_j), \tag{2.18}$$

The total phase shift produced by the perturbed coating (relative to the unperturbed one) will be

$$\delta\varphi_\Sigma = -2k_0 \sum_{j=1}^{N} \left[z_{N+e} (-1)^{N-j} \widetilde{z}_j^{-1} \psi_j n_j - 1\right] \delta d_j, \tag{2.19}$$

where we took into account that inside $\lambda/4$-reflector all quantities are real and $\alpha_j = -2k_0 n_j \psi_j z_{N+e} (-1)^{N-j} \widetilde{z}_j^{-1}$.

It is also important to admit that in a "good mirror" approximation, when $1 - |\Gamma| \ll 1$ (in this case $Z_N \to 0$ or $Z_N \to \infty$ depending on the topmost layer) the amplitude reflection coefficient correction for $\lambda/4$-reflector produced by each layer $\beta_j = (-1)^{N-j} z_{N+e} \gamma_j \widetilde{z}_j^{-1} \dfrac{Z_j}{\eta_j} \to 0$.

The term before δd_j can be regarded as a noise coefficient showing a contribution of each layer into the total noise. This coefficient can have any sign, depending on the values of interferential

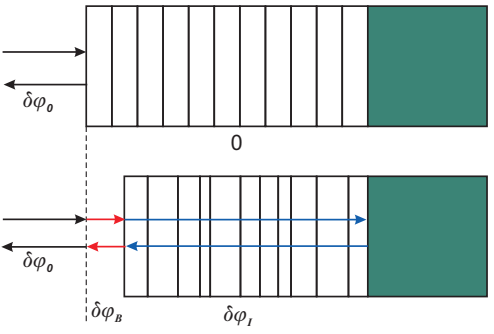

Fig. 2. Phase shift of the optical wave reflecting from an unperturbed (upper figure) and perturbed mirror. $\delta\varphi_0$, $\delta\varphi_g$ and $\delta\varphi_c$ are the shift in the total phase, the shift due to the surface displacement and the shift due to interference dephasing in the coating respectively ($\delta d_j < 0$).

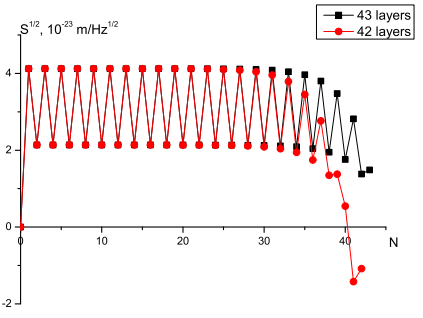

Fig. 3. Noise coefficient (keeping the sign) from each layer in a coating consisting of 42 (circles) or 43 (squares) layers on silicon substrate.

contribution ("$-$" sign) or surface displacement ("$+$"), but only its absolute value is significant as noise contributions from different layers are added incoherently.

Using the acquired formulas we can plot a diagram of the phase shift contribution of each layer and values of noise spectral densities in the whole. In Fig. 3 such a distribution is plotted, keeping the sign from (2.19). It can be seen that the interference part of noise plays a role in a few outer layers (order of penetration depth) [11] while Brownian (surface displacement) noise forms the major part. Several layers can even demonstrate nearly complete noise compensation.

The noise contribution of a layer is formally composed of three summands: the main Brownian (surface displacement) contribution, the interferential part and the photoelastic effect:

$$\delta\varphi_\Sigma = \sum 2k_0\delta d_j + \frac{\partial\varphi}{\partial d_j}\delta d_j + \frac{\partial\varphi}{\partial n_j}\frac{\partial n_j}{\partial d_j}\delta d_j, \tag{2.20}$$

where φ denotes the phase of total complex reflectivity of the mirror. Formulas (2.7)-(2.8) give analytical expression of the derivatives. Their sign distribution may be illustrated as follows. If the coating contracts, then the phase shift produced by each layer is positive due to the change of its thickness as the Brownian (surface displacement) noise is not really a phase shift acquired by

light inside the mirror, but outside it (Fig. 2). The contraction of each layer leads, at the same time, to an increase of the refraction index (as in normal materials it grows with density), providing a positive phase shift. Interference dephasing (phase shift due to reduction of the layer thickness itself), on the other hand, may compensate the phase shift produced by both effects. It looks like the photoelastic effect can play only a negative role; however, it can reduce too high interference dephasing in particular cases.

Equation (2.20) is quite suitable for numerical calculations as the partial derivatives in it may be calculated numerically. We used this approach for independent checking of formulas (2.7)-(2.8).

2.5. Noise spectral density

Using (2.19) one can estimate noise spectral densities if the noise spectral density of each layer is known. In the model of independent thin layers on an infinite half space substrate, each layer behaves just as if it was the only layer on the substrate. This model was heavily treated and the solution is well known [11, 12].However, we should split the total surface fluctuations of one layer into two parts for our purpose. The first one represents the fluctuations of the thickness of the coating layer S^c and the second one represents the fluctuations of the substrate surface induced by losses in the coating S^s. Interference and photoelastic effects influence only the first term. If the losses in the layer responsible for both fluctuations (shear and expansion losses) are equal, then these two spectral densities are uncorrelated. Otherwise cross correlation terms should be taken into account. We assume the losses equal in this paper. Using the approach presented in [11] this splitting may be easily obtained in the assumption that the noise produced by each layer is independent $\langle \delta d_j^2 \rangle \to S^c(\Omega)_j$, $\langle \delta d_j \delta d_k \rangle = 0$:

$$S(\Omega)_j = S^c(\Omega)_j + S^s(\Omega)_j = (\xi_j^c + \xi_j^s)\phi_j d_j = \xi_j \phi_j d_j, \tag{2.21}$$

$$\xi_j^c = \frac{4k_B T}{\pi w^2 \Omega} \frac{(1+\nu_j)(1-2\nu_j)}{Y_j(1-\nu_j)},$$

$$\xi_j^s = \frac{4k_B T}{\pi w^2 \Omega} \frac{Y_j(1+\nu_s)^2(1-2\nu_s)^2}{Y_s^2(1-\nu_j^2)} \tag{2.22}$$

where ν_j is the Poisson coefficient of layer j, Y_j – its Young's modulus (Y_s and ν_s are the parameters of the substrate), ϕ_j is the mechanical loss angle, w is the Gaussian beam radius on the mirror, Ω is the frequency of analysis, k_B is Boltzmann's constant and T is the temperature. Thereby we obtain spectral densities of phase and amplitude reflection fluctuations

$$S_\varphi = 4k_0^2 \sum_{j=1}^{N} [(\alpha_j - 1)^2 S^c(\Omega)_j + S^s(\Omega)_j], \tag{2.23}$$

$$S_\Gamma = 4k_0^2 \sum_{j=1}^{N} \beta_j^2 S^c(\Omega)_j. \tag{2.24}$$

The first sum can be simplified and the second is zero in assumption of a "good mirror" and $\lambda/4$ layers:

$$S_\varphi = 4k_0^2 \sum_{m=1}^{2} [S^c(\Omega)_m \left(\frac{a_m^2 \psi_m^2}{|n_1^4 - n_2^4|} - \frac{2a_m \psi_m}{|n_1^2 - n_2^2|} + N \right) + S^s(\Omega)_m N] \tag{2.25}$$

for $2N$ layers, and $S_\varphi + 4k_0^2 S_1$ for $2N+1$ layers, where $a_m = n_m^2$ for zero outer impedance ($2N$ layers with $n_1 > n_2$) and $a_m = n_2^2 n_1^2$ for infinite outer impedance ($2N+1$ layers).

From now on we turn phase noise into noise of effective reflecting surface displacement $S_x = \frac{S_\varphi}{4k_0^2}$, in units of m^2/Hz, at 100 Hz frequency to simplify the comparison of this type of noise with other types of noises and Fabry-Perot coordinate sensitivity.

Calculations were made for a silica-tantala mirror of 42-43 layers (21 pairs of SiO_2 Ta_2O_5 $\lambda/4$-layers on fused silica substrate with or without additional silica $\lambda/4$-layer) with he following parameters:

$$\begin{aligned} &\nu_l = 0.17, && n_l = 1.45, \\ &\nu_h = 0.23, && n_h = 2.06, \\ &Y_l = 7.2 \times 10^{10}\text{Pa}, && \phi_l = 0.4 \times 10^{-4}, \\ &Y_h = 14 \times 10^{10}\text{Pa}, && \phi_h = 2.3 \times 10^{-4}, \\ &\lambda = 1.064 \times 10^{-6}\ \text{m}, && w = 0.06\ \text{m}, \qquad T = 290\ \text{K}. \end{aligned}$$

The results are shown in Table 1 as a correction to Brownian (displacement) noise $\chi = \frac{\sqrt{S_{Br}} - \sqrt{S}}{\sqrt{S_{Br}}} \times 100\%$. Numerical estimates for the relative power transmittance noise $\delta\tau/\tau = 2\Gamma\sqrt{S_\Gamma}/(1-|\Gamma|^2)$ is less than 10^{-12} $\mathrm{Hz}^{-1/2}$.

Table 1. Silica-tantala mirror efficiencies relative to the Brownian noise. The standard LIGO coating consists of 41 Layers+$\lambda/2$ cap mirror. Modified cap has optical width $\lambda/4$ (42 layers case).

Type	$42 \times \lambda/4$	$41 \times \lambda/4 + \lambda/2$	$43 \times \lambda/4$
Transmittance τ, ppm	2.28	1.08	0.54
Brownian $10^{-20}\mathrm{m}/\sqrt{\mathrm{Hz}}$	0.632	0.635	0.645
χ with interference	1.96%	2.34%	1.75%
χ with photoelasticity	2.33%	1.85%	1.31%
χ modified cap	2.33%	2.76%	1.81%

The interference correction to thermal coating thickness noise is about 6%, or 7.5% when taking photoelasticity into account. The thickness fluctuations of the tantala layer are much smaller than its bending ($\xi_h^c = 0.36\xi_h^s$). That is why the interference correction to the total coating Brownian (displacement) noise is only about 2.0%, or 2.3% when taking photoelasticity into account.

3. Optimization strategies

3.1. Additional top layer-corrector

One may tweak the thickness of the topmost "correcting" layer in an attempt to minimize the noises using interference effects. This method proved to be useful for thermoelastic and thermorefractive

noises [10]. Using formulas (2.7)-(2.8) we can obtain

$$S_\varphi = \sum_{m=1}^{2} [S^c(\Omega)_m \left(\frac{a_m^2 \psi_m^2}{|n_1^4 - n_2^4|} - \frac{2a_m \psi_m}{|n_1^2 - n_2^2|} + N \right) + S^s(\Omega)_m N] + S_c'$$

$$S_c' = \left[\mathrm{Re} \left(\frac{z_{2N+c+e}}{\widetilde{z}_{2N+c}} \right) (1 \pm \gamma_c \sin(\phi_c)) n_c \psi_c - n_e \right]^2 S^c(\Omega)_c + S^s(\Omega)_c \tag{3.26}$$

for $2N$ layers, and $S_\varphi + 4k_0^2 S_1$ for $2N+1$ layers, where $a_m = n_m^2 n_c \,\mathrm{Re} \left(\frac{z_{2N+c+e}}{\widetilde{z}_{2N+c}} \right)$ and "+" for zero impedance of last but one layer ($2N+c$ layers with $n_2 < n_1$) and $a_m = \frac{n_2^2 n_1^2}{n_c} \,\mathrm{Re} \left(\frac{z_{2N+1+c+e}}{\widetilde{z}_{2N+1+c}} \right)$ and "$-$" for infinite impedance of last but one layer ($2N+1+c$ layers). The index "c" represents one cap layer corrector.

Results are quite unfavorable: for an even number of layers + cap the minimum of noise is at $n_c < 1$ while its suppression $\chi = \frac{\delta\sqrt{S}}{\sqrt{S_{unmod}}} \times 100\%$ is only 0.04%. For odd layers + cap absolute value of noise doesn't become lower than 6.198×10^{-20} m$/\sqrt{Hz}$, which means that the suppression is less than 0.69% (for $n_c = 3.6$; $d_c = 0.42\lambda/4$). Even after removing a pair of layers, the noise is about 6.04×10^{-20} m$/\sqrt{Hz}$, which is more than in the case of an even number of layers.

This means that standard coating with top silica $\lambda/2$ layer is reflectivity-optimized and "all $\lambda/4$" coating (cap$= \lambda/4$) is noise-optimized (see Table 1).

3.2. Layer-corrector inside the mirror

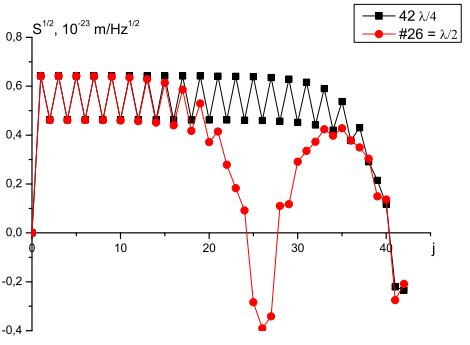

Fig. 4. Noise coefficient distribution in a coating with 42 layers, keeping the sign. Silica substrate, vacuum medium (squares – simple mirror; circles – a mirror with modified layer #26 (16 from top) $d_m = 0.98\lambda/2$).

The idea of inserting a resonant layer into the mirror is proposed in [15]. This case was studied numerically (Fig. 4). The maximum suppression of 4.4% was shown by layer-corrector close to

$d = \lambda/2$, which is the resonant cavity. But such modification increases power transmittance more than two orders of magnitude. If we add eight bilayers to restore transmittance, suppression will be more than eliminated (-14%).

3.3. Two-sided and double mirror.

A novel combined structure was proposed in [14]. This composite mirror has just a few layers on the front side of a big silica substrate, and other layers at the the bottom (two-sided mirror or Khalili etalon). The idea is that only top layers can imprint Brownian (displacement) noise on the phase of reflected light, while bottom layers do not contribute as they do not directly reflect incoming beam (just some residual power). In this case we should pay attention to interference effects, because first layers and substrate are well penetrated by light. This also means that coating noise and substrate noise in combined structures should be treated simultaneously as there is a possibility of interferential compensation (Figs. 5,2.13).

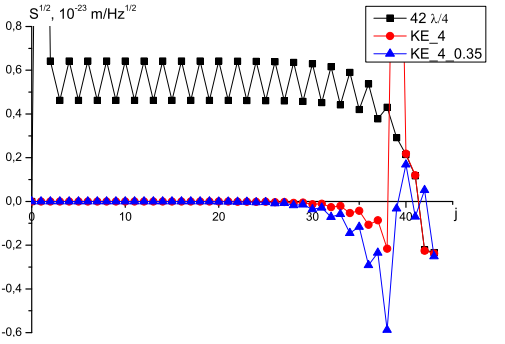

Fig. 5. Noise distribution in two-sided mirror, keeping the sign. Silica substrate, vacuum medium. Squares – $\lambda/4$ general coating; circles – corresponding etalon with $\lambda/4$ substrate; triangles – etalon, optimized for interference.

The main difficulty with the Khalili etalon is its high sensitivity to the manufacturing precision and fluctuations of its optical thickness produced by other sources. Namely the imprecision of substrate optical length by $0.07\lambda/4$, corresponding to the mirror's temperature variation of 6 mK, increases noise by 5%.

The same idea may be realized in another geometry (double mirror or Khalili cavity) with combined end mirror consisting of two individually suspended mirrors separated by a controlled gap. The first mirror has small number of layers and hence low noise, while the layers of the second one provide the required reflectivity. The sensitivity to the gap length is two times higher, though it may be controlled with actuators in real time yielding desired conditions. Our calculations show encouraging suppression of noise in both schemes. The deficiency of both schemes, however, is high power circulating in the mirror's substrate, which leads to various thermal lensing and detuning effects.

The absolute value of maximum effect is highly dependent on the ratio of thickness and bend noise spectral densities, which is yet unknown. This far we can only say that noise suppression and amplification effects decrease practically linearly with $\gamma'_s = \dfrac{\xi_s^c}{\xi_s}$ (Fig. 6).

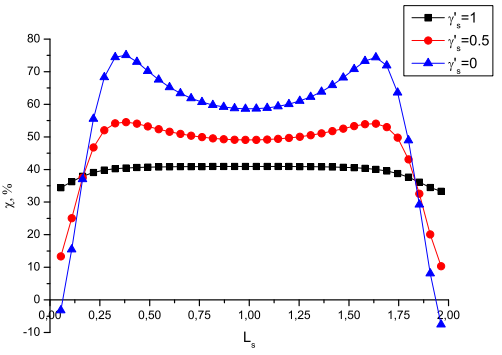

Fig. 6. Suppression as a function of excess substrate optical thickness (in units of $\lambda/4$) in addition to integer number of halfwavelengthes for different noise ratios $\gamma_s' = \dfrac{\xi_s^c}{\xi_s}$.

3.4. Modifying silica-tantala ratio

A promising way to reduce the thermal noise in the coating was proposed [3, 16], which suggests decreasing the thickness of lossy high-index (tantalum-oxide) layers, presumably preserving the total bilayer optical thickness to be $\lambda/2$ ($n_l d_l + n_h d_h = \lambda/2$). To keep the required reflectivity, more bilayers should be used. It was found numerically that there is an optimum in the ratio of layers' thickness and number of layers providing minimal noise at a given reflectivity.

It appears that noise suppression χ is highly dependent on the noise ratio in layers

$$\chi \propto \frac{S_h/d_h}{S_l/d_l} = \frac{\xi_h \phi_h n_l}{\xi_l \phi_l n_h} = \gamma, \tag{3.27}$$

For the LIGO parameters [1] $\gamma = 4.56$. In [16] coating was optimized for a chosen parameter $\gamma = 7$. An model silica-tantala mirror of 27 $\times\lambda/4$ layers+$\lambda/2$ cap was numerically optimized. Resulting coating had 16 silica-tantala bilayers with $n_l d_l = 1.383\lambda/4$, $n_h d_h = 0.617\lambda/4$, a thin cap $n_l d_l = 0.162\lambda/4$ and the first layer $n_h d_h = 0.556\lambda/4$ on substrate (34 layers total). In the experiment with this mirror design, noise suppression of $\chi_{exp} = (8.8 \pm 2.0)\%$ was observed. Our calculations with all material parameters taken from [16] yield $\chi_{th_7} = 8.2\%$, and if $\gamma = 9.23$ estimated from the same experiment is used [17], one gets $\chi_{th} = 9.1\%$.

4. Optimal coating

It is well known that for a fixed number of bilayers, a multilayer coating with quarter wave length layers (QWL) with $\varphi_h = \varphi_l = \pi$ provides the largest reflectivity [9]. The LIGO interferometers, however, require not only large reflectivity but also small noise added by the coating. The coating usually consists of two different materials having noticeably different mechanical losses. This fact stimulated mostly numerical attempts to construct more optimal coating which could have smaller noise with the increased number of layers but decreased total thickness of the "bad" component, while still preserving the desired reflectivity [3, 16]. Such coatings were found numerically and it is a common assumption that $\varphi_h + \varphi_l$ should be equal to 2π. It is possible, however, to construct a nearly perfectly optimized coating analytically and we will show that the "common knowledge"

is incorrect. In fact, previous numerical simulations clearly demonstrate that small correction is required (See Fig. 6 in [16]).

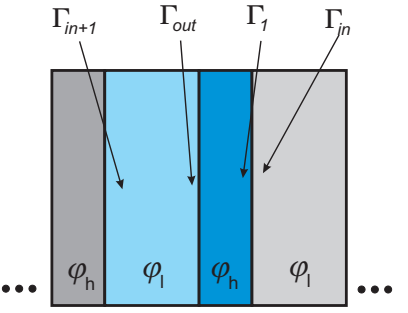

Fig. 7. A bilayer inside a multilayer coating

We would like to find optimal thicknesses of the components of a bilayer for a given thickness φ_h. Suppose we have a bilayer inside a coating and the amplitude reflectivity on the boundary to this bilayer from the side of the substrate is $\Gamma_{in} = \Gamma_0 e^{i\varphi_0}$, where Γ_0 is real amplitude and φ_0 is some initial phase. Let us introduce the following notations: $\Gamma_{in} = \widetilde{\Gamma}_0$ — initial reflectivity, Γ_1 — intermediate reflectivity, $\Gamma_{out} = \Gamma_2$ — output reflectivity, $\Gamma_{in+1} = \widetilde{\Gamma}_2$ — reflectivity, that will be initial for the next pair (see Fig. 7). Using formulas (2.5) and (2.4) two times we can find Γ_{in+1} as a function of (Γ_0, φ_0, φ_h, φ_l).

We can now find the optimal phase φ_0 maximizing $|\Gamma_{in+1}|$. Note that $|\Gamma_{in+1}| = |\Gamma_{out}|$ and does not depend on φ_l. After some math we find

$$\tan\varphi_0 = \frac{1 - g_{hl}^2}{1 + g_{hl}^2} \cot\frac{\varphi_h}{2}, \tag{4.28}$$

$$\varphi_0 \approx \frac{\pi - \varphi_h}{2} - g^2 \sin(\varphi_h). \tag{4.29}$$

In the last approximation we used the fact that $g_{hl} \simeq 0.17$ is small. It is also important that the reflectivity increases with a new pair of layers only if $\varphi_0 \in [-\frac{\pi}{2}; \frac{\pi}{2}]$ (this will be explained later). To optimize the next layer, we should provide the same input phase φ_{in} for it, which can be provided by φ_l as $|\Gamma_{in+1}|$ does not depend on it. Finally we obtain

$$\varphi_{l_j} = \varphi_{0_{j+1}} - \varphi_{0_j} - \varphi_{h_j} - 2\sin(\varphi_{h_j}) g_{hl_j}^2 + (\pi m), \tag{4.30}$$

where j stands for the bilayer number, m is integer number. For a series of identical bilayers that means

$$\varphi_l + \varphi_h = \pi m - 2\sin(\varphi_h) g^2 \tag{4.31}$$

It can be shown that in our case ($\varphi_0 \in [-\frac{\pi}{2}; \frac{\pi}{2}]$, $\varphi_h \in [0; 2\pi]$) $m > 0$ and even. As we need to shorten the coating $m = 2$. From the last equation it is clear that only in the case of QWL coating $\varphi_H + \varphi_L = 2\pi$. In other cases, however, there should be a small correction to maximize the reflection. Note that for the first layer $\Gamma_{in} = 0$ with undefined phase, thus satisfying the requirement on φ_0.

To get analytical approach consider a bilayer somewhere in the middle of coating. Suppose that incoming reflectivity is close to 1:

$$|\Gamma_{in}| = \left|\widetilde{\Gamma}_{2k}\right| = 1 - \epsilon \tag{4.32}$$

Then, expanding formulas for $|\Gamma_{out}|$ into series to the second order of ϵ and using (4.29) we obtain

$$|\Gamma_{out}|^2 = 1 - 2\alpha\epsilon - \alpha(1-2\alpha)\epsilon^2, \tag{4.33}$$

where

$$\alpha = \frac{(1-g^2)^2}{\left(g\sqrt{2(1-\cos(\varphi_1))} \pm \sqrt{1-2g^2\cos(\varphi_1)+g^4}\right)^2} \tag{4.34}$$

Here we have "+" sign, when $\varphi_0 \in [-\pi/2; \pi/2]$. It can be shown, that only in this case $\alpha \leq 1$, which means an increasing reflectivity.

Assuming $|2\alpha\epsilon| \ll 1$, $|(1-2\alpha)\epsilon| \ll 2$ we can rewrite local reflectivity as $|\Gamma_{out}| = 1 - \alpha\epsilon$ and get total power transmittance in the following form:

$$\tau = \beta(\varphi_h, \varphi_c)\alpha^N(\varphi_h)\epsilon(\varphi_e) \tag{4.35}$$

where

$$\beta = 2\frac{1-g_e^2}{1+2g_e\cos(\varphi_c + \dfrac{\pi+\varphi_h}{2} + g^2\sin(\varphi_h)) + g_e^2} \tag{4.36}$$

describes the coating-air boundary ($g_e = \dfrac{n_e - n_l}{n_e + n_l}$). For this formula to work we need to satisfy the assumptions we made. Calculations for $g = 0.17$ give $\alpha \in [0.55; 1]$. ($\alpha(\pi) = 0.55$) and $\epsilon \ll 0.5$. This also requires $\varphi_h \in [\pi/4; 7\pi/4]$. It can be shown numerically that all those requirements can be satisfied with just three initial layers on the substrate.

Now we can eliminate the total number of layers from equations to design an optimal mirror for a given power transmittance τ_0. As calculations by (2.7) - (2.8) for the total noise are rather complicated and provide small correction only, we consider the simplified formula (2.18). For the normalized spectral density we obtain

$$\begin{aligned}\frac{S_{Br}}{A} =& E\gamma\varphi_{\epsilon h} + E\varphi_{\epsilon l} - \varphi_{0\epsilon} + \varphi_0 + \\ & \frac{\ln\tau_0 - \ln\beta - \ln\epsilon}{\ln\alpha}(\gamma\varphi_h + \varphi_l) - \varphi_l + \varphi_c\end{aligned} \tag{4.37}$$

where $A = \dfrac{\xi_2\varphi_l}{2k_0 n_l}$ m^2/Hz is the dimensional constant. Here $\varphi_{\epsilon h}$ $\varphi_{\epsilon l}$ denote the phase thicknesses of the initial (first E from substrate) bilayers; $\varphi_{0\epsilon}$, φ_0 are the initial phases for initial and regular bilayers; φ_h, φ_l are regular layer thicknesses and φ_c is the cap layer thickness.

The results obtained are very close to numerical optimization in [16] (see table 2).

We found explicit formulas for the spectral density of phase noise produced by Brownian fluctuations in arbitrary multilayer coatings taking into account interference effects and photoelasticity. These effects play a role only in few top layers and give out correction of the order of 2%. Some optimization methods taking into account inerference were considered. The modifying silica-tantala ratio method was found to be the most efficient so far. Another promising approach is compound mirrors.

Table 2. Optimization results ($\gamma = 7$)

Type	$25 + \lambda/2$	[16]	Our Method
Power transmittance τ_0, ppm	277.5	277.7	277.7
χ, Brownian (displacement)	0	8.16%	8.4%
χ, with interference	3.37%	11.03%	11.27%
χ, with photoelasticity	2.63%	10.29%	10.5%
Real suppression	0	7.93%	8.18%

References

[1] Gravitational wave interferometer noise calculator (GWINC). http://gwastro.org/for scientists/gravitational-wave-interferometer-noise-calculator.

[2] B. Abbott et al. Ligo: the laser interferometer gravitational-wave observatory. *Rep. Progr. Phys.*, 72:076901:25, 2009.

[3] J. Agresti, G. Castaldi, R. DeSalvo, V. Galdi, V. Pierro, and I. M. Pinto. Optimized multilayer dielectric mirror coatings for gravitational wave interferometers - art. no. 628608. In *Proc. SPIE*, volume 6286, page 628608, 2006.

[4] B. Benthem and Yu. Levin. Thermorefractive and thermochemical noise in the beamsplitter of the geo600 gravitational-wave interferometer. *Phys. Rev. D*, 80:062004, 2009.

[5] V. B. Braginsky, M. L. Gorodetsky, and S. P. Vyatchanin. Thermodynamical fluctuations and photo-thermal shot noise in gravitational wave antennae. *Phys. Lett. A*, 264:1–10, 1999.

[6] V. B. Braginsky, M. L. Gorodetsky, and S. P. Vyatchanin. Thermo-refractive noise in gravitational wave antennae. *Phys. Lett. A*, 271:303–307, 2000.

[7] V. B. Braginsky and S. P. Vyatchanin. Thermodynamical fluctuations in optical mirror coatings. *Phys. Lett. A*, 312:244–255, 2003.

[8] M. Evans, S. Ballmer, M. Fejer, P. Fritschel, G. Harry, and G. Ogin. Thermo-optic noise in coated mirrors for high-precision optical measurements. *Phys. Rev. D*, 78:102003, 2008.

[9] Sh. A. Furman and A. V. Tikhonravov. *Basics of Optics of Multilayer Systems*. Atlantica Séguier Frontières, 1992.

[10] M. L. Gorodetsky. Thermal noises and noise compensation in high-reflection multilayer coating. *Phys. Lett. A*, 372:6813–6822, 2008.

[11] A. Gurkovsky and S. Vyatchanin. The thermal noise in multilayer coating. *Phys. Lett. A*, 374(33):3267–3274, 2010.

[12] G. M. Harry, A. M. Gretarsson, S. E. Saulson, P. R. Kittelberger, S. D. Penn, W. J. Startin, S. Rowan, M. M. Fejer, D. R. M. Crooks, G. Cagnoli, J. Hough, and N. Nakagawa. Thermal noise in interferometric gravitational wave detectors due to dielectric optical coatings. *Clas. Quantum Grav.*, 19(5):897–917, 2002.

[13] H. A. Haus. *Waves and Fields in Optoelectronics*. Prentice Hall, 1993.

[14] F. Ya. Khalili. Reducing the mirrors coating noise in laser gravitational-wave antennae by means of double mirrors. *Phys. Lett. A*, 334:67–72, 2005.

[15] H. J. Kimble, B. L. Lev, and J. Ye. Optical Interferometers with Reduced Sensitivity to Thermal Noise. *Phys. Rev. Lett.*, 101:260602, 2008.

[16] A. E. Villar, E. D. Black, R. DeSalvo, K. G. Libbrecht, C. Michel, N. Morgado, L. Pinard, I. M. Pinto, V. Pierro, V. Galdi, M. Principe, and I. Taurasi. Measurement of thermal noise in multilayer coatings with optimized layer thickness. *Phys. Rev. D*, 81:122001, 2010.

[17] A. V. Villar, E. Black, G. Ogin, T. Chelermsongsak, R. DeSalvo, I. Pinto, V. Pierro, and M. Principe. Loss angles from the direct measurement of brownian noise in coatings. In *LSC-Virgo meeting in Krakow*, number G1000937, Sep. 2010.

[18] D. A. Wille and M. C. Hamilton. Acousto-optic deflection in Ta_2O_5 waveguides. *Appl. Phys. Lett.*, 24:159, 1974.

[19] A. Yariv and P. Yeh. *Optical Waves in Crystals: Propagation and Control of Laser Radiation*. Wiley-Interscience, 2003.

S.Mayburov
Lebedev Institute of Physics,
Leninsky pr. 53, Moscow, Russia*

Photonic Communications and Information Encoding in Biological Systems

The structure of optical radiation emitted by the samples of loach fish eggs is studied. It was found earlier that such radiation perform the communications between distant samples, which result in the synchronization of their development. The photon radiation in form of short quasi-periodic bursts was observed for fish and frog eggs, hence the communication mechanism can be similar to the exchange of binary encoded data in the computer nets via the noisy channels. The data analysis of fish egg radiation demonstrates that in this case the information encoding is similar to the digit to time analogue algorithm.

Keywords: photonic communications; communication mechanism; biological systems. PACS number(s): 73.21.La, 03.67.Hk

1. Introduction

Currently, the term ”biophotons” is attributed to the optical and UV photons emitted by the living bio-systems in the processes which are different from standard chemi-luminescence. Their systematic measurements by the low-noise electronic photo-detectors was started about 1978 [1, 2]; the biophoton production (BP) in optical and close UV range was established now for large amount of bio-systems [3, 4]. It was found that its rate and other parameters are quite sensitive to the characteristics of bio-system and its development. Because of it, the biophoton measurements are applied now in many different fields from medical diagnostics to agriculture and ecology [2].

The energy spectrum of biophotons is nearly constant within optical and soft UV range practically for all studied bio-systems, so it essentially differs from the spectra expected for the system with the temperature about 300^0 K, which in this range should fall on 15 orders of magnitude [2,3]. The detailed BP mechanism is still unknown, but such excitations can be stipulated by the biochemical reactions, in which oxygen atoms are bound to the proteins and acids [2,3]. The typical bio-photon rates are quite low, however, the multiple experiments evidence that such radiation can perform the effective signaling between distant bio-systems. In particular, being radiated by the growing organism or plant and absorbed by the similar one at the distance about several cm, it can rise the rate of cell division (mitosis) in it up to 30% relative to the standard values. This phenomenon called mitogenetic effect (ME) is extensively studied in the last years [2,3]. Note that the artificial constant illumination by the visible light, even 10^4 times more intense, can’t induce the comparable gain. The communications of some other types were reported also; for the bio-systems in the state of abrupt stress or slow destruction (apoptosis) such radiation can change the state of other bio-systems in the similar depressive way [2,5].

*E-mail: mayburov@sci.lebedev.ru

Until now, ME and other biophoton properties can't be described within the standard framework of cellular biology. In our previous paper the model of information exchange between the bio-systems by means of optical radiation was proposed [6]. We've assumed that the main features of such communications can be similar to the information exchange between the distant computers by the binary encoded messages. This hypothesis is prompted by the experiments which show that the radiation of some species consists of narrow quasi-periodic bursts (fig. 1), so its time structure is similar to the sequence of electronic or photonic pulses which transfer information in the computer communication channels [1,4]. To check our model in more detail we performed the data analysis for the radiation from loach fish eggs measured by the photomultipliers [1,3]. Here some our results on the radiation structure are described, in particular, the possible algorithm of photon signal encoding in the fish egg communications is obtained.

2. Model of Bio-System Communications

Before considering the photon exchange between the distant bio-systems, it's worth to discuss how such communications can be released inside the same dense bio-system. The optical and UV excitations in the dense media exist as the quasi-particles called excitons which can spread freely through the whole media volume [7]. They are strongly coupled with electromagnetic field, so they can be effectively produced during the photon absorption by the media, the inverse process results in the photons emission from the system volume. It's established experimentally now that the excitons play the important role in the energy transfer inside the bio-systems, in particular, during the photosynthesis in plants and bacteria [8,9]. Photon production related to the nonlinear excitons in protein molecules was studied in [10]. In our model the excitations of biological media as the whole play the main role in biophotons generation and absorption by the bio-system. We don't considered any model dynamics, however, for such distances it's inevitably should have the solitonic properties [7]. Hence our model supposes that the excitons spread freely over all the volume of bio-system. In that case the exciton exchange can constitute the effective system of signaling and regulation of the bio-system development. The experiments evidence that such long-distance signaling regulates effectively the plant growth, preventing from the large fluctuations of its global form, i.e. defines their morphogenesis [2,3].

As was noticed above, BP rate is quite low, about $10\,photons/cm^2 sec$ from the surface of large, dense bio-system. If the corresponding field isn't coherent, then it described as the stochastic ensemble of photons. Then at its best the absorption of single photon or narrow bunch of photons can be detected by the bio-system as the single independent 'click' or one bit of information, analogously to standard photodetector devices. This is the photocounting regime of electromagentic field detection well-known in quantum optics [11]. We suppose that the same approach is applicable also for the excitons produced and absorbed in the same bio-system. Under these assumptions, the exciton signaling between two parts of the same bio-system and photon signalling between two distant bio-systems can be quite similar.

It can be expected that the signals which control the cell mitosis and other functions can be similar to the standard discrete (binary) encoded messages transferred between two computers via the noisy communication channels [6]. The origin of such similarity can be understood from the simple reasoning without exploit of information theory machinery. Plainly, for the low exciton or photon radiation rates, typical for bio-systems, the most important problem for the effective signal transfer is to suppress the background. Even for the bio-systems in complete darkness it induced by many sources, like the natural radioactivity, luminescent chemical impurities, etc.. Consequently, as the main criteria characterizing the efficiency of information exchange, the signal to noise ratio K_O can be used, i.e. the ratio of registrated 'clicks' induced by the bio-system signals and the background. It's natural to suppose that the evolution of living species made the information exchange by

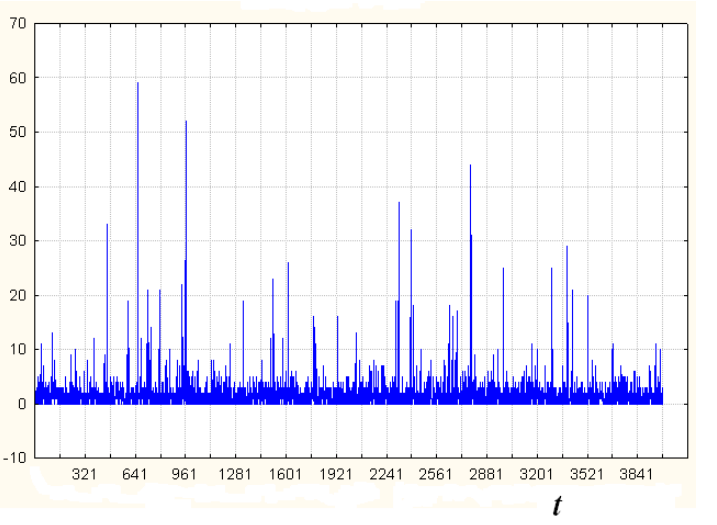

Fig. 1. Example of biophoton time spectra for development stage 16, full time scale 400 sec

means of photon radiation/absorption practically optimal. The average rate of background radiation normally should be constant in time, so for given bio-system with the limited radiation intensity the optimal method to achieve high K_O level is to make the main bulk of the bio-system radiation to be concentrated inside the short time intervals, i.e. the bio-system radiation should be in the form of bursts which would encode the signals transferred to other bio-systems. The experiments with fish eggs, fibroblast cells and other bio-systems demonstrated that the biophotons are radiated by the short-time (less than 1 msec) quasi-periodic bursts [1,4]; the typical time spectrum for fish eggs radiation is shown on fig. 1.

The influence of biophoton exchange on the organism development was found for many species, in particular their detailed study was performed for the eggs of loach fish ($Misgurnus fossilis$). Note that for the egg colony produced by the fish during its breeding the maximal rate of larvae survival is achieved, if all eggs would develop with the same speed. However, the small variations of temperature and water flow over colony volume and other external factors tend to violate this condition. It seems that the biophoton signaling between distant eggs of the same colony restore their simultaneous development. The results for the optical contacts during 30-50 min between two samples of fish eggs A,B of slightly different age demonstrate the significant synchronization of their development ([1] and refs. therein). However, it was found also that the optical contacts between the fish eggs of significantly different ages result in the serious violations of development in both samples, for fish eggs at early stages the development can simply stop. Those results evidence that the photon signals emitted by fish eggs of different age can have the essentially different structure, which encode the information about their age and corresponding development program.

3. Analysis of Experimental Data

The possible signal structure was exploited for the experimental data on the optical radiation of loach fish eggs. The studied sample is the colony about 200 eggs, which is confined in the quartz

container filled with water, their optical and soft UV radiation from the container surface was registrated by the photo-multiplier. Its intensity was summed over the nonoverlapping consequent time intervals (bins) with the duration $\Delta = .1$ sec; the experimental run normally consists of $6 * 10^3$ such bins [1]. The measurements were performed for the different development stages, from the earliest ones (cleavage) to the latest 33-35 stages, preceding the free larvae appearance; the average stage duration is about 1.5 hour. The background radiation was measured for the empty container .

Since the background is supposedly stochastic and there is no time correlations between its intensity at different time moments, then the burst periodicity or some other time correlations between them would help to discriminate the background more effectively. Simultaneously, the variations of such correlations can also encode the different signals send by the bio-system. It was supposed that such encoding is performed by the methods and algorithms similar to the standard ones used for noisy communication channels [6]. In this framework, as the model example it can be supposed that the separate message send by the bio-system consists of N bursts of the same height I_r with time interval T_r between them, such messages are divided by the periods of 'silence' T_s when the detectable radiation is similar to the stochastic background, i.e. each message constitutes the burst cluster and such messages divided by T_s intervals are repeated many times [6]. Plainly, for the realistic bio-systems those parameters would have some stochastic spread $\sigma_I, \sigma_T, \ldots$ around the average values.

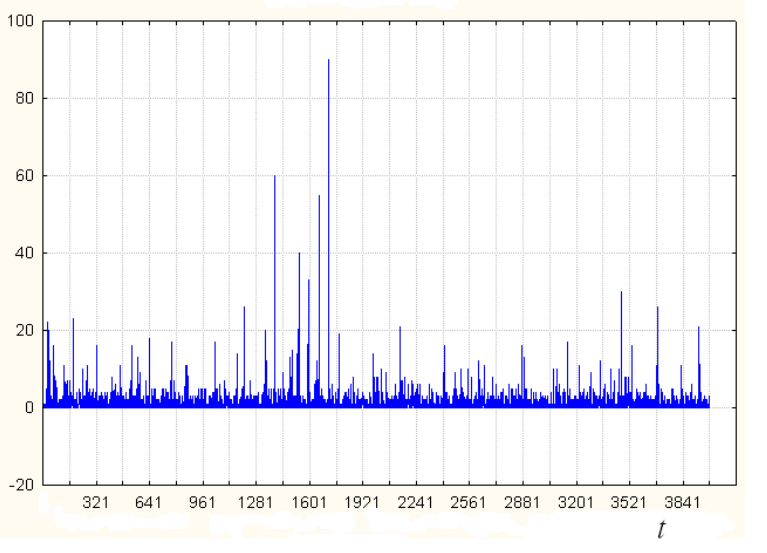

Fig. 2. Example of 'message' send by fish eggs at the development stage 32, full time scale 400 sec

First, we studied the discrimination of fish eggs radiation against the background, for which the burst distribution should be random with the arbitrary expectation values of burst amplitude $\bar{I}$ and time interval $\bar{T}$ between the neighbor bursts. The fish eggs radiation is expected to have more periodical structure, for example, if the burst radiation of fish eggs is strictly periodical, i.e. it can be approximated as:

$$A(t) = I_r \delta(t - nT)$$

for arbitrary integer n, then its fourier time spectra is equal to:

$$a_\nu = \int_0^\infty A(\tau)\cos\nu\tau\, d\tau = I_r\delta(\nu - \frac{\pi l}{T}) \tag{3.1}$$

for integer l and $0 < l \leqslant \infty$. Thus, the burst periodicity is reflected in fourier spectra as the sequence of periodical peaks, whereas for background one can expect $\bar{a}_\nu = \bar{I}$, i.e. is constant function with some fluctuations around its average value. Hence Fourier analysis of time spectra can be exploited to discriminate the periodic radiation from the background; STATISTICA-7.0 program packet was used for the data processing.

The preliminary analysis of radiation data has shown that in terms of our model example the typical duration of biophoton "message" is about 10^2 sec and $\bar{N} = 8.5$, i. e. $\bar{T}$ is about 12 sec, whereas T_s is about $4 * 10^2$ sec. From those estimates it follows that the density of fourier time spectra $f(\nu)$ should be calculated for each consequent set of 1200 bins in given run separately, i.e. 5 spectra for each run. In this template the density $f(\nu) = a_\nu^2 + b_\nu^2$ where b_ν is the value of corresponding fourier integral (3.1) for $\sin\nu\tau$. Then for each spectra f its autocorrelation:

$$g_l = \frac{\sum_0^M f(i)f(i+l)}{\sum_0^M f^2(i)} \tag{3.2}$$

was calculated for integer i, l, taking into account the finite length of run and its discreteness $M = \pi\Delta^{-1}$. The sum R of g_l modules over such set is used as the selection criteria:

$$R = \sum_0^M |g_l|$$

It was found that for arbitrary R threshold which selects about 80% of fish eggs runs, only $16 \pm 4\%$ backgorund runs are selected for $12 - 16$ stages ($10 \div 15$ hours after fertilization) and $23 \pm 6\%$ for $30 \div 34$ stages. It evidences that the fish eggs radiation has more periodical structure than the stochastic background, the possible candidate for such periodical signal (message) is shown on fig. 2. After such selection it was found that the individual messages have the length about $.6 \div 1.5 * 10^2$ sec and they are interspersed by the periods of silence about $3 \div 6 * 10^2$ sec. Each message consists of $6 - 14$ distinct high bursts, despite significant fluctuations, their amplitudes I demonstrate gaussian-like dependence on the time distance from the message centre (see fig. 2). In each individual message the time intervals T between the neighbor bursts with I higher than some threshold I_0 are nearly the same with some dispersion or differ by the whole number, i.e. are equal to $2T, 3T$, etc.. Yet T average value can differ from one message to another significantly, about factor 1.6.

Concerning the dependence of signal form on development stage, our analysis indicates that the most pronounced change suffers $\bar{T}$ value. To demonstrate it, the inclusive (i. e. over all run) T distributions for the bursts with I higher than $I_0 = 15$ units (see fig. 1) were obtained for several development stages. To enlarge statistics, we summed in the same plot the data for $8 - 11$, $12 - 16$ (fig. 3) and $30 - 34$ stages (fig. 4). Under these conditions the total exposition time for each plot was 130 min.. For each distribution the systematic errors are negligible, the statistical errors for each experimental point are equal to $N_{events}^{\frac{1}{2}}$, where N_{events} is the abcyssa value in this point. The obtained $\bar{T}$ expectation values are equal to $\bar{T} = 11.2 \pm .3$, $\bar{T} = 9.2 \pm .3$ and $7.1 \pm .2$, sec

for $8 \div 11$, $12 \div 16$ and $30 \div 34$ stages correspondingly. Meanwhile, the average number of bursts is nearly the same for all three cases, whereas the average burst amplitude $\bar{I}$ for $30 - 34$ stages is about $15 - 20\%$ larger than for $8 - 11$ stages, yet the overlap of their I distributions is essentially larger than for T distributions.

The essential feature of all three plots is the presence of several large peaks, which are effectively higher than the possible statistical error limits. Their parameters need further analysis, but it's worth to notice that for $8 - 11$ and $12 - 16$ stages two most prominent peaks seems to be generically connected, shifting from 5 to 6 sec and from 10.3 to 10.8 sec. Note also that T maxima positions of three largest peaks for $8 - 11$ stages are related approximately as $1 : 2 : 4$.

The obtained distinctions explain, probably, how the radiation from fish eggs of different age can influence the "detector" samples in a different way. Despite that the difference of signal parameters is only statistical, the multiple repetition of such messages can be eventually percepted by the "detector" fish eggs as the different instructions which would be fulfilled during their subsequent development. It seems that the most important for their encoding is T difference, because the burst amplitude produce mainly the threshold effect, i.e. only the condition like $I > I_0$ is accounted for some arbitrary I_0 which is proper for given bio-system. If those conclusions will be confirmed by further experiments, it would mean that the main encoding algorithm for fish eggs radiation has the analogue realization, despite the produced signal is constituted by the sequence of discrete bursts. Such information encoding is similar to the digital-time analogue (DTA) algorithm used in some electronic systems. Note that the similar encoding of electric pulses supposedly is exploited in the brain neuron chains [8].

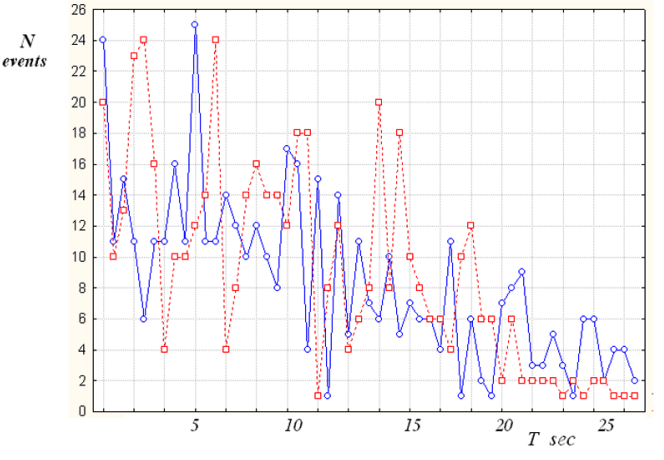

Fig. 3. T distribution for fish eggs radiation; solid line: $8 \div 11$ stages; broken line $12 \div 16$ stages

Our model assumes that the bio-system's field is noncoherent, yet it's worth to consider also the possibility that this e-m field of bio-system can possess the spacious short-time coherence within the observed photon bursts, similarly to the coherence of laser pulse. Some experiments evidence that such biophoton coherence really takes place [12]; in this experimental set-up the transparent quartz plate was installed between the inductor and detector bio-systems. In the first run the plate parallel surfaces were smooth and polished, so that it doesn't perturb the phase relations between the different pieces of wave front of incoming photons. In another run, the plate has the random deflections from the surface parallelism, which violated such phase relations, and so resuly in the violation of the impact wave coherence. It was found that in comparison with the control sample of

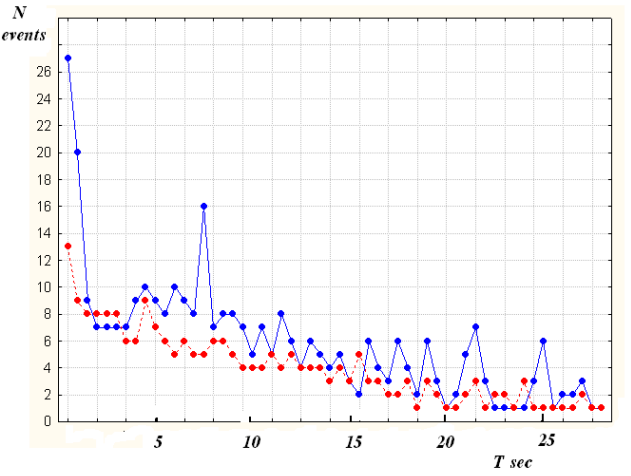

Fig. 4. T distribution for fish eggs radiation; solid line: $30 \div 34$ stages; broken line — background

isolated bio-system, the radiation passed through the random surface results in the gain of mitosis rate of 20%, yet for smooth surface it reach the rate of 45%. In our framework, it's reasonable to suppose that the field with such "transversal" coherence more effectively produce the collective excitations in the cells cluster, than noncoherent field. If this hypothesis is correct, then such coherence effects will not change the principal scheme of communications proposed here, rather, it would enlarge its efficiency.

For the conclusion the obtained results can help to reveal the mechanism of communications between the distant samples of fish eggs and permit to describe the universal features of biophoton signaling between the separate bio-systems. The similar mechanism can, on the all appearances, describe the exciton signaling inside the dense bio-system. The cell signaling and regulation features are well studied for the extracellular biochemical reactions [8]. Concerning the chemical signaling in the tissues, its efficiency and precision is principally restricted by the molecular diffusion effects inside the bio-system media and so can transfer the signals only for small distances. Note also that the exciton signaling inside organism can be much faster, than the chemical one by means of molecular messangers. Hence it can be efficient in case of stress or the abrupt change of external conditions. Experimental results show that under the different stress conditions the photon rates from bio-system can rise in short time significantly, probably, as the consequence of intensive internal signaling [2, 3].

Author is thankful L.V. Beloussoff and I.V. Volodiaev for providing the experimental data files and the extensive consultations on the related topics.

References

[1] Beloussov, L.V.: Ultraweak photon emission in cells and fish eggs. BioSystems 68, 199-212, (2003)

[2] VanWijk, R.: Biophotons and biocommunications. J. Sci. Explor. 15, 183-209, (2001)

[3] Popp, F.A. et al.: Photon radiation from organisms and plants. Collect. Phenomena 3, 187-198, (1981)

[4] Beloussov, L.V. , Burlakov, A.B.: Ind. J. Exp. Biol., Structure of photon radiation from biological systems. Ind. J. Exp. Biol. 41,424-430, (2003)

[5] Farhadi, A. et al.: Evidence of non-chemical, non-electrical intercellular signaling. Bioelectrochemistry Vol.71,142-148, (2008)

[6] Mayburov, S.: Biophoton production and communications. In Proc. of Int. Conf. on Nanotechnology and Nanomaterials, MGOU Publishing, Moscow, pp. 351-358, (2009)

[7] Davidov, A.: Solitons in Molecular Physics. Kluwer, Dortreht, (1991)

[8] Shubin, A.F.: Biophysics. Moscow, Nauka, (1998)

[9] Engel, G.S. et al.: Evidence for wave-like energy transfer in photosynthetic systems. Nature 446, 782-787, (2008)

[10] Brizhik, L.: Delayed luminescence of biological systems. Phys. Rev. E64, 031902-031917, (2005)

[11] Glauber, R.J.: Quantum Optics. Academic Press, N-Y, (1969)

[12] Budagovsky A.: In: Biophotonics and Coherent Systems in Biology. Springer, Berlin, pp. 81 - 94, 2007

V. Movchanskaya
Moscow State University of M.V.Lomonosov

Computation of the molecules' ground states and binding energies by Monte Carlo method

The structure of optical radiation emitted by the samples of loach fish eggs is studied. It was found earlier that such radiation perform the communications between distant samples, which result in the synchronization of their development. The photon radiation in form of short quasi-periodic bursts was observed for fish and frog eggs, hence the communication mechanism can be similar to the exchange of binary encoded data in the computer nets via the noisy channels. The data analysis of fish egg radiation demonstrates that in this case the information encoding is similar to the digit to time analogue algorithm.

Keywords: ground states; Monte Carlo method.
PACS number(s): 73.21.La

1. Introduction

The problem of finding molecular ground states and binding energies is a start of simulation of quantum dynamics. Monte Carlo method was chosen to perform this task.

In the quantum version of static diffusion Monte Carlo method particle is represented as a swarm of copies and after the process converges density of the swarm is equal to the modulus of the wave function of the ground state. This equation shows the limitations of the method, since it can't be used as a probabilistic model of quantum dynamics, where density of the swarm should be equal to the square-wave function. The underlying reason of this discrepancy is static nature of Monte Carlo method, i.e. it's not intended to simulate dynamics. Dynamics requires description of the excited states, not just the ground one. Nevertheless, Monte Carlo method can be regarded as a good beginning for the construction of real dynamic model.

2. Problem statement

We consider stationary Schredinger equation:

$$-\frac{\hbar^2}{2m}\triangle\psi + U\psi = W\psi$$

It's required to find the ground state of one or two atoms with one or two valence electrons. I.e. we need to find the function ψ_0 corresponded to the lowest energy eigenvalue $W_0 < W_1 \leq ... \leq W_{n-1} \leq W_n$. To resolve the task we need to know atom numbers and the distance between the nuclei in case of two atoms. Total energy of the system in the resulting state has to be close to the obtained experimentally value. Also we have to find the binding energy for two atoms, which corresponds to a well depth of the binding potential. Found values have to be compared with the

known values. Then it will be possible to make a conclusion about accuracy of the method and its future applicability.

3. Monte Carlo method

3.1. Description

The particle is represented as a swarm of copies, for which next principle of evolution is used:

1.Let the each instance jumps $\triangle x$ along any of the coordinate axes in positive or negative direction with the same small probability p. It remains in place with probability $1 - 6p$ in 3-dimensional case.

2.Let the instance be in potential U. Then next rule of creation / destruction of instances is used. If $U < 0$, then this instance creates the new one, located at the same point, if $U > 0$, then this instance destroys other one, located at a distance less than $\triangle x$.

This process converges to the modulus of the wave function of the ground state.

We consider Schredinger equation:

$$i\hbar\frac{\partial\psi}{\partial t} = -\frac{\hbar^2}{2m}\triangle\psi + U\psi$$

Making the substitution $t = -i\tau$, where $\tau = it$ is imaginary time, we obtain:

$$-\hbar\frac{\partial\psi}{\partial\tau} = -\frac{\hbar^2}{2m}\triangle\psi + U\psi$$

Rewrite it as:

$$\frac{\partial\psi}{\partial\tau} = \frac{\hbar}{2m}\triangle\psi - \frac{U}{\hbar}\psi \tag{3.1}$$

Consider one-dimensional case:

$$\triangle\psi = \frac{\psi(x+\triangle x) + \psi(x-\triangle x) - 2\psi(x)}{\triangle x^2}$$

If $U = 0$ and τ is real time, then equation (3.1) describes the change of the swarm's density in the static diffusion process (using the rule of jumps) up to a constant. In this case ψ is density of the swarm.

If $U \neq 0$, addition $-\frac{U}{\hbar}\psi$ corresponds exactly to the previously introduced rule of creation / destruction.

Consequently, equation (3.1) describes static diffusion process up to a constant, i.e. $\psi = C\rho$.

Further, we have the decomposition of the wave function:

$$\psi(t,x) = \sum_{n=0}^{\infty} C_n \cdot e^{-\frac{i}{\hbar}W_n t} \cdot \psi_n(x),$$

where W_n is energy eigenvalue.

Making the change $t = -i\tau$, we get:

$$\psi(t,x) = \sum_{n=0}^{\infty} C_n \cdot e^{-\frac{1}{\hbar}W_n \tau} \cdot \psi_n(x)$$

Decomposing exponent and noting that $W_0 < W_1 \leq ... \leq W_{n-1} \leq W_n$, we have:

$$\psi(t,x) = C_0\psi_0(x) + \sum_{n=1}^{\infty} C_n \cdot e^{-\frac{1}{\hbar}W_n\tau} \cdot \psi_n(x) \longrightarrow C_0\psi_0(x),$$

if $\tau \to \infty$.

Thus, indeed, the process should stabilize at a distribution proportional to the modulus of the ground state. Note that for this to execute C_0 is required to be large enough so that the initial distribution of the swarm is close to the one that should be in the ground state of the system. To make it, at the initial Hartree-Fock method is often used to the system, and the resulting state is taken as the initial for Monte Carlo method.

As can be seen instances don't have speed in Monte Carlo method, they have only the coordinates. It means Monte Carlo method is static and it's not intended to simulate dynamics.

Method can be directly generalized to the case of n(two or more) particles. In this case instance would be a tuple of n copies, one for each particle.

3.2. The case of two particles

The general function describing the state of a system of two electrons in the nuclear field, defined as the product of the coordinate functions Ψ and the spin functions Φ. This general function must be antisymmetric following the Pauli principle. Such antisymmetric expressions for the general function are the following four:

$$\Psi_S\Phi_a = \frac{1}{\sqrt{2}}(\psi_{ik} + \psi_{ki})[\varphi_+(1)\varphi_-(2) - \varphi_+(2)\varphi_-(1)], \tag{3.2}$$

$$\Psi_a\Phi_{S_1} = \frac{1}{\sqrt{2}}(\psi_{ik} - \psi_{ki})\varphi_+(1)\varphi_+(2),$$

$$\Psi_a\Phi_{S_2} = \frac{1}{\sqrt{2}}(\psi_{ik} - \psi_{ki})[\varphi_+(1)\varphi_-(2) + \varphi_+(2)\varphi_-(1)], \tag{2}$$

$$\Psi_a\Phi_{S_3} = \frac{1}{\sqrt{2}}(\psi_{ik} - \psi_{ki})\varphi_-(1)\varphi_-(2).$$

The first of these four functions (3.2) corresponds to the sum of the spin quantum numbers $m_{S_1} + m_{S_2} = 0$, the other three to the values: $m_{S_1} + m_{S_2} = +1, 0, -1$. Since each of the quantum numbers m_{S_i} determine projection of the spin moment p_{S_i} to the preferred direction, then, consequently, the sum of the quantum numbers $m_{S_1} + m_{S_2}$ determine projection of the result spin moment P_S on the same direction. This projection takes the four values corresponding to the four values of specified sum $m_{S_1} + m_{S_2}$. It means the quantum number S, that determines the result spin moment P_S, takes two values: $S = 0$ and $S = 1$. We have singlet terms of atoms and ions with two valence electrons and zero projection of the result spin moment P_s corresponding to the value $S = 0$, the triplet terms and three possible values of the projections P_S corresponding to the value $S = 1$. To get the singlet state of the system described by the first equation of (3.2), where the coordinate function Ψ_S is simmetric, at each step of the diffusion process we need to ensure the condition:

$$\rho(r_1, r_2) = \rho(r_2, r_1).$$

To obtain the triplet state of the system described by the other three equations of (3.2), where the coordinate function Ψ_a is antisimmetric, at each step of the method we need to realize the requirements:

$$\rho(r_1, r_2) = \rho(r_2, r_1),$$
$$\rho(r_1, r_1) = 0.$$

4. Algorithms

4.1. Algorithm of finding the ground state

1.We create object model with given parameters, this action includes definition of the nuclei's position and initial uniform distribution of electron instances in the space.

2. In the loop step of Monte Carlo method is performed, where the following actions are done over each instance:

1) Calculation of the potential acting on the instance. The potential U consists of the Coulomb interaction potential between the particles of one tuple and potential between the nuclei and the particles of one tuple.

2) Analysis of the directions' number, where the jumps could be done.

3) Making jumps in the neighbour cells with a small probability p , if we consider two electrons, then the symmetric instances perform the same jumps.

4) An instance remains at the same place with probability $1 - dim \cdot p$, where dim is the number of directions along which jumps were done.

5) Birth / destruction of instances in the current cell with probability $Cv \cdot U$, where $Cv = \frac{d\rho_j}{d\rho_V}$, $d\rho_j$ is the density's change of the tuple in consequence of jump, $d\rho_V$ is the density's change of the tuple in consequence of potential effect.

6) Destruction of instances with zero density.

7) If we consider two electrons, the density of symmetrical copies are made equal.

8) If we consider the triplet state, then the instances, in which both electrons are in the same cell of the configuration space, are removed.

3. Check for convergence: if the density of all instances at this step differs from the density at the previous lower than a number ε, then the process is finished and we exit the previous cycle.

4. In any case we control the constancy of particles' number by changing zero of potential energy.

5. If the process is converged, the density is normalized so that the sum of its square across the configuration space equal to unity.

6. If the process is converged, we calculate the total energy as the sum of interaction energies of nuclei and electrons, electrons with each other and nuclei themselves:

$$E = -\sum_n \sum_i \frac{{\rho^2}_i Z_n}{r(i, i_n)} + \sum_{j1,j2} \frac{{\rho_{j1j2}}^2}{r(j_1, j_2)} + \frac{Z_1 Z_2}{r(i_1, i_2)},$$

where ρ_i is the density at the i-th point, Z_n is the charge of the n-th nucleus, $r(i, j)$ is the distance between the i-th and j-th points, i_n is a cell that contains the n-th nucleus, ρ_{j1j2} is the density of the tuple at the point(j_1, j_2) and $e = 1$. The last term is absent if we consider a single nucleus.

4.2. Algorithm of finding the binding energy of two atoms

1. We carry out a number of experiments described in previous algorithm, where we increase the distance between the nuclei.

2. Compute the difference between the minimum energy and the energy, calculated for the maximum distance between the nuclei.

5. Results

The table shows the values of the obtained energy taking into account electron-electron interaction (E_0) , without it (E_1) and experimentally obtained values E in Hartree units, values of calculation error are in parentheses:

	H	H_2+	$BeH+$	$CH+$	He (singlet)	He (triplet)	H_2 (singlet)
E_0	-0.5	0.08082(7%)	0.11200(8%)	0.13200(0.3%)	-2.663(8%)	-2.304	0.150(10%)
E_1	-0.5	0.08082(7%)	0.11200(8%)	0.13200(0.3%)	-3.461(19%)	-2.681	0.195(17%)
E	-0.5	0.09701	0.12127	0.13229	-2.904		0.166

Fig. 1

Energy value of the helium atom in the triplet state is greater than in case of the singlet state, it coordinates with the theory. Since energetically most profound state of the helium atom corresponds to symmetric (singlet) solution of the Schredinger equation.

Resulting potential of the hydrogen molecule in the triplet state is not binding.

The figure shows the characteristic shape of the total energy's dependence on the distance between two Coulomb centers (nuclei) for one and two electrons:

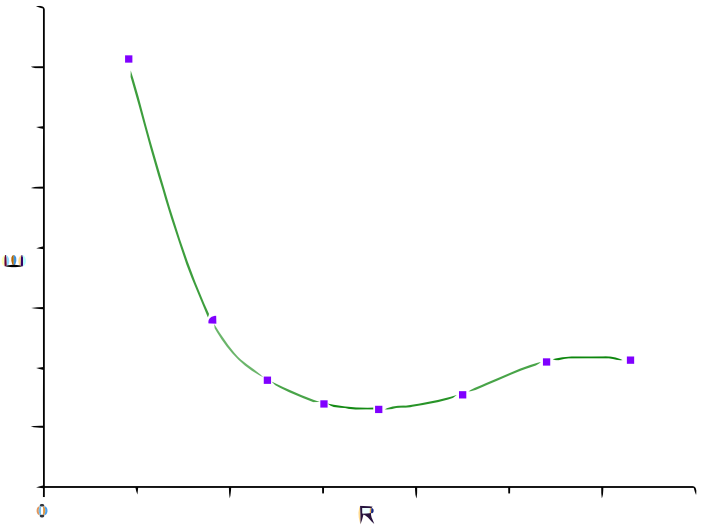

6. Conclusion

Thus, the algorithms for building the ground states and calculating the binding energies of molecules with one or two valence electrons are constructed. Monte Carlo method was chosen as a base.

These data of the total energies and binding energies for some of the particles are verified with experimental results. Based on this comparison, we can say that the built implementation has a good accuracy and can be used to find the binding energies.

References

[1] Yu.I.Ozhigov *Constructive physics.* M.; Izhevsk: RCD, 2010; Nova Science Publisher, 2011.

[2] S.E.Frish *The optical spectra of atoms.* M.; L.: Physmatgiz, 1963.

[3] *Tables of physical quantities. Reference book.* Edited by academician I.K.Kikoin. M.: Atomizdat, 1976.

[4] John Preskill *Lecture Notes for Physics 229: Quantum Information and Computation.* 1998.

[5] R. Feynman, R. Leighton, M. Sands *The Feynman Lectures on Physics. Vol. 8, 9. Quantum mechanics.* M.:Mir,1978.

[6] A.S.Davydov *Quantum mechanics.* M.:Nauka, 1973.

[7] L.D.Landau E.M.Lifshitz *Quantum mechanics. Nonrelativistic theory.* M.:Nauka, 1989.

Martín Rivas
Theoretical Physics Department, University of the Basque Country, Bilbao, Spain *

The mechanism of tunneling and formation of bound pairs of electrons

The classical description of elementary spinning particles shows that the center of mass and center of charge of an elementary particle are different points. This separation is half Compton's wave length and because of this the interaction of two electrons with their spins parallel can produce a bound pair provided the internal phase is opposite and the relative velocity of their centers of mass is below a certain limit. It is also this separation which justifies that an electron under a potential barrier can cross it with an energy below the top of the potential provided the spin is properly oriented and the barrier has a narrow range. This can justify the spin polarized tunneling effect.

Keywords: tunneling effect; bound pairs of electrons.
PACS number(s): 73.21.La

1. Two centers

Let us think that the following classical analysis was performed before 1920, i.e., before the emergence of quantum mechanics. The assumption is that the center of mass $\boldsymbol{iq}$ and the center of charge $\boldsymbol{ir}$, of a charged elementary spinning particle are two different points. If this is the case we can define the angular momentum of the particle with respect to both points. Let us call $\boldsymbol{iS}$ the angular momentum w.r.t. the center of charge (CC for short) and $\boldsymbol{iS}_{CM}$ the corresponding angular momentum w.r.t. the center of mass (CM for short). They are not independent, because if $\boldsymbol{ip}$ is the linear momentum of the particle, then $\boldsymbol{iS}_{CM} = (\boldsymbol{ir} - \boldsymbol{iq}) \times \boldsymbol{ip} + \boldsymbol{iS}$. But both spins satisfy two different dynamical equations in the free case and under some external electromagnetic interaction.

For any arbitrary inertial observer, the total angular momentum of the particle w.r.t. the origin of observer's frame can be written either as

$$\boldsymbol{iJ} = \boldsymbol{ir} \times \boldsymbol{ip} + \boldsymbol{iS}, \quad \text{or} \quad \boldsymbol{iJ} = \boldsymbol{iq} \times \boldsymbol{ip} + \boldsymbol{iS}_{CM}.$$

If the particle is free, $\boldsymbol{iJ}$ is conserved and thus

$$\frac{d\boldsymbol{iJ}}{dt} = 0 = \frac{d\boldsymbol{ir}}{dt} \times \boldsymbol{ip} + \frac{d\boldsymbol{iS}}{dt}, \quad \text{or} \quad \frac{d\boldsymbol{iJ}}{dt} = 0 = \frac{d\boldsymbol{iq}}{dt} \times \boldsymbol{ip} + \frac{d\boldsymbol{iS}_{CM}}{dt},$$

so that

$$\frac{d\boldsymbol{iS}}{dt} = \boldsymbol{ip} \times \boldsymbol{iu}, \quad \text{or} \quad \frac{d\boldsymbol{iS}_{CM}}{dt} = 0,$$

because the conserved $\boldsymbol{ip}$ is along the CM velocity $\boldsymbol{iv} = d\boldsymbol{iq}/dt$, but not along the CC velocity $\boldsymbol{iu} = d\boldsymbol{ir}/dt$. The CM spin is a conserved observable for a free particle while the CC spin is not. It is moving in an orthogonal direction to the linear momentum, and only its projection on $\boldsymbol{ip}$, the helicity $\boldsymbol{iS} \cdot \boldsymbol{ip}$, is conserved.

*martin.rivas@ehu.es

Let us assume now that the particle is under some external electromagnetic force $\boldsymbol{i}F$ defined at the CC position. In this case, $\boldsymbol{i}J$ and $\boldsymbol{i}p$ are no longer conserved and thus $d\boldsymbol{i}J/dt = \boldsymbol{i}r \times \boldsymbol{i}F$ and $d\boldsymbol{i}p/dt = \boldsymbol{i}F$.

$$\frac{d\boldsymbol{i}J}{dt} = \boldsymbol{i}r \times \boldsymbol{i}F = \frac{d\boldsymbol{i}r}{dt} \times \boldsymbol{i}p + \boldsymbol{i}r \times \frac{d\boldsymbol{i}p}{dt} + \frac{d\boldsymbol{i}S}{dt},$$

$$\text{or} \quad \frac{d\boldsymbol{i}J}{dt} = \boldsymbol{i}r \times \boldsymbol{i}F = \frac{d\boldsymbol{i}q}{dt} \times \boldsymbol{i}p + \boldsymbol{i}q \times \frac{d\boldsymbol{i}p}{dt} + \frac{d\boldsymbol{i}S_{CM}}{dt},$$

$$\frac{d\boldsymbol{i}S}{dt} = \boldsymbol{i}p \times \boldsymbol{i}u, \quad \text{or} \quad \frac{d\boldsymbol{i}S_{CM}}{dt} = (\boldsymbol{i}r - \boldsymbol{i}q) \times \boldsymbol{i}F.$$

The CC spin satisfies the same dynamical equation as in the free case, it moves in an orthogonal direction to the linear momentum, although now $\boldsymbol{i}p$ is not conserved. The CM spin satisfies the usual torque equation: the torque of the external force w.r.t. the CM is the time variation of this spin.

Both spins can be found in the literature. The Bargmann-Michel-Telegdi spin [1] is the covariant generalization of the CM spin. The CC spin satisfies the same dynamical equation as Dirac's spin operator in the quantum case.

2. Classical model of a Dirac particle

If an elementary spinning particle has two separate centers, the free motion implies that the CM is moving at a constant velocity $\boldsymbol{i}v$. But, what about the CC motion? If the motion is free it means that we are not able to distinguish, at two different instants, a different dynamical behaviour. But if the trajectory of the CC is a regular curve (i.e. a continuous and differentiable trajectory) it means that the velocity of the CC has to be of a constant modulus, the same at any time, and the trajectory of a constant curvature and torsion. The CC travels along a helix at a constant velocity, and this description must be valid for any inertial observer.

This implies that the CC velocity has to be unreachable for any inertial observer. Otherwise, if some inertial observer is at rest w.r.t. the CC at a certain instant t, because the CC motion is accelerated, it will have for that observer, a velocity different from zero at a subsequent time, and thus contradictory with the assumption that the velocity is of constant absolute value for any inertial observer. The only possibility is that the CC velocity is the speed of light and only a relativistic treatment is allowed.

This is precisely the main feature of a classical model of an elementary particle, which satisfies Dirac's equation when quantized, we have developped [2]. The free motion of this model is depicted in Figure 1, where we see the straight motion of the CM and the helical motion at the speed of light of the CC. We also depict the two above mentioned spins, $\boldsymbol{i}S$ and $\boldsymbol{i}S_{CM}$. The total spin $\boldsymbol{i}S$ has two parts $\boldsymbol{i}S = \boldsymbol{i}Z + \boldsymbol{i}W$, one $\boldsymbol{i}W$ related tom the rotation of the particle and in the direction of the angular velocity while the *zitterbewegug part* $\boldsymbol{i}W$ is due to the separation between CC and CM and has the opposite direction, as depicted in figure 2.

3. Dirac's analysis of the electron

In his original 1928 papers [3, 4] Dirac describes an electron in terms of a four-component spinor $\psi(t, \boldsymbol{i}r)$, defined at point $\boldsymbol{i}r$, and a Hamiltonian

$$H = c(\boldsymbol{i}p - e\boldsymbol{i}A(t, \boldsymbol{i}r)) \cdot \boldsymbol{\alpha} + \beta mc^2 + e\phi(t, \boldsymbol{i}r)$$

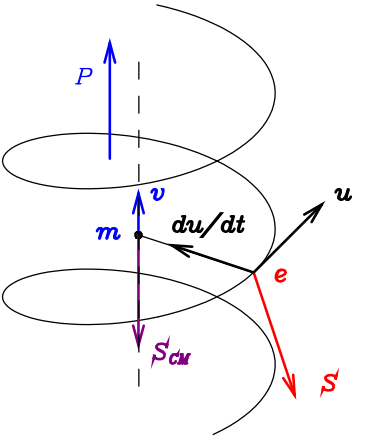

Fig. 1. Model of a free classical Dirac particle, with two separate centers, showing the precession of the CC spin $\boldsymbol{i}S$ and the conserved CM spin $\boldsymbol{i}S_{CM}$. The CC moves along a helix at the speed of light. The CC spin is always orthogonal to the velocity and acceleration of the charge and precesses around $\boldsymbol{i}p$. The separation between CC and CM is $\hbar/2mc$, half Compton's wavelength, and the frequency of this internal motion, in the CM frame, is $2mc^2/h$. It is described in [2].

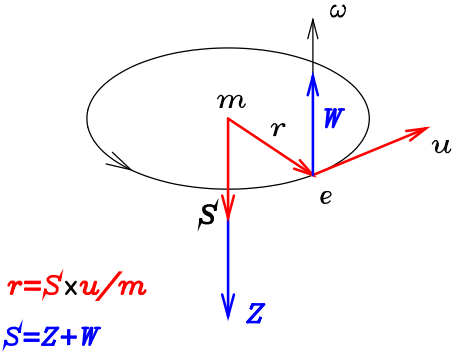

Fig. 2. The classical description of a spinning Dirac particle in the CM frame. The CC $\boldsymbol{i}r$ moves at the speed of light. The spin has two parts, one $\boldsymbol{i}W$ related to the rotation of the particle and another in the opposite direction $\boldsymbol{i}Z$ related to the zitterbewegung part of the motion of the CC around the CM.

where β and $\boldsymbol{\alpha}$ are Dirac's matrices and ϕ and $\boldsymbol{i}A$ the scalar and vector external potentials, also defined at the point $\boldsymbol{i}r$.

When computing the velocity of point $\boldsymbol{i}r$, Dirac arrives at: $\boldsymbol{i}u = i/\hbar[H, \boldsymbol{i}r] = c\boldsymbol{\alpha}$, which is expressed in terms of α matrices and writes, '*... a measurement of a component of the velocity of a free electron is certain to lead to the result* $\pm c$. *This conclusion is easily seen to hold also when there is a field present*', because it holds even if the external potentials are not vanishing.

The point $\boldsymbol{i}r$ oscillates in a region of order of Compton's wavelength: '*The oscillatory part of* x_1 *is small, ... , which is of order of magnitude* $\hbar/mc$, ...'. This is the amplitude of the motion of the CC around the CM in our model.

The linear momentum does not have the direction of the velocity $\boldsymbol{i}u$, but must be related to some average value of it: ... '*the* x_1 *component of the velocity,* $c\alpha_1$, *consists of two parts, a constant part* $c^2 p_1 H^{-1}$, *connected with the momentum by the classical relativistic formula, and an oscillatory part, whose frequency is at least* $2mc^2/h$, ...', the same as in the above classical model.

The total angular momentum w.r.t. the origin of observer's frame, takes the form

$$\boldsymbol{i}J = \boldsymbol{i}r \times \boldsymbol{i}p + \frac{\hbar}{2}\boldsymbol{\sigma} = \boldsymbol{i}r \times \boldsymbol{i}p + \boldsymbol{i}S$$

where the orbital part $\boldsymbol{i}r \times \boldsymbol{i}p$ and the spin part $\boldsymbol{i}S = \hbar\boldsymbol{\sigma}/2$, are not separately conserved for a free electron but the spin satisfies,

$$\frac{d\boldsymbol{i}S}{dt} = \frac{i}{\hbar}[H, \boldsymbol{i}S] = \boldsymbol{i}p \times c\boldsymbol{\alpha} = \boldsymbol{i}p \times \boldsymbol{i}u.$$

even under some external interaction. This is the dynamical equation of the CC spin.

The electron, *'... behaves as though it has a magnetic moment given by*

$$\mu = g\frac{e}{2m}\boldsymbol{i}S = \frac{e\hbar}{2m}\boldsymbol{\sigma}, \quad g = 2,$$

an also an instantaneous electric dipole'

$$\boldsymbol{i}d = \frac{ie\hbar}{2mc}\boldsymbol{\alpha}.$$

If the previous classical analysis of an elementary particle with two separate centers is taken into account, it is not difficult to conclude that Dirac's electron is an object with two centers, described by a spinor $\psi(t, \boldsymbol{i}r)$ which is a function of the CC position $\boldsymbol{i}r$. The linear momentum is not lying along the velocity of point $\boldsymbol{i}r$, but around some average value of it. Dirac spin operator is not the angular momentum w.r.t. the CM, but it represents the angular momentum w.r.t. the CC, even under some external interaction. The magnetic moment is produced by the motion of the charge, and the separation between these two points defines an electric dipole moment $\boldsymbol{i}d = e(\boldsymbol{i}r - \boldsymbol{i}q)$.

All these features of Dirac's analysis are contained in the classical description depicted in figure 2 in which the velocity of the CC is always c.

4. Electron dynamical equations

If we call the position of the CM $\boldsymbol{i}q$, and its velocity $\boldsymbol{i}v = d\boldsymbol{i}q/dt$, $v < c$, and for the CC position $\boldsymbol{i}r$, and $\boldsymbol{i}u = d\boldsymbol{i}r/dt$, in the relativistic case always $u = c$. The dynamical equation of the spinning electron in an external electromagnetic field is computed in [5] and are given by the expressions (4.1) and (4.2). In the nonrelativistic case, the second equation (4.2) is replaced by the third (4.3) showing that the relative motion of the CC around the CM is a kind of harmonic motion with a constant frequency ω while in the relatistic case the internal frequency depends on the velocity of the CM. The internal frequency of a relativistic electron decreases with its velocity, so that a faster electron a slower internal frequency as suggested by the so called twin paradox.

$$\frac{d\boldsymbol{i}p}{dt} = e(\boldsymbol{i}E(t, \boldsymbol{i}r) + \boldsymbol{i}u \times \boldsymbol{i}B(t, \boldsymbol{i}r)), \quad \boldsymbol{i}p = \gamma(v)m\boldsymbol{i}v \tag{4.1}$$

$$\frac{d^2\boldsymbol{i}r}{dt^2} + \frac{c^2 - \boldsymbol{i}v \cdot \boldsymbol{i}u}{(\boldsymbol{i}r - \boldsymbol{i}q)^2}(\boldsymbol{i}r - \boldsymbol{i}q) = 0, \quad \text{(RELATIVISTIC)} \tag{4.2}$$

$$\frac{d^2\boldsymbol{i}r}{dt^2} + \omega^2(\boldsymbol{i}r - \boldsymbol{i}q) = 0, \quad \text{(NON REL)} \tag{4.3}$$

We shall use these dynamical equations to analyze the classical behaviour of a spinning electron in two situations: The analysis of an electron-electron interaction, and the analysis of the

interaction of a transversally polarized electron with a triangular potential barrier. In the firs case we shaw that, in addition to the usal sccatering between electrons, it is also possible that two spinning electrons with their spins parallel, can form bound states. This is done in next section. The analysis of tunnelling is defered till section 6.

5. Formation of bound pairs

We shall use the above dynamical equations to analyze the electron-electron interaction but for particles with spin. Here the fields are the electromagnetic field produced by either particle on each other.

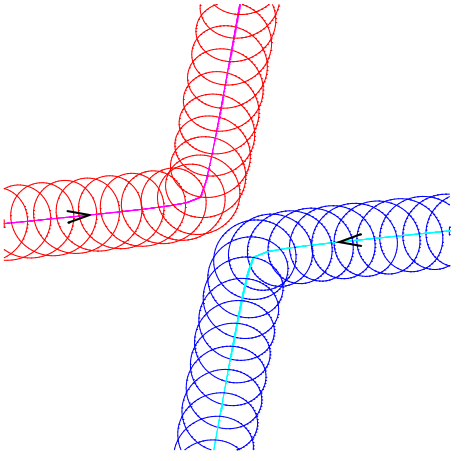

Fig. 3. Scattering of two equal charged particles with parallel spins.

See in figure 3 the scattering of two equal charged particles with parallel spins. The centre of mass motion of each particle is depicted with an arrow. If the two particles do not approach each other too much these trajectories correspond basically to the trajectories of two spinless point particles interacting through an instantaneous Coulomb force (see figure 4). By too much we mean that their relative separation between the corresponding centres of mass is always much greater than Compton's wavelength. For high energy interaction the two particles approach each other to very small distances where the interaction term and the exact position of both charges, becomes important. In this case new phenomena appear. We can have, for instance, a forward scattering, which is not described in the classical spinless case, or even the formation of bound pairs for particles of the same charge, which we shall analyse in what follows.

In figure 5 we represent an initial situation for two equal charged particles with parallel spins such that the corresponding centres of mass are separated by a distance below Compton's wavelength. Remember that the radius of the internal motion is half Compton's wavelength. We locate the charge labels e_a at the corresponding points ir_a and the corresponding mass labels m_a to the respective centre of mass iq_a. We see that a repulsive force between the charges when both charges have opposite phases implies an atractive force between the corresponding centres of mass. If the initial situation is such that the centres of mass separation is greater than Compton's wavelength, the force is always repulsive irrespective of the internal phases of the particles.

The analysis of this interaction is treated in more detail in [5]. In figure 6 we show the bound motion of both particles when their centres of mass are initially separated $q_{1x} = -q_{2x} = = 0.2\times$Compton's wavelength, $\dot{q}_{1x} = -\dot{q}_{2x} = 0.008c$ and $\dot{q}_{1y} = -\dot{q}_{2y} = 0.001c$, and opposite phases.

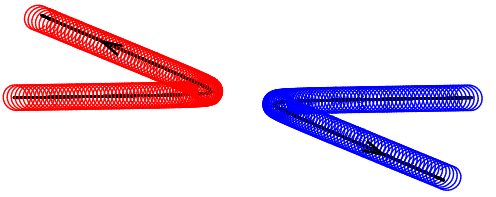

Fig. 4. Scattering of two spinning particles with parallel spins. The inner black lines represent the motion of two spinless electrons interacting through a Coulomb force, which have as initial conditions the same positions and velocities as the CM's positions and velocities of the spinning electrons. There is a small difference provided the CC's do not approach each other too much.

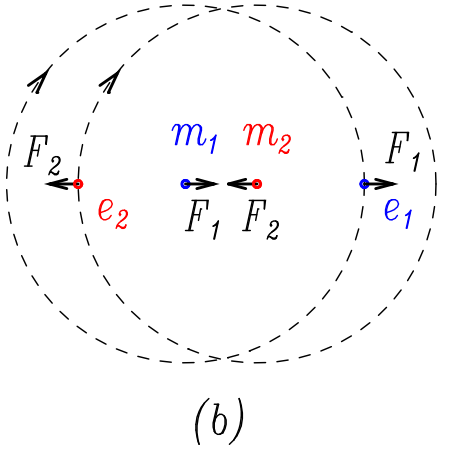

Fig. 5. Boundary values for two Dirac particles with parallel spins and with a separation between the centres of mass below Compton's wavelength. The dotted lines represent the previsible clockwise motion of each charge. If the phases are opposite the repulsive force between charges becomes an atractive force between the CM's.

We have found bound motions provided the velocity of each electron, in the CM frame, will be below $0.01c$. If the phases of the two particles are the same (or almost the same) there is no possibility of formation of a bound state. The two fermions of the bound state have the same spin and energy. They differ that their phases and linear momenta are opposite to each other. Is this difference in the phase a way to overcome at the classical level, the Pauli exclusion principle?

6. Tunneling

As a consequence of the zitterbewegung and therefore of the separation between the center of mass and center of charge, we shall see that spinning particles can have a non-vanishing crossing of potential barriers.

Let us consider the potential barrier depicted in figure 7. On the left side AC the electrostatic field produces a force on the electrons to the left while on the right side region CB, the force is to

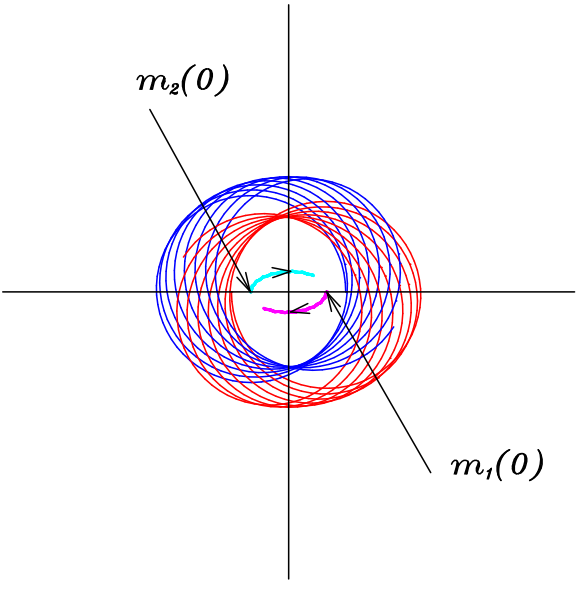

Fig. 6. Bound motion of the CC's and CM's of two spinning particles with parallel spins, and with a centre of mass velocity $v \simeq 0.008c$, for an initial separation between the centres of mass of $0.2\times$Compton's wavelength.

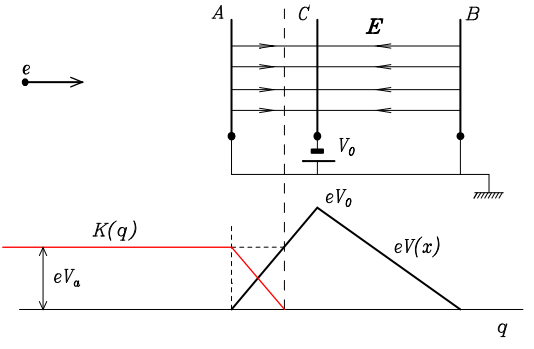

Fig. 7. Uniform field triangular potential barrier. We show in red, the variation of the kinetic energy $K(q)$ of a spinless electron. It goes to zero, when the eelctron penetrates into the barrier. Then the electron stops and is rejected backwards. A spinless electron never crosses the barrier.

the right. A spinless electron, accelerated with a potential V_a has a kinetic energy $K(q)$ such that when the electron enters into the field decreases till zero, stops and is finally rejected. A spinless electron with kinetic energy below eV_0, never crosses that barrier. However, a tranversally polarized spinning electron can tunnel the above device.

We solve the electron dynamical equations (4.1) and (4.2) in that potential of left width a and right width b, respectively, and depict in figure 8 the variation of the kinetic energy during the crossing. In this figure, the width of the potential is $a = b = 1$, i.e., in units of the separation between the CC and CM. In figure 9 we depict the variation of the kinetic energy when the right side of the potential has a width of $b = 10$ times this separation. The whole classical analysis is dimensionless so that the crossing is independent of the absolute value of the potential V_0. A more detailed analysis is done in [6]

To compare the classical crossing with the quantum one we use the solution of this quantum mechanical problem as solved by Landau [7]. The quantum probability depends on the potential V_0 and for different V_0 values is depicted in figure 10 as a function of the right width b of the barrier,

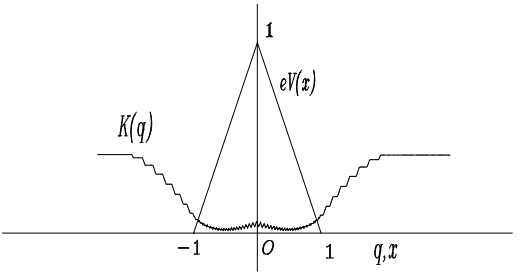

Fig. 8. Evolution of the kinetic energy of a transversally polarized electron in a triangular potential barrier of left width $a = 1$ and right width $b = 1$.

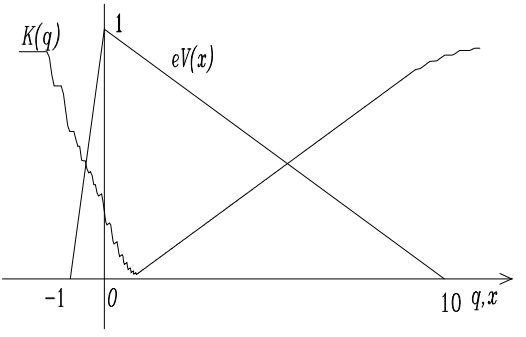

Fig. 9. Evolution of the kinetic energy of a transversally polarized electron in a triangular potential barrier of left width $a = 1$ and right width $a = = 10$.

with a fixed value for the left width a. This quantum probability has been obtained by assuming that we have electrons of a uniform distribution in energy, below the top of the potential. Simmilarly, in the same figure we shaw the classical probability of tunneling $P(b)$ computed from the previous solved equations for different values of b. If we consider for the classical spinning particle the same uniform distribution of particles, then, the function $P(b) = 1 - K_c(b)$, where $K_c(b)$ is the minimum dimensionless kinetic energy for crossing computed before, represents the ratio of the particles that with kinetic energy below the top of the potential cross the barrier because of the spin contribution.

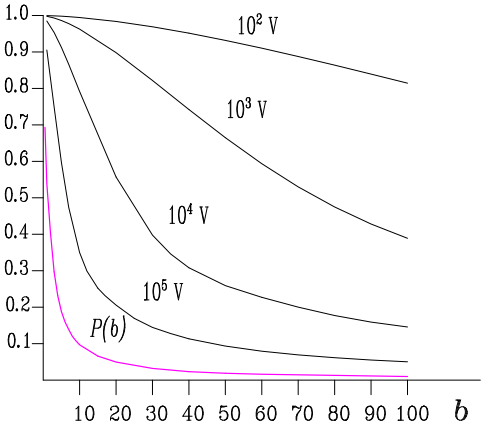

Fig. 10. Classical probability $P(b)$ and Quantum probability of tunneling for various potentials V_0. Classical Probability is independent of the potential and quantum probability decreases with V_0. The Quantum Probability is greater than the Classical Probability for crossing because of the Uncertainty Principle.

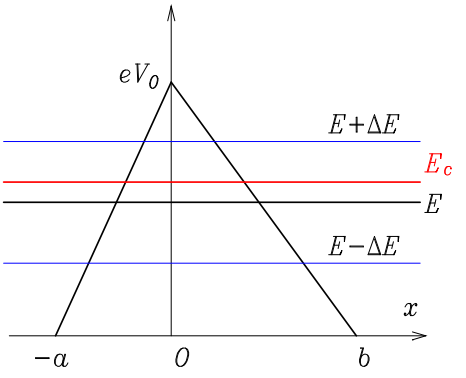

Fig. 11. Potential barrier where E_c represents the minimum kinetic energy for crossing for the classical spinning particle. For a quantum particle of kinetic energy E, the value of the crossing energy is between $E+\Delta E$ and $E-\Delta E$, with $\Delta E \Delta t_c \geqslant \hbar$, being Δt_c the uncertainty in the time of crossing. It thus implies that a quantum particle with an energy below the crossing energy, has a probability of having a greater energy than E_c and thus it crosses the barrier.

The classical probability of crossing is smaller then the quantum one because of the uncertainty principle. But when the potential V_0 rises, the quantum probability approaches the classical one. The reason is described in figure 11. If Δt_c is the uncertainty in the time of crossing the uncertainty principle implies that the uncertainty in the energy of the electron satisfies $\Delta E\ \Delta t_c \geqslant \hbar$. It therefore implies that a quantum particle with an energy below the crossing energy can have a nonvanishing probability of having a greater energy than E_c if this value lies in the range $E_c \in (E-\Delta E, E+ + \Delta E)$. This ΔE decreases when the uncertainty Δt_c increases which is the case for faster particles. This means that a quantum particle with an average energy below the crossing energy E_c, and an uncertainty $\pm\Delta E$ can cross the barrier while the classical spinning particle does not. When the potential V_0 increases the quantum probability of crossing approaches the probability computed for the classical spinning particle.

We acnokledge that this work was supported by The University of the Basque Country (Research Grant 9/UPV00172.310-14456/2002).

References

[1] Bargmann V, Michel L and Telegdi VL *Precession of the Polarization of particles moving in a homogeneous electromagnetic field Phys. Rev. Lett.* **2** 435 (1959).

[2] Rivas M *Kinematical theory of spinning particles* (Dordrecht: Kluwer) 2001.

[3] Dirac PAM *The Quantum Theory of the Electron Proc. Roy. Soc. Lon.* **A117**, 610 (1928).

[4] Dirac PAM 1928 *The quantum theory of the electron. Part II Proc. Roy. Soc. Lon.* **A118**, 351 (1928).

[5] M. Rivas *The dynamical equation of the spinning electron*, J. Phys. A, **36**, 4703, (2003), ArXiv:physics/0112005.

[6] M. Rivas *Is there a classical spin contribution to the tunnel effect?*, Phys. Lett. **A 248**, 279 (1998).

[7] L. Landau and E. Lifchitz, *Mécanique quantique*, Mir Moscow (1988), 3rd. edition.

D.A.Slavnov

Department of Physics, Moscow State University,
Moscow 119899, Russia*

Causality and probability in quantum mechanics

We discuss the causality problem in quantum theory. We show that there exists a formulation of quantum theory that, on one hand, preserves the mathematical apparatus of the standard quantum mechanics and, on the other hand, ensures the satisfaction of the causality condition for each individual event including the measurement procedure.

Keywords: quantum mechanics.
PACS number(s): 73.21.La, 03.65.-w

The causality problem has become more and more relevant in recent years. This is because it passes more and more from the domain of theoretical reasonings and Gedankenexperiments into the domain of actual experiments. Moreover, the first attempts are begin made to construct prototypes of engineering constructions in the domain of so-called quantum telecommunication. The causality (locality) problem plays a key role in this domain. The axiom of causality has different formulations [1, 2]; however, without going into mathematical subtleties, it can be reduced to the following: boson fields must commute at space-like separated points, while fermion fields must anti-commute.

The following argument is often used as a physical justification of this axiom. The results of the measurement in a bounded domain of a Minkowski space (a local measurement) are determined by boson-field values and by bilinear combinations of fermion fields in this domain.

Such locality requirement is purely mathematical in its nature. It can be formulated only in the framework of a particular mathematical formalism, and it is a part of that formalism. In a general discussion of causality it is desirable to proceed from requirements that can be formulated in physics terminology and that can be checked in the experiment directly. That is, such formulation must be fairly obvious.

It is Einstein causality. If two bounded domains $\mathcal{O}_1$ and $\mathcal{O}_2$ of the Minkowski space are space-like separated, then the results of measurements in the domain $\mathcal{O}_1$ do not depend on any manipulations in the $\mathcal{O}_2$.

Practically no one argues with the above formulation. However, the situation changes radically when we try to supplement the above requirement with the following one. There exists a certain physical reality, which determines the results of a local measurement.

Many people object to such an extension of the causality requirement. The arguments on this matter began a long time ago. One can recall the famous debates between Einstein [3] and Bohr [4]. Einstein was in favor of the above extension, while Bohr was against it.

Later on, the majority's opinion within the physics scientific community leaned towards the Bohr side. The results of many modern experiments related to this problem are currently considered as proof that the physical reality mentioned above does not exist.

However, if we abandon the extension formulated above, we almost completely lose the physical foundation behind the locality axiom accepted in the quantum field theory. This rejection

*E-mail: slavnov@theory.sinp.msu.ru

would force us to assume that neither local fields, nor their combinations describe a local reality (because it does not exist). Then, it is not clear why these combinations must commute in space-like separated domains.

Thus we have a deadlock situation. The assumption of the existence of a local physical reality contradicts the mathematical formalism of the quantum theory. At the same time, the rejection of this assumption denies the physical foundation one of the main axioms in the mathematical formalism of the quantum field theory.

However, the mathematical formalism of the quantum theory can be compatible with the assumption of the existence of physical reality determining the results of local measurements [5, 6]. The often-produced incompatibility proofs have the following two flaws. First, these proofs often point out toward a contradiction between the experimental data and certain mathematical assumptions, which are used in the construction of mathematical formalism. The questions of physical validity of these assumptions and their necessity are usually not discussed. Second, the interpretation given to the obtained experimental data is far from being always adequate.

The so-called de Broglie waves can be considered as one of the most striking examples of inadequate interpretation. In the beginning of practically any textbook on quantum mechanics it is said that a de Broglie wave with the wavelength

$$\lambda = \frac{2\pi\hbar}{k} \tag{1}$$

is associated with any quantum particle having the momentum k. The results of electron interference are mentioned as examples supporting the above statement. In agreement with (1) a clear interference pattern was observed in the experiment.

Equation (1) became the basis of subsequent assertions, that the distinctive feature of quantum particles is the presence of both corpuscular and wave properties.

These assertions seem to be quite well supported experimentally. Nevertheless, we would like to examine if this is indeed the case.

Let us turn to the results of more recent experiments performed by Tonomura [7]. These experiments investigated electron beam scattering by a biprism, which by its physical properties is analogous to a double-slit screen. The beam intensity was so low, that on average there was less than one electron in the experimental apparatus at any single moment. This allowed one to neglect the influence of electron interaction on the results of the experiment. Moreover, it was possible to register the results of passage of a small number of electrons in this experiment.

The experimental results are shown in Fig. 1. The individual photographs correspond to different exposure times. The photograph (1) registered traces of 10 electrons, (2) — 200, (3) — 6000, (4) — 40000, (5) — 140000.

When only a small number of electrons are registered (the photographs (1) and (2)) the interference is not showing through. A pattern appears only after a very large number of electrons were registered (the photographs (4) and (5)). If we try to determine the electron wavelength with a help of the photographs (1) and (2), we do not obtain anything similar to de Broglie Eq. (1).

These results speak in favor of the fact that wave properties are not revealed by a single electron. They become apparent only in a specially prepared ensemble of electrons. In the considered case, all electrons had approximately the same momentum.

Just as interference pattern, quantum state is not the characteristic of an individual physical object. It describes ensemble of such objects. Therefore, the commonly used in textbooks formulation of the mathematical formalism of the quantum theory, with wave functions or state vectors as the basic elements, is not ideal for discussions of the locality problem, because these objects themselves are obviously nonlocal.

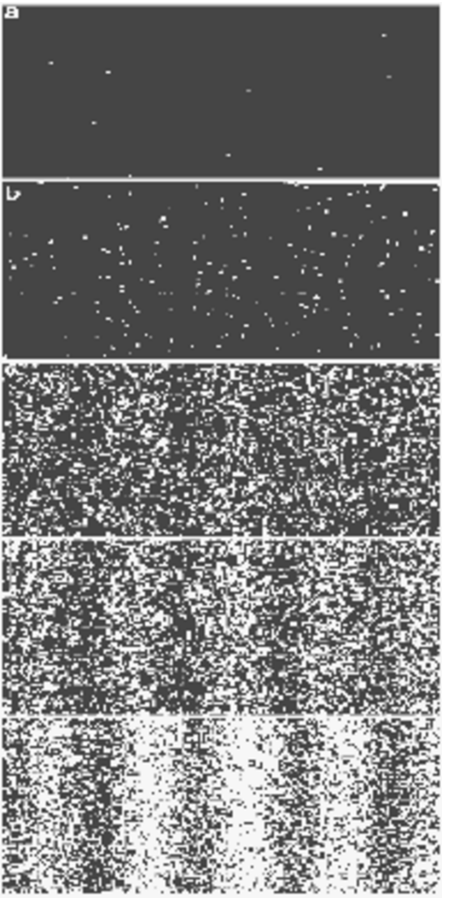

Fig. 1. Interference pattern in electron scattering: 10; 200; 6000; 40000; 140000 events

The so-called algebraic approach [8, 9] is much better suited for these purposes. Unlike the traditional approach, the Hilbert's space of state vectors is no longer a primary object of the theory within the algebraic approach, and observables are no longer defined as operators in the Hilbert space.

Observables, more specifically, local observables are considered as the primary elements of the theory. Heuristically, an observable is defined as such an attribute of the investigated physical system for which one can obtain some numerical value with the help of a certain measuring procedure. Accordingly, for local observables one can obtain numerical values with the help of local measurements.

Initially the observables are not related to operators in a Hilbert space at all. The Hilbert space itself is constructed with the help of observables as some secondary object. After that a connection between the observables and the operators in this space is established.

We will conduct the subsequent examination in the framework of a special version of the algebraic approach.

We begin from stating the basic properties of observables. The main property is the following one. The observables can be multiplied by real numbers, added to each other, and multiplied by one another. This property is formulated as the following postulate.

POSTULATE 1. The observables $\hat{A}$ of a physical system are Hermitian elements of some C^*-algebra [10].

Postulate 1 (and all the subsequent ones) is valid for classical systems as well. The set of observables will be denoted $\mathfrak{A}_+$ ($\mathfrak{A}_+ \subset \mathfrak{A}$). In classical systems all observables are compatible with each other (can be measured simultaneously). In a quantum system they can be either compatible or incompatible.

POSTULATE 2. The set of compatible with each other observables is a maximal real associative commutative subalgebra $\mathfrak{Q}_\xi$ of the algebra $\mathfrak{A}$ ($\mathfrak{Q}_\xi \subset \mathfrak{A}_+$).

The index ξ, which runs through the set Ξ, distinguishes one such subalgebra from another. For a classical system the set Ξ contains just a single element, for a quantum system Ξ contains infinitely many elements.

The set of observables $\mathfrak{A}_+$ can be considered as a mathematical model of a quantum system. Accordingly, the subset $\mathfrak{Q}_\xi$ can be considered as observables of some classical subsystem. This subsystem is open, because the quantum-system's degrees of freedom corresponding to observables from different subsets $\mathfrak{Q}_\xi$ can interact with each other.

Moreover, these classical subsystems may not have their own dynamics, because the generalized coordinates and momenta corresponding to the same degree of freedom, may belong to different subsets of $\mathfrak{Q}_\xi$. Therefore, the traditional approach for defining the state as a point of a phase space is not suitable for such subsystems. But, specifying a point in the phase space is equivalent to setting initial conditions for the equations of motion. This allows one to fix the values of all observables of the considered system.

However, one can avoid using equations of motion and the initial condition, and fix the values of all observables directly. Such an approach is suitable for open systems as well.

Measuring the sum of observables in any concrete classical system yields the sum of the values of the individual observables, and measuring the product of observables yields the product of their individual values. In other words, specifying the values of all observables is equivalent to specifying some homomorphic map of the algebra of observables into the set of real numbers. For commutative associative algebra, such a map is called a character. Therefore we accept the following postulate.

POSTULATE 3. The state of a classical subsystem, whose observables are elements of a subalgebra $\mathfrak{Q}_\xi$, is described by a character of this subalgebra.

This definition of the state of a classical subsystem has an important advantage, that it can be generalized to the quantum case. Each quantum observable belonging to $\mathfrak{A}_+$, simultaneously belongs to some subalgebra $\mathfrak{Q}_\xi$. This allows one to consider a quantum system as a family of classical subsystems. If we knew the states of all these subsystems, we could have predicted the result of measuring any observable of the quantum system. This gives us grounds for accepting the following postulate.

POSTULATE 4. The result of measuring any observable of a physical system is determined by its elementary state φ.

Here, φ is a family $\varphi = [\varphi_\xi]$ of characters φ_ξ of all subalgebras $\mathfrak{Q}_\xi$. Each subalgebra $\mathfrak{Q}_\xi$ in the family is represented by a single character.

At first it may seem that the last postulate contradicts the fact that one cannot predict the measurement results for all observables of a quantum system. However, there is no contradiction here. The point is that we can measure simultaneously (that is in a compatible way) only compatible

observables. These observables belong to a certain subalgebra $\mathfrak{Q}_\xi$. Lets say for instance they belong to the subalgebra with the index $\xi = \eta$. Then, from the complete set $[\varphi_\xi]$ we can specify only one character φ_η.

Endowed with such information we can predict only the measurement results for observables belonging to $\mathfrak{Q}_\eta$. We will not be able to say anything certain about the values of other observables. Additional measurements, if they are not compatible with the previous ones, will not improve the situation. They will produce new information about the quantum system; however, simultaneously the additional measurements will disturb the state of our system and will make the information obtained earlier worthless.

Figuratively speaking, an elementary state is a holographic image of the system under investigation. Using classical measuring devices we can look at it from one side only, and, hence, obtain a two-dimensional image. Moreover, the measurement will disturb the system and will change its original holographic image.

Therefore, if later we will look at the system from another side, we will see a two-dimensional projection of the new holographic image. Thus, we will never be able to see the entire holographic image.

In connection with the above it is useful to introduce the notion of φ_η-equivalence. Two elementary states $\varphi = [\varphi_\xi]$ e $\varphi' = [\varphi'_\xi]$ will be called φ_η-equivalent, if $\varphi_\eta = \varphi'_\eta$. The relations between the remaining characters φ_ξ and φ'_ξ can be arbitrary. The class of φ_η-equivalent elementary states will be denoted $\{\varphi\}_{\varphi_\eta}$. The most that one can possibly learn about an elementary state φ is that it belongs to some equivalence class $\varphi \in \{\varphi\}_{\varphi_\eta}$.

There is one more obstacle preventing unambiguous predictions of measurement results.

One and the same observable $\hat{A}$ may belong simultaneously to several subalgebras $\mathfrak{Q}_\xi$: $\hat{A} \in \mathfrak{Q}_\xi \cap \mathfrak{Q}_{\xi'}$ $(\xi \neq \xi')$.

Therefore, it is not clear which of the functionals (characters) φ_ξ or $\varphi_{\xi'}$ will describe the results of a particular measurement.

At first it may seem that this additional ambiguity can be easily eliminated with the help of the additional condition

$$\varphi_\xi(\hat{A}) = \varphi_{\xi'}(\hat{A}), \text{ if } \hat{A} \in \mathfrak{Q}_\xi \cap \mathfrak{Q}_{\xi'}. \tag{2}$$

However, this condition leads to numerous contradictions. On the other hand, one can show that the condition (2) is not a necessary one. Indeed, the measurement result may depend not only on the system under investigation, but on the characteristics of the measuring device as well.

From the observer's point of view such dependence is extremely objectionable, and experimentalists try to minimize it as much as possible.

We have come to think that measurement results are virtually independent of the characteristics of "good" measuring devices. However, for this to be true all the devices used for measuring the observable of interest must at least be calibrated in a consistent way. One can show that the existence of incompatible measurements in the quantum case makes such calibration far from being always possible. In particular, if we assign a certain type of measuring devices (ξ-type) to every subalgebra $\mathfrak{Q}_\xi$, then, as it turns out, the devices of different types cannot be calibrated consistently. Therefore, one cannot get rid of a possible dependence of the measurement results on the device type (or, on the index ξ).

Thus, value of an observable is not attribute of physical system. Such attribute (local physical reality) is the elementary state.

The above assertion does not exclude that for some elementary states φ Eq. (2) will be valid for all $\mathfrak{Q}_\xi$, $\mathfrak{Q}_{\xi'}$, containing the observable $\hat{A}$. In this case we shall say that the elementary state φ is stable with respect to the observable $\hat{A}$.

Measurements allow one to establish that the elementary state φ of the system under investigation belongs to some equivalence class $\varphi \in \{\varphi\}_{\varphi_\eta}$. Thereafter, we can make the following predictions. Measuring devices of the η-type will yield the value $A = \varphi_\eta(\hat{A})$ for the observable $\hat{A} \in \mathfrak{Q}_\eta$. From now on the measurement result is denoted by the same symbol as the observable itself, but without the "hat."

If the elementary state φ is stable with respect to the observables $\hat{A} \in \mathfrak{Q}_\eta$, then the same result will be obtained by using measuring devices of any type ξ. One cannot say anything definite about measurement results for observables $\hat{A} \notin \mathfrak{Q}_\eta$, because we will obtain different values for different elementary states $\varphi \in \{\varphi\}_{\varphi_\eta}$.

Within the standard mathematical formalism of quantum mechanics all the physical properties mentioned above are exhibited by quantum states specified by particular values of a complete set of commuting observables. This allows one to state the following definition of a quantum state within the proposed approach.

DEFINITION. A quantum state Ψ_{φ_η} is the class $\{\varphi\}_{\varphi_\eta}$ φ_η- equivalent elementary states, which are stable with respect to the observables $\hat{A} \in \mathfrak{Q}_\eta$.

It is usually assumed that a quantum state Ψ_{φ_η} appears as a result of measuring the observables $\hat{A} \in \mathfrak{Q}_\eta$, where a specified value is registered for each of the observables $\hat{A}$ Of course, this is not always true, at least, because some particles of the investigated system can be absorbed by the device in the measuring process. In order for a measurement to be simultaneously a preparation of a quantum state, it must be reproducible. If repeated measurements of an observable $\hat{A}$ give identical results, we shall mean the measurements reproducible. Note that the repeated measurements are not necessarily performed by measuring devices of the same type.

Within the standard mathematical formalism of quantum mechanics pure states are defined as vectors $|\Phi >\rangle$ of some Hilbert state $\mathfrak{H}$.

These vectors are used for calculating the average values of observables in the corresponding quantum states. This definition works very well for applied purposes; however, it does not have an intuitively clear physical interpretation. Within the approach proposed in the present work the average value of an observable is connected in a natural way with the probability distribution of the elementary states φ within the equivalence class $\varphi \in \{\varphi\}_\eta$.

One has to bear in mind that the elementary states satisfy the standard properties of elementary events from the classical Kolmogorov probability theory [11]. Namely, each random experiment results in one and only one elementary event. Different elementary events are mutually exclusive.

Note that the standard approach to quantum mechanics does not have such an ingredient. This became an insurmountable obstacle for application of the classical probability theory to quantum mechanics. Such an obstacle is absent within the approach used here. Therefore, there is no need for creating some artificial quantum probability theory. Instead one can use the well-developed formalism of the classical probability theory. Therefore, the following postulate appears to be fairly natural.

POSTULATE 5. The equivalence class $\{\varphi\}_{\varphi_\eta}$ corresponding to the quantum state Ψ_{φ_η} can be equipped with the structure of a probability space.

Then, the mean value of the observable $\hat{A}$ in the quantum state Ψ_{φ_η} is given by the formula

$$\Psi_{\varphi_\eta}(\hat{A}) = \int_{\varphi \in \Psi_{\varphi_\eta}} P_{\hat{A}}(d\varphi)\, \varphi_\xi(\hat{A}), \tag{3}$$

where

$$P_{\hat{A}}(d\varphi) = P(\varphi : \varphi_\xi(\hat{A}) \le A + dA) - P(\varphi : \varphi_\xi(\hat{A}) \le A),$$

and $P(\varphi : \varphi_\xi(\hat{A}) \le A)$ is probability measure corresponding to the event $\varphi : \varphi_\xi(\hat{A}) \le A$.

In order for formula (3) to define the quantum average, the probabilistic measure must satisfy the following postulates.

POSTULATE 6. The functional Ψ_{φ_η} is linear over the algebra $\mathfrak{A}$.
and

POSTULATE 7. The functional does not depend on the particular choice of ξ.

One can show [5] that such distribution actually exists.

With the C^*-algebra and a linear positive normalized functional $\Psi_{\varphi_\eta}(\cdot)$ defined over this algebra, we can construct a representation of the algebra $\mathfrak{A}$ by using the Gelfand-Naimark-Segal canonical construction [12]. In other words, we can construct Hilbert space $\mathfrak{H}$, in which there is an operator $\Pi(\hat{A})$ acting over a space $\mathfrak{H}$ that corresponds to each element $\hat{A} \in \mathfrak{A}$, while the expectation value $\langle\Phi|\Pi(\hat{A})|\Phi\rangle$, where $|\Phi\rangle \in \mathfrak{H}$ is the corresponding vector in Hilbert space — to the quantum average $\Psi_{\varphi_\eta}(\cdot)$. This is the way the standard mathematical apparatus of quantum mechanics is reproduced.

Thus, there are two paths leading to the same result. One can fix the algebra of observables, and build on it a set of elementary states corresponding to some quantum states. Then, one can endow this set by the structure of a probability space and, finally, calculate the probabilistic averages.

The alternative path is the following one. Fix a Hilbert space, define observables as linear operators in that space, while quantum states are either vectors of that space, or density matrices. The average values of observables are defined as the mathematical expectations of the corresponding operators with respect to either vectors of the Hilbert space, or density matrices.

Usually the second path turns out to be much more convenient from the pragmatic point of view. However, the first path has a better physical foundation. This allows one to create a more or less intuitively clear picture of the quantum world. In particular, our model allows one to present an intuitively appealing interpretation of quantum phenomena [6], whose traditional interpretation looks absolutely absurd from the classical physics point of view.

The list of such phenomena includes quantum particle scattering on a double-slit screen, the Einstein-Podolsky-Rosen paradox [13], the delayed choice experiment [14], and quantum teleportation [15].

References

[1] *N. N. Bogolioubov and D. V. Shirkov* Introduction to the Theory of Quantized Fields. World Sci., Singapore, 1982.

[2] *R. Streater and A. S. Wightman* PCT, Spin and Statistics and All That. Benjamin, New York, 1964.

[3] *Einstein A.* Physics and Reality // Journal of the Franklin Institute, V. 221, PP. 313-347, 1936.

[4] *Bohr N.* Discussion with Einstein on Epistemological Problems in Atomic Physics, in Albert Einstein: Philosopher-Scientist, Ed. by PA. Schlipp (La Salle, Open Court, 1949), P. 201.

[5] *Slavnov D.A.* // Phys. Part. Nucl, V.38, P. 147, 2007.

[6] *Slavnov D.A.* // Phys. Part. Nucl, V.41, P. 149, 2010.

[7] *Tonomura A.*// PNAS V.102. No 42. P.14952, 2005.

[8] *Araki H.* // Progr.Theor.Phys. V. 32, No 5. P. 844, (1964).

[9] *Haag R., Kastler D.* // J. Math. Phys. V. 5, No 7. P. 848, 1964.

[10] *Dixmier J.S.* , C^*-Algebras, Elsevier, North-Holland, Amsterdam, 1977.

[11] *Kolmogorov A. N.* // Foundations of the Theory of Probability, Chelsea, New York, 1956.

[12] *Naimark M. A* , Normed Algebras, Wolters-Noordhoff, Groningen, 1972.

[13] *Einstein A., Podolsky B., and Rozen N.* // Phys. Rev. V. 47, P. 777, 1935.

[14] *Wheeler J.A.* Mathematical Foundation of Quantum Theory. New York: Academic Press 1978

[15] Physics of Quantum Information, Ed. by Bouwmeester D., Ekert A., and Zeilinger A., Springer, Berlin, Heidelberg, 2001

A.A. Suzko and E.P. Velicheva
Joint Institute for Nuclear Research, 141980 Dubna, Russia
JIPENP, National Academy of Sciences of Belarus, Minsk

Darboux transformations for generalized Schrödinger equations

The Darboux transformation technique and point canonical method are used to obtain a family of exactly solvable Schrödinger equations with a position-dependent effective mass and with linearly energy-dependent potentials. The approach is illustrated by some examples.

Keywords: Darboux transformation technique, position-dependent effective mass, energy-dependent potentials.
PACS number(s): 73.21.La, 03.65.-w

1. Introduction

In resent years quantum mechanical systems with position-dependent mass and with energy-dependent potentials have attracted attention due to their applications in quantum micro- and nanoelectronics, photoelectronics and optoelectronics, nuclear and atomic physics, semiconductor theory and so on. There are many different theoretical methods are used to study of these systems, in particular such modern and power technique as Darboux transformation method. Darboux transformations have been constructed for a variety of linear and nonlinear equations [1–3]. Among the linear equations to which the Darboux transformations are applicable, there are common Schrödinger equations, Schrödinger equations with position-dependent effective mass [4–9], Schrödinger equations with energy-dependent potentials [10–13] and so on. Darboux transformations are usually constructed by means of the intertwining relations technique. Within the intertwining operator method, solutions of two differential equations of the same type, e.g. two Schrödinger equations, are connected by means of a linear differential operator, called the Darboux or intertwining operator. If the initial Hamiltonian is exactly solvable, then the Darboux transformation generates a new solvable Hamiltonian with the spectrum different from the initial one by a single bound state. The iterative applications of the procedure allow one to generate families of Hamiltonians with a predetermined spectrum, removing or adding new bound states. We think that the method of Darboux transformations for the Schrödinger equation with effective mass and with energy dependent potentials extends the set of exactly solvable models and this, in its turn, extends the opportunities for study of low-dimensional structures needed in quantum engineering.

The position-dependent mass equation is an important particular case of the generalized Schrödinger equation, since it is extensively used in condensed matter physics. The Darboux transformation allows one to obtain a family of exactly solvable equations from each of exactly solvable equation with position-dependent mass. However, a few exactly solvable effective mass Schrödinger equations are known that can be used by physicists as generic equations. In resent years the point canonical transformation method is often used [14], [15] to convert a general second order differential equation into another solvable equation. However, this approach can be applied to very

particular equations with position-dependent mass functions (see, for example, [5], [9], [14], [16]). The conventional Schrödinger equation has a variety of soluble potentials. The following question arises: can one use these soluble equations for obtaining exact solutions to the position-dependent mass equation? The positive answer to this question would make quantum engineering more flexible and active, providing the opportunities to develop a set of novel quantum devices.

We outline a possible strategy of the solution of this problem. In this paper we elaborate the Darboux transformations of an arbitrary order for Schrödinger equations with position-dependent effective mass and weighted energy. We combine the point canonical transformation with the intertwining technique to construct exactly solvable position-dependent Hamiltonians and corresponding solutions. To this end, we convert the Schrödinger equation with constant mass into the equation with position-dependent mass and construct the generic exactly soluble potentials, which can be used for generation of a family of exactly solvable equations. The paper is organized as follows. Section 2 is devoted to intertwining relations and generalized Darboux transformations of nth-order in the differential form. In Section 3 we suggest to apply the intertwining technique together with the point interaction method to Hamiltonians with effective mass to construct potentials which support the desirable spectrum. Finally, we give an explicit example to illustrate the method.

2. Darboux transformations

2.1. First-order Darboux transformations

For the purpose of simplification of the description below we briefly introduce Darboux transformations of the first-order obtained in [17]. We start by considering the Schródinger equation with position-dependent mass and weighted energy

$$-\left[\frac{d}{dx}\left(\frac{1}{m(x)}\right)\frac{d}{dx}\right]\phi(x)+v(x)\phi(x)=q(x)\mathcal{E}\phi(x)\ , \tag{2.1}$$

where $m(x)$ stands for the particle's effective mass, $q(x)$ and $v(x)$ denote the potentials, $\phi(x)$ is the wave function and ε denotes real-valued energy, and we use atomic units. We expand the conventional intertwining relations on our generalized equation (1). To the end we use the intertwining relations

$$\mathcal{L}\mathcal{H}=\mathcal{H}_1\mathcal{L}\ , \tag{2.2}$$

$$\phi_1\ =\ \mathcal{L}\ \phi \tag{2.3}$$

and find out the intertwining operator $\mathcal{L}$ in the form

$$\mathcal{L}=\frac{1}{\sqrt{q\ m}}\left(\frac{d}{dx}+K\right)\ ,\qquad K=-\frac{\mathcal{U}^{'}}{\mathcal{U}}. \tag{2.4}$$

The operator equation (2.2) intertwines the two generalized Hamiltonians H and $\mathcal{H}_1$

$$\mathcal{H}=-\frac{1}{q(x)}\left[\frac{d}{dx}\left(\frac{1}{m(x)}\right)\frac{d}{dx}\right]+\frac{v(x)}{q(x)}\ ,\qquad \mathcal{H}\phi=\mathcal{E}\phi\ , \tag{2.5}$$

$$\mathcal{H}_1=-\frac{1}{q(x)}\left[\frac{d}{dx}\left(\frac{1}{m(x)}\right)\frac{d}{dx}\right]+\frac{v_1(x)}{q(x)}\ ,\qquad \mathcal{H}_1\phi_1=\mathcal{E}\phi_1\ , \tag{2.6}$$

where Hamiltonians $\mathcal{H}$ and $\mathcal{H}_1$ differ only in potentials v and v_1. The intertwining relation (2.3) allows one to construct a solution for $\mathcal{H}_1$, if a solution for $\mathcal{H}$ is known. The potential $v_1(x)$ and solutions $\phi_1(x)$ are defined as

$$v_1 = v + 2\sqrt{\frac{q}{m}}\frac{d}{dx}\left[\frac{K}{\sqrt{q\,m}}\right] - \sqrt{\frac{q}{m}}\frac{d}{dx}\left[\frac{1}{q}\frac{d}{dx}\left(\sqrt{\frac{q}{m}}\right)\right] \tag{2.7}$$

$$= v - \sqrt{\frac{q}{m}}\left[2\frac{d}{dx}\left(\frac{1}{\sqrt{q\,m}}\frac{\mathcal{U}'}{\mathcal{U}}\right) + \frac{d}{dx}\left(\frac{1}{q}\frac{d}{dx}\left(\sqrt{\frac{q}{m}}\right)\right)\right],$$

$$\phi_1 \;=\; \mathcal{L}\,\phi = \frac{1}{\sqrt{qm}}\left[\frac{d}{dx} - \frac{\mathcal{U}'}{\mathcal{U}}\right]\phi = \frac{1}{\mathcal{U}}\frac{1}{\sqrt{qm}}W_{\lambda,\,\varepsilon}\;, \tag{2.8}$$

where $W_{\lambda,\,\varepsilon} = \mathcal{U}\phi' - \phi\mathcal{U}'$ is the Wronskian of the functions $\mathcal{U}$ and $\phi(x)$. From (2.4), (2.7) and (2.8) it follows that the intertwiner $\mathcal{L}$, the transformed potential v_1 and solutions ϕ_1 depend not only on the potential v and on the additional potentials m and q in contrast to the conventional Schrödinger equation. These results generalize usual first-order Darboux transformations for the Schrödinger equation. It is easy to see that all expressions are reduced to the well known ones if potential functions m and q are taken to be constants.

2.2. Chain of Darboux transformations

By considering iterative applications of the first-order Darboux transformations n times, we obtain Darboux transformations of nth-order. In this case the intertwining operator $\mathcal{L}$ is obtained from a sequence of n first-order Darboux transformations

$$\mathcal{L} = \mathcal{L}_n\mathcal{L}_{n-1}...\mathcal{L}_1, \quad \mathcal{L}_n = \frac{1}{\sqrt{q\,m}}\left(\frac{d}{dx} + K_n\right), \quad K_n = -\frac{\chi'_{n-1}}{\chi_{n-1}}. \tag{2.9}$$

This procedure being applied n times leads to generalized Darboux transformations for potential and solutions

$$v_n = v_{n-1} + 2\sqrt{\frac{q}{m}}\frac{d}{dx}\frac{K_n}{\sqrt{q\,m}} - \sqrt{\frac{q}{m}}\frac{d}{dx}\left[\frac{1}{q}\frac{d}{dx}\left(\sqrt{\frac{q}{m}}\right)\right], \tag{2.10}$$

$$\phi_n = \mathcal{L}\phi = \mathcal{L}_n\phi_{n-1} = \mathcal{L}_n\mathcal{L}_{n-1}...\mathcal{L}_1\phi\;. \tag{2.11}$$

The solution χ_n can be obtained by applying the operator $\mathcal{L}$ to an auxiliary solution $\mathcal{U}_n$ of (5) at energy λ_n. Evidently, $\mathcal{L}_1$ is $\mathcal{L}$ given in (2.4), K_1 coincides with K determined in (2.4). The operator $\mathcal{L}_2$ is determined as

$$\mathcal{L}_2 = \frac{1}{\sqrt{q\,m}}\left(\frac{d}{dx} + K_2\right), \quad K_2 = -\frac{\chi_1'}{\chi_1}\;. \tag{2.12}$$

The function χ_1 is obtained by means of the first-order Darboux transformation (8), applied to an auxiliary solution $\mathcal{U}_2$ of equation (5) at energy λ_2

$$\chi_1 = \mathcal{L}_1\mathcal{U}_2 = \frac{1}{\sqrt{q\,m}}\left(\frac{d}{dx} + K_1\right)\mathcal{U}_2. \tag{2.13}$$

Clearly, χ_1 is the solution of the transformed equation (2.6) with the potential v_1, defined as in (2.7), and χ_1 can be taken as a new transformation function to generate the potential v_2 and corresponding

solutions ϕ_2.

$$v_2 = v_1 + 2\sqrt{\frac{q}{m}}\frac{d}{dx}\left[\frac{K_2}{\sqrt{q\,m}}\right] - \sqrt{\frac{q}{m}}\frac{d}{dx}\left[\frac{1}{q}\frac{d}{dx}\left(\sqrt{\frac{q}{m}}\right)\right], \tag{2.14}$$

$$\phi_2 = \mathcal{L}_2\phi_1 = \frac{1}{\sqrt{q\,m}}\left(\frac{d}{dx} + K_2\right)\phi_1, \quad \phi_1 = \mathcal{L}_1\phi. \tag{2.15}$$

The iteration of this procedure n times leads to the operator $\mathcal{H}_n$ with the transformed potential v_n which satisfies the recurrent relation (2.10).

Notice that the recursion in (2.9) - (2.11) can be removed, leaving the transformed potentials and solutions in terms of the initial potentials and the family of auxiliary solutions $\mathcal{U}_j,\ j = 1, 2, .., n$ of the initial equation (2.5)

$$v_n = v + 2\sqrt{\frac{q}{m}}\frac{d}{dx}\frac{K}{\sqrt{q\,m}} - n\sqrt{\frac{q}{m}}\frac{d}{dx}\left[\frac{1}{q}\frac{d}{dx}\left(\sqrt{\frac{q}{m}}\right)\right], \quad K = K_1 + K_2 + ... + K_n\ . \tag{2.16}$$

Indeed, using the explicit expression for v_1 which appears in the first-order Darboux transformation (2.7), we present the formula (2.16) for the potential v_2 as

$$v_2 = v + 2\sqrt{\frac{q}{m}}\frac{d}{dx}\frac{K}{\sqrt{q\,m}} - 2\sqrt{\frac{q}{m}}\frac{d}{dx}\left[\frac{1}{q}\frac{d}{dx}\left(\sqrt{\frac{q}{m}}\right)\right], \quad K = K_1 + K_2\ . \tag{2.17}$$

Now transform $K = -\mathcal{U}_1{}'/\mathcal{U}_1 - \chi_1{}'/\chi_1$, representing χ_1 as

$$\chi_1 = \frac{1}{\sqrt{q\,m}}\frac{W_{1,2}}{\mathcal{U}_1}\ , \tag{2.18}$$

where is the Wronskian of the functions $\mathcal{U}_1$ and $\mathcal{U}_2$. Substituting (2.18) into the formula for K_2, we get

$$K_2 = -\frac{\chi_1{}'}{\chi_1} = -\frac{d}{dx}\left[\ln\left(\frac{1}{\sqrt{q\,m}}\frac{W_{1,2}}{\mathcal{U}_1}\right)\right] \tag{2.19}$$

and with account $K_1 = -\mathcal{U}_1{}'/\mathcal{U}_1$ we find

$$K = -\frac{d}{dx}\left[\ln\frac{W_{1,2}}{\sqrt{q\,m}}\right]. \tag{2.20}$$

With the last expression after some manipulations, the new potential v_2 can be expressed as

$$v_2 = v - 2\sqrt{\frac{q}{m}}\frac{d}{dx}\left[\frac{1}{W_{1,2}}\ \frac{d}{dx}\frac{W_{1,2}}{\sqrt{q\,m}}\right] - 2\sqrt{\frac{q}{m}}\frac{d}{dx}\left[\frac{1}{q}\frac{d}{dx}\left(\sqrt{\frac{q}{m}}\right)\right]\ . \tag{2.21}$$

The corresponding functions ϕ_2 defined as in (2.11) can be presented as

$$\phi_2 = \mathcal{L}\phi = \frac{1}{q\,m}\frac{W_{1,2,\mathcal{E}}}{W_{1,2}}\ , \quad \mathcal{L} = \mathcal{L}_1\mathcal{L}_2. \tag{2.22}$$

It is easily seen from (2.21) and (2.22) that due to the 2nd-order Darboux transformations, the potential and solutions are completely expressed in terms of the known potential functions, v, m and q and the solutions $\mathcal{U}_1$, $\mathcal{U}_2$, $\phi(\varepsilon)$ of the initial equation, with no use of the solutions to the

intermediate equation with the potential $v_1(x)$. Clearly, for the next transformation step to be made, one should take a new transformation function χ_2, that corresponds to the potential v_2 at energy λ_3. The solution χ_2 can be obtained by applying the operator $\mathcal{L} = \mathcal{L}_1\mathcal{L}_2$ to solution $\mathcal{U}_3$ at energy λ_3 that is

$$\chi_2 = \mathcal{L}\mathcal{U}_3 = \mathcal{L}_2\mathcal{L}_1\mathcal{U}_3. \tag{2.23}$$

By analogy with (2.22), the fixed solution χ_2 can be written as

$$\chi_2 = \frac{W_{1,2,3}}{q\ m\ W_{1,2}}. \tag{2.24}$$

Then it can be used to produce a new transformed operator $\mathcal{L}_3$, given by

$$\mathcal{L}_3 = \frac{1}{\sqrt{q\ m}}\left(\frac{d}{dx} + K_3\right), \quad K_3 = -\frac{\chi_2{}'}{\chi_2} \tag{2.25}$$

for generating a new potential v_3 with corresponding solution ϕ_3 and so on according to (2.9)–(2.11). As a result, we can express the transformed potentials v_n in terms of the initial potentials v, q, effective mass m and the family of auxiliary solutions $\mathcal{U}_j, j = 1, 2, ..n$ of the initial equation (2.5) at energies λ_j conformity with (2.16). This construction enables us to generate a family of new Hamiltonians of any order and corresponding solutions directly from the initial Hamiltonian and solutions without generating intermediate Hamiltonians. When $\mathcal{L}$ is the nth-order differential operator, the intertwining relation

$$\mathcal{L}\mathcal{H} = \mathcal{H}_n\mathcal{L} \tag{2.26}$$

is valid.

3. Constructing exact solutions for effective mass Schrödinger equations

In resent years particular interest has been given to physical systems with position-dependent mass. This interest is due to the recent progress of crystal-growth techniques for the production of nonuniform semiconductor devices. Therefore in this section we shall consider the Schrödinger equation with position-dependent mass

$$-\left[\frac{d}{dx}\left(\frac{1}{m(x)}\right)\frac{d}{dx}\right]\phi(x) + v(x)\phi(x) = \mathcal{E}\phi(x)\ , \tag{3.27}$$

which is a particular case of the equation (1). To construct equations (3.27) admitting exact solutions we shall combine the inverse point canonical transformation with the intertwining technique. We suggest to convert the equation with constant mass into the equation with position-dependent mass in contrast with the standard canonical approach, when the equation with position-dependent mass is transformed into the Schrödinger equation. The point canonical method, like Liouville transformations, consists in transformations of functions and coordinate variables. Introducing a new function $\phi(x) = exp(f(x))\psi(x)$and a new variable $\xi = \xi(x)$, effective mass Schrödinger (3.27) equations is converted to

$$\begin{aligned} -\left(\frac{\xi_x^2}{m}\right)\psi_{\xi\xi} - \left(\frac{2\ f_x\ \xi_x}{m} - \frac{m_x\ \xi_x}{m^2} + \frac{\xi_{xx}}{m}\right)\psi_\xi \\ - \left(\frac{f_x^2 + f_{xx}}{m} - \frac{f_x\ m_x}{m^2}\right)\psi + v\ \psi = \mathcal{E}\ \psi, \end{aligned} \tag{3.28}$$

where ξ_x denotes the derivative of x. The equation (3.28) is transformed to a conventional Schrödinger equation under the following conditions: the coefficient at $\psi_{\xi\xi}$ is equal to $1/m_o$ (m_o corresponds to constant mass) and the coefficient of ψ_ξ vanishes

$$\frac{\xi_x^2}{m} = \frac{1}{m_o}\ , \qquad \frac{2\ f_x\ \xi_x}{m} - \frac{m_x\ \xi_x}{m^2} + \frac{\xi_{xx}}{m} = 0. \tag{3.29}$$

The solutions of equations (3.29) give us

$$\xi_x = \left(\frac{m(x)}{m_o}\right)^{1/2}\ , \qquad f_x = \frac{1}{4}\frac{m_x}{m}. \tag{3.30}$$

As a result we have

$$f(x) = \ln\left(m(x)\right)^{1/4} \quad and \quad \xi = \frac{1}{\sqrt{m_o}}\int \exp(2\ f(x))dx. \tag{3.31}$$

Finally, we obtain the Schrödinger equation in ξ-representation

$$-\frac{1}{m_o}\ \psi_{\xi\xi} + V\psi = \mathcal{E}\ \psi\ , \tag{3.32}$$

where the effective potential V is written in the old coordinates as

$$V = v - \frac{1}{4\ m}\left(\frac{m_{xx}}{m} - \frac{7}{4}\left(\frac{m_x}{m}\right)^2\right). \tag{3.33}$$

It is apparent that the potential and mass in the initial x-space and in the transformed ξ-space have different functional dependence and the effective potential V depends on position-dependent mass m. It should be noted that m can give a very complex function $V(\xi)$ for which the Schrödinger equation (3.33) cannot be solved analytically. To obtain the explicit expressions for mass m and the potential V in ξ-space we need to know how x depends on ξ. Even the dependence ξ on x is known the inverse procedure is not always solved. In general case both these factors make the problem of solution of the Schrödinger equation (3.32) is very complicated.

We suggest to use the inverse point transformation. First, we start from the Schrödinger equation (3.32), for which there are a lot of exactly soluble potentials. On the second stage we transform the Schrödinger equation, given in ξ-space to the effective mass Schrödinger equation in x-space. Next, knowing exact solutions of the Schrödinger equation in ξ-representation, we find $m(x)$, $V(x)$ and solutions $\phi(x)$ for the position dependent Schrödinger equation in x-space and use the soluble effective mass equation as generic ones for constructing a whole family of exactly solvable equations with the desired spectrum by using the intertwining technique.

This approach allows one to consider another class of exactly solvable models and thus expands opportunities constructing exactly solvable equations with position dependent mass on the base of combination of two methods of point interaction transformation and intertwining technique.

Let us consider the inverse point transformation as follows. We shall apply the inverse point transformation to the Schrödinger equation (3.32) introducing change of variables $\xi = \xi(x)$ and functions $\psi(x) = exp(g(\xi))\phi(x(\xi))$. This transformation converts the Schrödinger equation (3.32) to

$$-\frac{1}{m_o}\left(\ (x_\xi^2\phi_{xx} + (\ 2\ g_\xi x_\xi + x_{\xi\xi})\phi_x + (g_{\xi\xi} + g_\xi g_\xi)\right)\phi + V(\xi)\phi = \mathcal{E}\ \phi\ . \tag{3.34}$$

Now we transform (3.34) into the effective mass Schrödinger equation (3.27) by requiring that the coefficient at ϕ_{xx} is equal to $1/m(x)$, the coefficient at ϕ_x is equal to $(1/m(x))_x$ and the coefficient at ϕ is equal to the effective potential. These conditions give us

$$x_\xi = \left(\frac{m_o}{m}\right)^{1/2} \quad \to x = \int \left(\frac{m_o}{m}\right)^{1/2} d\,\xi\ , \tag{3.35}$$

$$2\ g_\xi x_\xi + x_{\xi\xi} = \left(\frac{m_o}{m}\right)_x \quad \to g(\xi) = \ln\left(\frac{1}{m(\xi)}\right)^{1/4}\ , \tag{3.36}$$

$$v(\xi) = V(\xi) - \frac{1}{m_o}\left(g_{\xi\xi} + g_\xi g_\xi\right)\ . \tag{3.37}$$

Using (3.35) and (3.36) in (3.37) we find the expression for the potential in terms of mass functions

$$v = V + \frac{1}{4\ m_o}\left(\frac{m_{\xi\xi}}{m} - \frac{5}{4}\left(\frac{m_\xi}{m}\right)^2\right). \tag{3.38}$$

Now, with regard to our approach we would like to find out $m(\xi)$. To this end, we shall solve the equation (3.37) that is the nonlinear second order differential equation, in fact, it is the Riccati equation. As it is known, the Riccati equation can be analytically solved for a lot of cases. Let us introduce the function $g_\xi = N_\xi/N$ which reduce the equation (3.37) to the linear second order differential equation

$$-\frac{1}{m_o}N_{\xi\xi} + (V - v)N = 0\ . \tag{3.39}$$

Let assume that this equation can be exactly solvable with respect to $N(\xi)$. Once we have found $N(\xi)$, we can determine $m(\xi)$ via $N(\xi) = m^{-1/4}(\xi)$. The further solution of the problem depends on integrability of (as one can see from (3.35)) and existence of the inverse function $\xi = \xi(x)$. If these conditions are fulfilled we can find out the potential v, the mass-position function m and the solutions ϕ in x-space. Now by using the soluble effective mass equation as the initial ones one can construct a whole family of exactly solvable equations with the given spectrum. Let's consider the example. We are given the transparent potential in the ξ-space in the form of modified Pöschle-Teller potential

$$m_o(V - v) = -\frac{2\alpha^2}{\cosh^2(\alpha\xi)} + \alpha^2\ , \tag{3.40}$$

where is α real constant. The solution of the equation (3.39) with this potential is known:

$$N(\xi) = \frac{\sqrt{\alpha/2}}{\cosh(\alpha\xi)}\ . \tag{3.41}$$

Hence, from (3.41) one gets

$$m(\xi) = \frac{4\cosh^4(\alpha\xi)}{\alpha^2}\ , \qquad x = \frac{\sqrt{m_o}}{2}\tanh(\alpha\xi)\ + \text{const.} \tag{3.42}$$

From the second equation of (3.42) we immediately get

$$\xi = \frac{1}{\alpha}\,\text{arctanh}(2\ x/\sqrt{m_o}). \tag{3.43}$$

Particular solutions of the Schrödinger equation (3.32) in ξ-representation with the effective potential (3.40) at energy $\varepsilon = \kappa^2$ can be written as

$$\psi = (-i\gamma + \alpha \tanh(\alpha\xi)) \exp(i\gamma\xi) \ , \tag{3.44}$$

where $\gamma^2 = k^2 - \alpha^2$. The linearly independent solutions are

$$\hat{\psi} = (i\gamma + \alpha \tanh(\alpha\xi)) \exp(-i\gamma\xi) \ . \tag{3.45}$$

For the simplicity let us suppose that the initial potential v in (3.33) is equal to zero. The corresponding solutions of position-dependent mass Schrödinger equation (3.27) with

$$m(x) = \frac{4\cosh^4(\operatorname{arctanh}(2\ x/\sqrt{m_o}))}{\alpha^2}$$

can be written as

$$\phi_{\pm}(x) = \frac{\sqrt{\alpha/2}}{\cosh(\operatorname{arctanh}(2x/\sqrt{m_o}))}(\mp i\gamma + \alpha(2x/\sqrt{m_o}))\times$$
$$\times \exp \pm \left(i\ \frac{\gamma}{\alpha} \operatorname{arctanh}(2\ x/\sqrt{m_o})\right) .$$

Thus we obtained the initial exactly solvable equation with position-dependent mass in x presentation. Next, by using the above intertwining technique, we can construct a family of exactly solvable equations (3.27).

Let us construct potentials with one and two bound states and investigate the influence of distance between levels on the form of potentials. First we obtain potentials with one bound state at energy $\mathcal{E}_1 = -\kappa_1^2$ and corresponding solutions by applying first-order Darboux transformations. The transformation functions have been chosen as follows

$$\eta_1 = -\cosh(\kappa_1 y) + \alpha \tanh(\alpha y) \frac{\sinh(\kappa_1 y)}{\kappa_1}, \tag{3.46}$$

where $y = \operatorname{arctanh}(2x/\sqrt{m_o})$. Here we select $\alpha = 1.0$ and $m_o = \text{const} = 6.0$. By using (2.6) with $q(x) = 1$ and the transformation kernel $K(x)$ determined by $K(x) = -\frac{\eta_1'}{\eta_1}$ we obtain a set of potentials, the width and depth of which depend on the choice of the bound state values (see Fig. 1a).

Now we would like to construct potentials with two bound states. The transformation functions have been used as:

$$\eta_1 = -\cosh(\kappa_1 y) + \alpha \tanh(\alpha y) \frac{\sinh(\kappa_1 y)}{\kappa_1}, \tag{3.47}$$

$$\eta_2 = -\sinh(\kappa_2 y) + \alpha \coth(\alpha y) \frac{\cosh(\kappa_2 y)}{\kappa_2}, \tag{3.48}$$

With using the second-order Darboux transformations we obtain a family of potentials with two bound states. The form of potentials depends on the distance between levels. One can see if levels are sufficiently distant from one another we construct simple symmetric potentials presented in Fig.1b (curve 1), if the levels are close to each other, we construct symmetric double well potentials Fig.1b (curves 2, 3). As a final remark, let us note that different distances between levels give us different shapes of potentials. It can be very important for construction and investigation of quantum systems with needed spectral properties, e.g. in nanoelectronics.

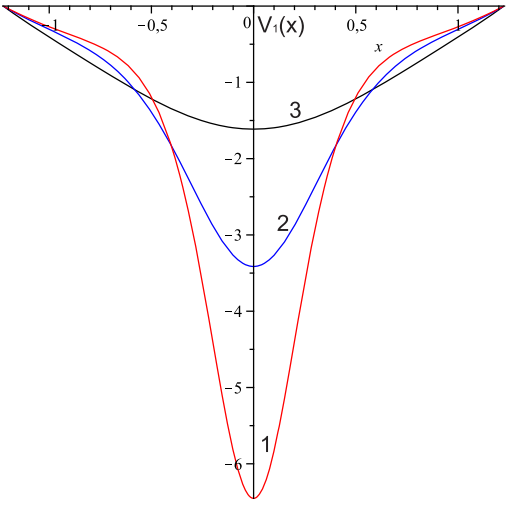

Fig. 1 a) The change in form of potentials $V_1(x)$ with one bound state:
$1 : \mathcal{E}_1 = -19.36$,
$2 : \mathcal{E}_1 = -10.24$,
$3 : \mathcal{E}_1 = -4.84$;

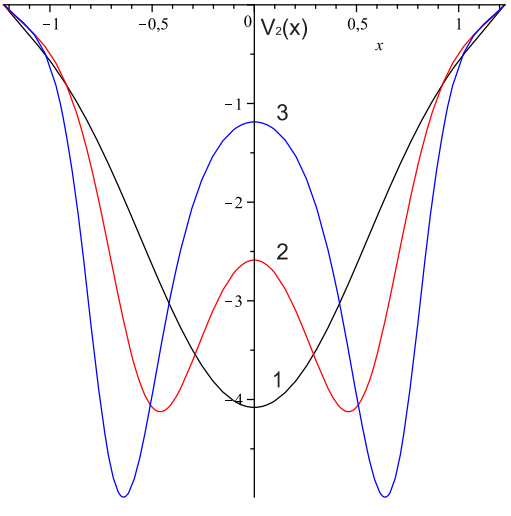

Fig. 1 b) The change in form of potentials $V_2(x)$ with two bound states as the levels come close to each other:
$1 : \mathcal{E}_1 = -16.0,\ \mathcal{E}_2 = -5.76$,
$2 : \mathcal{E}_1 = -16.0,\ \mathcal{E}_2 = -10.24$,
$3 : \mathcal{E}_1 = -16.0,\ \mathcal{E}_2 = -14.44$.

4. Conclusion

Darboux transformations have been constructed for generalized Schrödinger equation with position-dependent mass and with linearly energy-dependent potentials. The iterative procedure of the first-order Darboux transformations allows one to generate families of Hamiltonians with a predetermined spectrum. A combination of intertwining technique with the point canonical transformation method is used for constructing position-dependent mass Schrödinger equations, admitting exact solutions.

Acknowledgments. This work was partially supported by RFFI grant 09-01-00770.

References

[1] Matveev V.B. and Salle M.A. Darboux transformations and solutions. Springer, Berlin, 1991. 123 p.

[2] Gu C., Hu H. and Zhou Z., Darboux transformations in integrable systems. The Netherlands: Mathematical Physics Studies 26, Springer, Dordrecht, 2005. 310 p.

[3] Junker G., Supersymmetric Method in Quantum and Statistical Physics. Springer, New York, 1996. P. 173.

[4] Einevoll G.T., Hemmer P.C. and Thomesn J., Operator Ordering in Effective-mass Theory for Heterostructures. I. Comprason with Exact Result for Superlattices, Quantum Wells and Localized Potentials // Phys. Rev. B. 1990. Vol. 42. P. 3485.

[5] Plastino A.R. et al., Supersymmetric Approach to Quantum Systems with Position-dependent Effective mass//Phys. Rev. A. 1999. Vol. 60. P. 4318–4325.

[6] Milanović V., Iconić Z., Generation of Isospectral Combinations of the Potential and the Effective-mass Variations by Supersymmetric Quantum Mechanics // J. Phys. A: Math. Gen. 1999. Vol. 32. P. 7001–7015.

[7] Roy B. and Roy P., A Lie Algebraic Approach to Effective mass Schrödinger Equations // J. Phys. A. 2002. Vol. 35. P. 3961.

[8] Koç R. and Koca M., A Systematic Study on the Exact Solution of the Position Dependent mass Schrödinger Equation // J. Phys. A. 2003. Vol. 36. P. 8105–8112.

[9] Suzko A.A. and Schulze-Halberg A., Intertwining Operator Method and Supersymmetry for Effective mass Schrödinger Equations//Phys. Lett. A. 2008. Vol. 372. P. 5865–5871.

[10] Suzko A.A., Giorgadze G., Darboux Transformations for the Generalized Schrödinger Equations//Physics of Atomic Nuclei. 2007. Vol. 70, No. 3. P. 607–610;

[11] Suzko A.A., Tralle I., Reconstruction of Quantum Well Potentials via the Intertwining Operator Technique//Acta Physica Polonioca B. 2008. Vol. 39, No. 3. P. 1001–1023.

[12] Zakhariev B.N. and Suzko A.A. Direct and inverse problems. (Potentials in quantum scattering). Springer, New York, 1990. P. 223.

[13] Suzko A.A. //Physica Scripta. 1985. Vol. 31. P. 447; Physica Scripta. 1986. Vol. 34. P. 5; in Lect Notes in Phys. ”Quantum Inversion Theory and its Applicationsin”; Sov. J. Nuclear Physics. 1992. Vol. 55. P. 1359.

[14] Sara Cruz y Cruz, Oscar Rosa-Ortiz, Position-dependent Mass Oscillators and Coherent States// J. Phys. A: Math. Theor. 2009. Vol. 42. P. 185205.

[15] Suzko A.A. and Schulze-Halberg A., Darboux transformations and Supersymmetry for the Generalized Schrödinger Equations in (1+1) Dimensions // J. Phys. A. 2009. Vol. 42. P. 295203-14;

[16] Cruz y Cruz S., Negro J. and Nieto L.M., On Position-dependent Mass Harmonic Oscillators // J. Phys.: Conference Series. 2008. Vol. 128. P. 012053-12 pages.

[17] Suzko A.A., Velicheva E.P., Darboux Transformations in Integral and Differential Forms for the Generalized Schrödinger Equations//Physics of Atomic Nuclei. 2011. Vol. 74, No. 7. P. 1106–1111.